IMPORTANCE OF ARP2/3 COMPLEX AND NUCLEATION PROMOTING FACTORS LIKE WISKOTT-ALDRICH VERPROLIN SYNDROME PROTEIN (WAVE) IN BRANCHING OF ACTIN FILAMENTS

A DISSERTATION

SUBMITTED IN PARTIAL FULFILLMENT OF THE REQUIREMENTS

FOR THE DEGREE OF DOCTOR OF PHILOSOPHY

IN THE GRADUATE SCHOOL OF THE

TEXAS WOMAN'S UNIVERSITY

DEPARTMENT OF BIOLOGY

COLLEGE OF ARTS AND SCIENCES

BY

AMRUTA C. MAHADIK

DENTON, TEXAS

DECEMBER 2016

TEXAS WOMAN'S UNIVERSITY
DENTON, TEXAS

JULY 15, 2016

To the Dean of the Graduate School:

I am submitting herewith a dissertation written by Amruta C. Mahadik entitled "Importance of Arp2/3 Complex and Nucleation Promoting Factors like Wiskott Aldrich Verprolin Syndrome Protein (WAVE) in Branching of Actin Filaments." I have examined this dissertation for form and content and recommend that it be accepted in partial fulfillment of the requirements for the degree of Doctor of Philosophy with a major in Molecular Biology.

_____
DiAnna L. Hynds Ph.D., Major Professor

We have read this dissertation and recommend its acceptance:

_____
Dr. Brian W. Beck

_____
Dr. Nathaniel C. Mills

_____
Dr. Douglas Root

_____
Dr. Lynda Uphouse

_____
Department Chair

Accepted:

_____
Dean of the Graduate School

DEDICATION

To my mom and dad, Mrs. Kusum C. Mahadik and Mr. Chandrakant A. Mahadik,

The individual I am today is by your grace and upbringing.

To my loving brother Amol and sister Aparna,

Thank you for taking on my responsibilities and leading the family.

To my beloved husband, Mr. Sheokant Diwakar,

I am complete because of you.

Thank you for the unconditional love, patience, and endless support.

And

To my father-in-law, Dr. Ramakant Sharma,

Thank you for demonstrating how to fight odds in the life with a smile.

ACKNOWLEDGMENTS

The work presented in this thesis would not have been possible without my close association with many people. I take this opportunity to extend my sincere gratitude and appreciation to all those who made this Ph.D thesis possible.

First and foremost, I would like to thank my former research guide, Dr. Brian W. Beck, for introducing me to this exciting field of science and for his dedicated help, advice, inspiration, encouragement, and continuous support throughout my Ph.D. His enthusiasm, integral view on research, and his mission for providing high-quality work have made a deep impression on me. During our course of interaction, I have learned extensively from Dr. Beck, including how to raise new possibilities, how to regard an old question from a new perspective, how to approach a problem by systematic thinking, data-driven decision-making, and exploiting serendipity. I owe Dr. Beck lots of gratitude for having shown me this way of research. I would also like to thank Dr. Dianna Hynds, one of the committee members and my current mentor, for stepping in to act as my committee chair in order to facilitate my actual mentor continuing to train me.

My special words of thanks go to my research committee members Dr. Nathaniel C. Mills, Dr. Douglas Root, Dr. Junalyn NavarraMadsen (former member), and Dr. Lynda Uphouse for their continuous support, guidance, cooperation, and encouragement.

I am also grateful to Dr. Lynda Uphouse (Professor), Dept. of Biology, Texas Woman's University for her guidance and advice regarding the statistical analysis. I would also like to thank Dr. Shazia Ahmed (Biology Lab's Coordinator), Dept. of Biology, Texas Woman's University for her guidance and support in difficult moments.

I thank my friends and lab-mates for their help in various ways during my Ph.D.

I thank to my destiny for strengthening me as an "individual" by offering ups and downs in the life, especially during the course of my Ph.D.

ABSTRACT

AMRUTA C. MAHADIK

IMPORTANCE OF ARP2/3 COMPLEX AND NUCLEATION PROMOTING FACTORS LIKE WISKOTT-ALDRICH VERPROLIN SYNDROME PROTEIN (WAVE) IN BRANCHING OF ACTIN FILAMENTS

DECEMBER 2016

Initiation of branching in actin cytoskeletal filaments requires an active Arp2/3 complex binding to the side of an existing actin filament. Arp2 and Arp3, the major subunits of the Arp2/3 complex, nucleate actin branches by forming the first short pitch dimer of the daughter actin filament. Nucleation promoting factors like Wiskott-Aldrich syndrome VErprolin (WAVE) from the WASP family of proteins are thought to activate the Arp2/3 complex and promote the elongation process by orienting and enhancing actin monomer binding to the daughter actin filament. Previous kinetics and cross-linking studies have established the importance of binding the VCA/WH2 domains of WAVE proteins in Arp2/3 complex activation, but the quaternary interactions are not well understood.

Here, we used molecular dynamics simulations to study the conformational changes in actin, Arp2, and Arp3 upon binding of the V and C peptide of the VCA domain of WAVE protein. We found that peptide binding induces larger conformational changes than the nucleotide-binding. The C-domain-bound Arp3 produced a more

compact structure than the V-domain-bound Arp3 or Arp2. Based on the binding energy calculations, actin binds tighter to V-domains than do the Arps, while Arp2 binds C-domains more tightly than does Arp3, suggesting the C-domain of V-bound actin interacts with Arp2 first. Additionally, binding of the C peptide reduced the average inter domain distance between SD1:SD3 and SD3:SD4, suggesting amino acid residues at the Arp2:Arp3 dimer interface play an important role in stabilizing the "inactive" state of the complex. Therefore, we used Baker's computational alanine scanning method and identified "hot spots" residues (R123, S188, and R409) that stabilized the "inactive" state of the complex. We further proposed point mutants for each of the identified hot spots (R123A, S188Q, and R409A).

We performed site-directed mutagenesis and transient transfection of GFP-tagged R123A Arp3 expressed in B35 neuroblastoma cells. Morphology of B35 neuroblastoma cells was changed to spherical structures with altered neurite growth and excess cortical actin. The Arp2/3 complex was preserved; however, Arp3: R123A successfully altered the quaternary interactions at the dimer interface, making the complex constitutively active.

TABLE OF CONTENTS

Page

LIST OF TABLES

LIST OF FIGURES

CHAPTER I

INTRODUCTION

Background of actin

In eukaryotic cells, cell shape and motility depend on actin cytoskeleton.[1, 2] Actin cytoskeleton consists of the network of actin filaments that provides a scaffold to the different regulatory factors and mechanical supports to the cells to change the shape.[3] These filaments also serve as the tracks for the motor proteins during intracellular trafficking and also promote formation of various cellular structures such as spikes, ruffles, filopodia, lamellipodia, and actin bundles. The major component of these filaments is actin, an ATPase enzyme that exists in two forms: Globular actin (G-actin) and Filamentous actin (F-actin).[4] Hydrolysis of ATP into ADP and inorganic phosphate (Pi) is the main factor that stimulates the transition of G-actin into F-actin to form polar actin filaments with a fast growing end, called the barbed or plus ("+") end, and a slower-growing end, "pointed" or negative ("-") end. Both the ends have distinct biochemical properties.[5] In vitro, addition of actin monomers occurs at the barbed end followed by the nucleotide hydrolysis in the filament and a faster release of the ADP-actin from the pointed end.[4] Therefore, the rate of actin filament assembly is dependent on the presence of free barbed ends that provide templates for new polymerization processes.

Known mechanisms to generate free barbed ends are by uncapping the pre-existing actin filaments, severing of filaments, or *de novo* filament nucleation.[6]

Uncapping of the barbed ends is the primary mechanism that generates the free barbed ends in the cells. Capping molecules, such as *gelsolin*, dissociates from the barbed ends by the removal of Ca^{2+} ions, releasing the free barbed end to polymerize. *Cofilin* as well as *Actin Depolymerising Factor* (ADF) (other cofilin family proteins) severs the filament to generate free barbed ends, whereas the *de novo* mechanism involves association of the *Actin related proteins 2/3* (Arp2/3) complex with the preexisting actin filament. However, Arp2/3 complex requires activation by nucleation promoting factors to nucleate and promote new actin filaments in response to upstream signal.[7, 8]

Arp2/3 complex

The Arp 2/3 complex is composed of seven subunits that include two major subunits (Arp2 and Arp3) and five accessory subunits (ArpC1-ArpC5).[9] Arp2 and Arp3 subunit share 30-60% sequence identity with actin.[10] Like actin, Arps are composed of a small domain and a large domain.[11] The small domain consists of SD1 and SD2, whereas the large domain is comprised of SD3 and SD4.[9] The adenine nucleotide-binding cleft is present between the small and large domain.[11] Both the major subunits, Arp2 and Arp3 undergo conformational changes to form an "active-like" dimer that act as a template for the daughter actin subunit at the barbed end. However, none of the available crystal structures of the Arp2/3 complex represents the "active" state of the complex, as the conformational arrangement of Arp2 and Arp3 subunits is not consistent with their binding conventional actin subunits to nucleate a new filament with a free barbed end.[9, 12]

Electron Microscopy (EM) and reconstruction studies have suggested different orientation of Arp2 relative to Arp3 within the complex in an active state.[9, 13] The

transition from inactive to active state involves closing of the nucleotide-binding cleft of Arp2 and Arp3 upon nucleotide-binding, a ~15° rotation of SD's 3 and 4 relative to SD's 1 and 2 of Arp2, and the movement of Arp2 and Arp3 relative to each other. [13, 14]

The proposed conformational changes in Arp2 and Arp3 for the activation of the complex require interactions with the NPFs and the preexisting actin filament. Molecular dynamics simulation study by Pfaendtner and his collaborators revealed that the number of salt bridges and hydrophobic contacts were formed/broken at the interface between the pointed end of the Arp2/3 complex and the preexisting actin filament.[15] These dynamic salt bridges stabilize the association of the Arp2/3 complex and preexisting actin filament at the pointed end of the complex. On the other hand, the NPF's are thought to be involved in conformational rearrangement and delivery of the actin molecule at the barbed end of the complex.[13]

Nucleation promoting factors

Arp2/3 complex has low intrinsic nucleation activity and can be activated by different NPFs. The family of NPFs constitute a large number of proteins that includes the evolutionarily conserved Wiskott-Aldrich syndrome protein (WASP),[7, 16-18] N-WASP ,[19] suppressor of cAR (Scar)/WASP family verprolin homologous (WAVE) proteins.[16] All NPFs form transient oligomeric complexes with different proteins and perform diverse functions.[20] However, a minimal peptide sequence located at the C-terminus of the NPFs interacts with Arps and activates the complex.[21, 22] The minimal peptide sequence is consist of three major domains: V (Verprolin) domain made up of ~22 amino acid residues, C domain (central domain), and the A domain (Acidic domain) stretch of

few acidic amino acid residues.[22] The CA domain interacts with Arp2 and Arp3 but cannot activate the complex exclusively.[23, 24] The interaction between actin and the V domain is equally important for the activation of the complex.[22]

The crystal structure of the V domain bound to actin in the presence of DNase I have been resolved (PDB ID: 2A40, 2.4 Å resolution).[22] The C domain is thought to form an amphipathic helix like the V domain and to bind between the extended hydrophobic groove between the sub-domain 1 and 3 of Arp2 and Arp3.[21] However, the proposed binding site for V or C peptide is "pre" occupied by the C terminal end of Arp2 and Arp3.[25] Thus, the V or C peptide competes with the C-tails of Arps for the binding site. The binding of the V or C peptide in the "pre" occupied hydrophobic groove may displace the C-tail of the Arp2 or Arp3 and promote the conformational changes required for the rearrangement. This may lead to the formation of an active, actin-like, "short-pitch" dimer, where short-pitch refers to a dimer across the transverse axis of an actin filament.[26, 27] However, there is no experimental evidence that suggest the binding of V or C peptide in the hydrophobic groove displaces the C-tail of Arps and leads to the conformational changes required for the activation of the complex.

Different models were proposed to address the conformational changes and rearrangement of the subunits that were involved in the activation of the Arp2/3 complex.[28-30] Unfortunately, due to the lack of the crystal structure that represents the "active" state of the complex, the problem is still unsolved. One of the models proposed by Padrick et al. suggest that the delivery of actin, bound to a V peptide of a VCA peptide, to Arp2 occurs with high affinity but activates the Arp2/3 complex weakly, while actin, bound to

a V domain of a VCA peptide, is delivered slowly to Arp3, but results in strong activation of the complex.[30] ITC and FRET studies have also shown that the V-domain bound actin binds first to Arp2 and ArpC1 which in turn produces a partial conformational change at the barbed end of Arp3.[28]

Apart from the V and C peptide interactions, nucleotides also bind to the Arps.[10] Le Clainche et al. have shown that ATP hydrolysis regulates Arp2/3 function.[24] Arp2 hydrolyzes the ATP after branching, whereas Arp3 did not hydrolyze ATP. However, the relative role of the accessory subunits present within the complex and NPFs that bind to the Arps was not considered explicitly in this study.

Comparison of "OFF" and "ON" state of Arp2/3 complex

The electron microscopy data suggest that the crystal structure available of Arp2/3 complex is in the "OFF" state. During the branching, the two major subunits of the Arp2/3 complex, Arp2 and Arp3, form an active "actin-like" short pitch dimer in the presence of VCA peptide of the WASP family of proteins that act as a template for the daughter actin filament to polymerize. The activated conformation of Arp2/3 complex by a VCA peptide of WASP was analyzed using the single-particle reconstruction method at 32Å resolution.[31] The cryo-electron micrograph showed overall features consistent with the crystal structure. However, at a 35Å resolution it is difficult to predict the conformational changes in small subunits of Arp2/3 complex upon activation. On the other hand, the three-dimensional reconstructions from cryo-electron micrographs of branching point suggest a substantial conformational difference between the activated and crystal structure of Arp2/3 complex.[14] It is postulated that the association of Arp2/3

complex with the existing actin filament, interaction with the regulatory peptide (VCA) of WASp, and nucleotide-binding stabilizes the activated Arp2/3 complex.

Computational Approach to assess the quaternary interactions

We used computational modeling methods such as computational alanine scan and molecular dynamic simulations to characterize the conformational and energetic variations upon quaternary interaction. The regulatory mechanisms involved in the activation of the Arp2/3 complex rely on the conformational perturbations generated by VCA peptides as well as the interactions between the specific interfacial residues of the Arp2:Arp3 dimer. A full regulated complex, consisting of an Arp2/3 complex bound to a WA family protein, would be a large, complex system that would likely prove extremely challenging for structural analysis using NMR and X-ray methods. Size alone (>200 kDA) may preclude tractable analysis via NMR spectroscopy. Crystallographic methods have a challenge in that the Arp2/3 complex crystallizes in the inactive "OFF" state, while active conformers may lead to the polymerization of filaments that do not readily crystallize. In addition, experimental design, synthesis, and testing of all possible mutants at each residue in the Arp:Arp3 dimer interface would be time consuming and expensive. Finally, it is challenging to design experimental protocols that can analyze only monomeric response to single quaternary interactions in systems that spontaneously form oligomeric complexes. Computational modeling methods, by comparison, allow hypothesis design, analysis, and testing of the smallest possible components necessary to demonstrate putative responses to quaternary interactions. We will be using computational alanine scan modeling, designed to calculate the change in pseudo-free

energy due to alanine substitution for every interfacial residue, and molecular dynamics simulations to understand the conformational stability and dynamics of actin, Arp2, Arp3 in different peptide and nucleotide bound states.

In Chapter 2, we assessed the affinity of the V- and C-domains of the VCA peptide of the WAVE to monomeric actin, Arp2, and Arp3 in the nucleotide bound and free state using molecular dynamic simulations. Each of the systems was simulated over a period of 2ns using the CHARMM 27 force field parameters for all atoms in conjunction with the particle-mesh Ewald sum method to calculate long-range electrostatic interactions in the system.[32, 33] The trajectories were analyzed to assess the perturbations to the conformational dynamics of actin, Arp3, and Arp2 as a function of V and C peptide binding. The average RMSDs of four sub-domains of each of the molecule in different binding states suggest the stability of the sub-domain in different binding states, whereas the average inter-domain distances estimate the compactness of the molecule as a function of peptide binding. Besides the effect of the regulatory peptide binding, nucleotide-binding, the average nucleotide-binding cleft distance was computed by using the definition of nucleotide-binding cleft by Nolen and Pollard.[34] The conformational study suggests that the nucleotide bound Arp3 upon C peptide binding results in a substantial conformational change in the sub-domain 3.

The observed conformational change in Arp3 suggest that the interfacial residues might play a crucial role in shifting the conformational equilibrium required for the active dimer orientation. Therefore, we further assessed the role of interfacial residues at the Arp2:Arp3 dimer interface in the rearrangement of Arp2 next to Arp3 that promotes the

active complex formation. In Chapter 3, we used Baker's computational alanine scanning method to identify "hot spot" residues that stabilize the Arp2:Arp3 interface in the inactive state.[35] These "identified hot spots" were further analyzed and point mutations were proposed. The proposed mutants (R123A, R409W, and S188Q) were expected to change the quaternary interactions at the Arp2:Arp3 interface, and that would result in the destabilization of the inactive state and shift the complex to the active state.

Our predictions were validated using mutagenesis and transient transfection of GFP-tagged R123A Arp3 expressed in B35 neuroblastoma cells. Cells changed morphology to more spherical structures with altered neurite growth and excess cortical actin while preserving the function of the Arp2/3 complex. Mutated Arp2/3 complex was constitutively active suggesting the Arp3: R123A mutant successfully altered the quaternary interactions at the interface of Arp2:Arp3 dimer.

The effect of Arp3:R123A mutant was further assessed in terms of the the number of neurite bearing cells, number of neuritis per cell, and branches of neurites per cell in Chapter 4. Quantification study of these characteristics suggests that excessive actin branch formation due to constitutively active Arp2/3 complex favors the lamellipodia formations instead of filopodia, thus reducing the neurite outgrowth.

ABBREVIATIONS AND SYMBOLS

A-domain: Acidic domain

Arp: Actin Related Protein

Arp 2/3 Complex: Actin Related Protein 2/3 Complex

ATP: Adenosine Tri Phosphate

ADF : Actin Depolymerising Factor

ADP: Adenosine Di Phosphate

CAS: Computational Alanine Scanning

C-domain: Central domain

EM : Electron Microscopy

FRET : Fluroscence Resonance Energy Transfer

ITC : Isothermal Titration Calorimetry

NPF: Nucleation Promoting Factors

RMSD: Root Mean Square Deviation

SD: Sub Domain

V-domain: Verprolin domain

WA Family: Wiskott-Aldrich Family

WASP: Wiskott-Aldrich Syndrome Protein

WAVE: Wiskott-Aldrich syndrome VErprolin homolog

REFERENCES

1. Mogilner A, Oster G. Cell motility driven by actin polymerization. Biophys J 1996 Dec;71(6):3030-45.
2. Carlier MF, Pantaloni D. Control of actin dynamics in cell motility. J Mol Biol 1997 Jun 20;269(4):459-67.
3. Welch MD, Mullins RD. Cellular control of actin nucleation. Annu Rev Cell Dev Biol 2002;18:247-88.
4. Dominguez R, Holmes KC. Actin structure and function. Annu Rev Biophys 2011;40:169-86.
5. Wegner A, Isenberg G. 12-fold difference between the critical monomer concentrations of the two ends of actin filaments in physiological salt conditions. Proc Natl Acad Sci U S A 1983 Aug;80(16):4922-5.
6. Pollard TD, Borisy GG. Cellular motility driven by assembly and disassembly of actin filaments. Cell 2003;112(4).
7. Higgs HN, Blanchoin L, Pollard TD. Influence of the C terminus of wiskott-aldrich syndrome protein (WASp) and the Arp2/3 complex on actin polymerization. Biochemistry 1999 Nov 16;38(46):15212-22.
8. Svitkina TM, Borisy GG. Arp2/3 complex and actin depolymerizing factor/cofilin in dendritic organization and treadmilling of actin filament array in lamellipodia. J Cell Biol 1999 May 31;145(5):1009-26.

9. Robinson RC, Turbedsky K, Kaiser DA, Marchand JB, Higgs HN, Choe S, Pollard TD. Crystal structure of Arp2/3 complex. Science 2001 Nov 23;294(5547):1679-84.

10. Kelleher JF, Atkinson SJ, Pollard TD. Sequences, structural models, and cellular localization of the actin-related proteins Arp2 and Arp3 from acanthamoeba. J Cell Biol 1995 Oct;131(2):385-97.

11. Kabsch WW. Atomic structure of the actin:DNase I complex. Nature (London) 1990;347(6288):37-44.

12. Nolen BJ, Pollard TD. Insights into the influence of nucleotides on actin family proteins from seven structures of Arp2/3 complex. Mol Cell 2007 May 11;26(3):449-57.

13. Rodal AA, Sokolova O, Robins DB, Daugherty KM, Hippenmeyer S, Riezman H, Grigorieff N, Goode BL. Conformational changes in the Arp2/3 complex leading to actin nucleation. Nat Struct Mol Biol 2005 Jan;12(1):26-31.

14. Rouiller I, Xu XP, Amann KJ, Egile C, Nickell S, Nicastro D, Li R, Pollard TD, Volkmann N, Hanein D. The structural basis of actin filament branching by the Arp2/3 complex. J Cell Biol 2008 Mar 10;180(5):887-95.

15. Pfaendtner J, Volkmann N, Hanein D, Dalhaimer P, Pollard TD, Voth GA. Key structural features of the actin filament Arp2/3 complex branch junction revealed by molecular simulation. J Mol Biol 2012 Feb 10;416(1):148-61.

16. Machesky LM, Mullins RD, Higgs HN, Kaiser DA, Blanchoin L, May RC, Hall ME, Pollard TD. Scar, a WASp-related protein, activates nucleation of actin

filaments by the Arp2/3 complex. Proc Natl Acad Sci U S A 1999 Mar 30;96(7):3739-44.

17. Winter D, Lechler T, Li R. Activation of the yeast Arp2/3 complex by Bee1p, a WASP-family protein. Curr Biol 1999 May 6;9(9):501-4.

18. Yarar D, To W, Abo A, Welch MD. The wiskott-aldrich syndrome protein directs actin-based motility by stimulating actin nucleation with the Arp2/3 complex. Curr Biol 1999 May 20;9(10):555-8.

19. Rohatgi R, Ma L, Miki H, Lopez M, Kirchhausen T, Takenawa T, Kirschner MW. The interaction between N-WASP and the Arp2/3 complex links Cdc42-dependent signals to actin assembly. Cell 1999 Apr 16;97(2):221-31.

20. Kurisu S, Takenawa T. The WASP and WAVE family proteins. Genome Biol 2009;10(6):226,2009-10-6-226. Epub 2009 Jun 15.

21. Panchal SC, Kaiser DA, Torres E, Pollard TD, Rosen MK. A conserved amphipathic helix in WASP/scar proteins is essential for activation of Arp2/3 complex. Nat Struct Biol 2003 Aug;10(8):591-8.

22. Chereau D, Kerff F, Graceffa P, Grabarek Z, Langsetmo K, Dominguez R. Actin-bound structures of wiskott-aldrich syndrome protein (WASP)-homology domain 2 and the implications for filament assembly. Proc Natl Acad Sci U S A 2005 Nov 15;102(46):16644-9.

23. Dayel MJ, Holleran EA, Mullins RD. Arp2/3 complex requires hydrolyzable ATP for nucleation of new actin filaments. Proc Natl Acad Sci U S A 2001 Dec 18;98(26):14871-6.

24. Le Clainche C, Pantaloni D, Carlier MF. ATP hydrolysis on actin-related protein 2/3 complex causes debranching of dendritic actin arrays. Proc Natl Acad Sci U S A 2003 May 27;100(11):6337-42.

25. Dalhaimer P, Pollard TD, Nolen BJ. Nucleotide-mediated conformational changes of monomeric actin and Arp3 studied by molecular dynamics simulations. J Mol Biol 2008 Feb 8;376(1):166-83.

26. Pollard TD, Blanchoin L, Mullins RD. Molecular mechanisms controlling actin filament dynamics in nonmuscle cells. Annu Rev Biophys Biomol Struct 2000;29:545-76.

27. Xu XP, Rouiller I, Slaughter BD, Egile C, Kim E, Unruh JR, Fan X, Pollard TD, Li R, Hanein D, Volkmann N. Three-dimensional reconstructions of Arp2/3 complex with bound nucleation promoting factors. EMBO J 2012 Jan 4;31(1):236-47.

28. Boczkowska M, Rebowski G, Kast DJ, Dominguez R. Structural analysis of the transitional state of Arp2/3 complex activation by two actin-bound WCAs. Nature Communications 2014;5.

29. Ti SC, Jurgenson CT, Nolen BJ, Pollard TD. Structural and biochemical characterization of two binding sites for nucleation-promoting factor WASp-VCA on Arp2/3 complex. Proc Natl Acad Sci U S A 2011 Aug 16;108(33):E463-71.

30. Padrick SB, Doolittle LK, Brautigam CA, King DS, Rosen MK. Arp2/3 complex is bound and activated by two WASP proteins. Proc Natl Acad Sci U S A 2011 Aug 16;108(33):E472-9.

31. Volkmann N, Amann KJ, Stoilova-McPhie S, Egile C, Winter DC, Hazelwood L, Heuser JE, Li R, Pollard TD, Hanein D. Structure of Arp2/3 complex in its activated state and in actin filament branch junctions. Science 2001 Sep 28;293(5539):2456-9.

32. Brooks BR, Bruccoleri RE, Olafson BD, States DJ, Swaminathan S, Karplus M. CHARMM: A program for macromolecular energy, minimization, and dynamics calculations. Journal of Computational Chemistry 1983;4(2).

33. Kolafa J, Perram JW. Cutoff errors in the ewald summation formulae for point charge systems. Molecular Simulation 1992;9(5):351.

34. Nolen BJ, Pollard TD. Structure and biochemical properties of fission yeast Arp2/3 complex lacking the Arp2 subunit. J Biol Chem 2008 Sep 26;283(39):26490-8.

35. Kortemme T, Kim DE, Baker D. Computational alanine scanning of protein-protein interfaces. Sci STKE 2004 Feb 3;2004 (219):pl2.

CHAPTER II

MOLECULAR DYNAMIC SIMULATIONS OF MONOMERIC ARP2 AND ARP3 IN THE PRESENCE OF V AND C PEPTIDE OF WAVE.

Amruta C. Mahadik[1], Brian W. Beck[2†]

1 Department of Biology, Texas Woman's University, Denton, Texas, United States of America

2 Texas Advanced Computing Center, University of Texas at Austin, Austin, Texas, United States of America

†Author to whom correspondence should be addressed: bbeck@tacc.utexas.edu

Running title: "Molecular Dynamics Simulations of Monomeric actin, Arp2, and Arp3"

Manuscript pages: 47, supplementary material pages: 0, tables: 6, figures: 13, Supplementary figures: 3

ABSTRACT

The Arp2/3 complex is an oligomeric protein, composed of two major subunits, Arp2 and Arp3, and five accessory subunits (ArpC1, ArpC2, ArpC3, ArpC4, and ArpC5). Arp2 and Arp3 nucleate to form an "actin-like" dimer and provide a template for actin monomers to polymerize into a daughter actin filament. Nucleation promoting factors like WAVE, WASP, and N-WASP interact with the Arp2/3 complex and regulate the activation of Arp2/3 complex. While a number of critical studies have been undertaken to identify the important conformational changes involved in the activation of the Arp2/3 complex at the atomistic level, the changes and events required during activation of the complex remain poorly understood. Here, we report the results of eighteen 2ns NpT (isobaric/isothermal) molecular dynamic simulations at 1 atm pressure and 300^0 K designed to characterize the conformational changes in monomeric Arp2 and Arp3 in the presence of V and C peptide peptides from the VCA domain of WAVE. We found that peptide binding induces larger conformational changes than nucleotide-binding and produces long-range interdomain conformational changes. The C-domain bound Arp3 produced a more compact structure than the V peptide bound Arp3 or Arp2. Based on the binding energy calculations, actin binds tighter to V peptides than do the Arps while Arp2 binds C peptides more tightly than does Arp3, suggesting the C peptide of V-bound actin interacts with Arp2 preferentially than Arp3. Conformational changes in SD3 of Arp3 upon C binding suggest a mechanism for activation of the Arp2/3 complex.

KEYWORDS

Arp2/3 complex, actin branching, molecular modeling, molecular dynamic simulations, NPT simulations.

IMPORTANCE/IMPACT

The Arp2/3 complex plays important role in branching of the actin filaments. Here we used molecular dynamic simulations to understand the conformational changes and fluctuations that occur when different domains of the WAVE regulatory protein are bound to monomeric Arp2 and Arp3.

ABBREVIATIONS AND SYMBOLS

A-peptide: Acidic domain of Wiskott-Aldridge family of proteins

Arp: Actin Related Protein

Arp 2/3 Complex: Actin Related Protein 2/3 Complex

CAS: Computational Alanine Scanning

C peptide: Central domain of Wiskott-Aldridge family of proteins

DIC Microscopy: Differential Interference Contrast Microscopy

FRET : Fluorescence Resonance Energy Transfer

ITC : Isothermal Titration Calorimetry

IDD : Inter domain distance

MD : Moleculer Dynamics

NBC: Nucleotide-binding Cleft

NPF: Nucleation Promoting Factors

NpT: Isothermal-isobaric ensemble

ns : Nano seconds

PDB: Protein Data Bank

RMSD: Root Mean Square Deviation

RMSF: Root Mean Square Fluctuations

SD: Sub-domain, (1,2,3,4) = sub-domain number.

For example SD1:SD2 suggests Sub-domain 1 and Sub-domain 2.

V peptide: Verprolin domain of Wiskott-Aldridge family of proteins

WA Family: Wiskott-Aldrich Family

WASP: Wiskott-Aldrich Syndrome Protein

WAVE: Wiskott-Aldrich syndrome VErprolin homolog

WHAMM: WASP homolog-associated protein with actin, membranes and microtubules

NOTE

Actin: $NTD_{ØATP}$: PEP_V : Actin without ATP and with V peptide

Actin: $NTD_{ATP:}$ PEP_V : Actin with ATP and with V peptide

Actin: $NTD_{ØATP}$: PEP_C :Actin without ATP and with C peptide

Actin: NTD_{ATP} : PEP_C : Actin with ATP and with C peptide

Actin: $NTD_{ØATP}$: $PEP_{ØV/ØC}$: Actin without ATP and without V and C peptide

Actin: NTD_{ATP} : $PEP_{ØV/ØC}$: Actin with ATP and without V and C peptide

Arp3: $NTD_{ØATP}$: PEP_V : Arp3 without ATP and with C peptide

Arp3: NTD_{ATP}: PEP_V : Arp3 with ATP and with V peptide

Arp3: $NTD_{ØATP}$: PEP_C : Arp3 without ATP and with C peptide

Arp3: NTD_{ATP} : PEP_C : Arp3 with ATP and with C peptide

Arp3: $NTD_{ØATP}$: $PEP_{ØV/ØC}$: Arp3 without ATP and without V and C peptide

Arp3: NTD_{ATP} : $PEP_{ØV/ØC}$: Arp3 with ATP and without V and C peptide

Arp2: $NTD_{ØATP}$: PEP_V : Arp2 without ATP and with V peptide

Arp2: NTD_{ATP}: PEP_V : Arp2 with ATP and with V peptide

Arp2: $NTD_{ØATP}$: PEP_C : Arp2 without ATP and with C peptide

Arp2: NTD_{ATP} : PEP_C : Arp2 with ATP and with C peptide

Arp2: $NTD_{ØATP}$: $PEP_{ØV/ØC}$: Arp2 without ATP and without V and C peptide

Arp2: NTD $_{ATP}$: $PEP_{ØV/ØC}$: Arp2 with ATP and without V and C peptide

INTRODUCTION

Actin cytoskeleton plays important roles in various cellular processes such as cell locomotion, migration, adhesion, division, phagocytosis, and intracellular motility of vesicles, organelles, and certain pathogens.[1-3] These extracellular and intracellular processes require actin filament networks that consist of linear and branched filaments.[4] Globular actin (G-actin) polymerizes as filamentous actin (F-actin) at the "barbed" or "+" end of the filament. Linear filaments are thought to support cellular structures like filopodia (β-actin) and stress fibers (γ-actin), whereas branched filaments are enriched in lamellipodia in eukaryotic cells. [5, 6]

Polymerization and depolymerization of acti filaments involves many Actin Binding Proteins (ABP) such as profilin, cofilin/ADF, Actin Related Protein 2/3 complex (Arp2/3 complex), and Nucleation Promoting Factors (NPF) such as Wiskott-Aldrich family proteins (WASP, WAVE, and NWASP, WHAMM).[7-9] ABPs are involved in processes such as branching (Arp2/3 complex), delivery of actin to the NPFs (profilin), and depolymerization (cofilin/ADF). NPFs are thought to help deliver actin to the "+" end as well as activating the Arp2/3 complex.[9-16]

The Arp2/3 complex consists of two major subunits (Arp2 and Arp3) along with five accessory subunits (ArpC1, ArpC2, ArpC3, ArpC4, ArpC5) [7, 14, 17] (Figure 2.1 and 2.2). Like actin, Arp2 and Arp3 are members of the actin family (PFAM PF00022) and the actin-like ATPase superfamily (PFAM CL0108) that includes amongst its 29 members the Arps, actins, several sugar kinases, and the HSP70s. [18, 19] Actin, Arp2, and Arp3 fold into two large domains, which are further divided to produce four total sub-

domains, SD1 to SD4. Like actin, Arp2 and Arp3 have a nucleotide-binding site present between SD1 and 3.[20] Also both the subunits are presumed to have a regulatory protein-binding site in SD1 (hereafter referred to as the WA peptide-binding site).[13, 15] The accessory subunits, ArpC1-5, facilitate the binding of the Arp2/3 complex to existing actin filaments by mediating quaternary interactions between cofactors and the existing mother filament (Figure 2.1).[8]

NPFs are one type of regulatory protein that stimulates the activity of the Arp2/3 complex during the branching of actin filaments. In the absence of NPFs, the Arp2/3 complex has low intrinsic nucleation activity.[8] Members of the NPF family of proteins are all oligomeric complexes, each of which contain a carboxy-terminal VCA region in common (Figure 2.1).[9, 10, 21] The VCA region can be divided into three sub-domains: a ~25 amino acid N-terminal Verprolin domain (V peptide) that is often tandom-repeated, a ~20 amino acid centrally ordered hydrophobic region (C peptide), and a C-terminal domain rich in aspartate and glutamate residues referred to as the acidic domain (A peptide).[10] The VCA region regulates nucleation and branching by modulating interactions between actin (V peptide) and either Arp2 or Arp3 (CA peptide) at actin branch points whereas other subunits in WA complexes facilitate cellular localization.[10-12, 16]

A V peptide-bound actin complex has been crystallized in the presence of DNase I (PDB ID: 2A40). Though not a native interaction, DNase I inhibits actin polymerization. The V peptide is characterized by ~20 residues that include a predicted amphipathic α-helix at the N-terminus and an LKKT "signature" sequence.[10] The

presence of DNase I during crystallization restricts sub-domains 2 and 4 from sampling filament favoring conformational space in the crystal structure. Crystal coordinates of actin (PDB ID: 3MFP) in filament favoring forms differ somewhat from either V bound actin or monomeric actin (PDB ID: 1ATN), though the general topology is the same.[22] In cells, the Arp2/3 complex adopts three major nucleotide-binding cleft conformations, "open," "intermediate," and "closed." All three species exist in approximately equal ratio but have variable spacing across the major nucleotide-binding cleft between the SD1 and 2 group, and the SD3 and 4 group.[23]

Available crystal structures of the Arp2/3 complex in different conformations (PDB IDs 1K8K, 2P9*, 1TYQ,) are generally incompletely resolved.[8, 14, 23, 24] The coordinates for SD1 and 2 of Arp2 are generally not reported suggesting Arp2 has either dynamic interdomain movement or lacks a well-defined structure. The sequence similarity of Arp2 and Arp3 with actin is large (>69% and >61%, respectively).[25]

While Arp2 and Arp3 share substantial structural similarity with actin, there are a few dissimilarities, such as the presence of a long α helix in SD3 and a different orientation of the DNase binding loop in SD2. Arps are thought to undergo tertiary and quaternary conformational rearrangements during formation of an active "short-pitch" F-actin-like dimer. This active dimer provides a template surface for actin subunits to polymerize into a branched daughter filament.[8, 14, 24, 26] Attempts to determine the "active" structure of the complex using electron microscopy and reconstruction studies have been partially successful.[8, 23, 24, 27] However, none of the reported structures were in the "active" state but reported as representing an "active-like", "intermediate", and "inactive" state

(PDB ID: 2P9* family). The lack of "active" state structures greatly increases the difficulty of characterizing quaternary conformational changes during the activation of the Arp2/3 complex. Likely modulation of conformational changes by the VCA segment of WA family proteins adds to the complexity. As the VCA segment is generally a component of the WAVE Regulatory Complex (WRC), the structure of which has only been partially-resolved, additional uncertainty in the mechanism is present.[28, 29]

Panchal and co-workers have reported the crystal structure of V peptide bound actin in the presence of DNase I, whereas the CA peptide is thought to form an amphipathic helix that interacts with Arp2 and Arp3.[10, 13, 15, 28] Actin monomers, when at cellular concentration ≥ 100 μM, are the preferred binding sites for V peptides of NPFs, with relatively high affinity (Kd <1.0 μM).[10, 30-33] Activation of the complex involves transition of the "open" inactive Arp2/3 to a "closed" active structure by closing of the nucleotide-binding cleft, a ~15° rotation of SD3 and 4 relative to SD1 and 2.[8] Arp2 and Arp3 interact with ArpC1 and ArpC2 subunits differently in the active state than the inactive. In addition to this, the active complex buried surface area is 1700 $Å^2$ larger than the contacts that occur in the inactive complex.[8] We were interested in understanding these predicted changes in Arp2 and Arp3 upon V and C binding, as the VCA peptide free simulations of Arps by Dalhaimer and Pollard did not reproduce the known nucleotide cleft closures or the ~15° rotation of the two halves of both Arps. This suggests that the interactions with NPFs or the mother filament are most likely required for these conformational changes to take place during branch formation.[34]

Padrick and co-workers have postulated, based on the affinity of V bound actin to Arp2 and Arp3 and the level of the activation of the complex, that V bound actin has a strong affinity towards Arp2 but activates the complex weakly. On the other hand, they found V bound actin has a weak affinity towards Arp3 but activates the complex strongly.[13] Recent ITC and FRET studies have shown that V peptide bound actin prefers to bind Arp2 and ArpC1 which in turn is associated with a partial conformational change at the barbed end of Arp3.[35] The Boczkowska model differs from the Rosen model of activation in terms of the delivery of first V bound actin to Arps. However, both these models confirm the conformational changes in Arp3 are involved in activating the Arp2/3 complex.

Like actin, Arp2 and Arp3 have ATPase activity and hydrolyze ATP to ADP + Pi however Arps are known to have less nucleotide dependency than actin.[24, 36-38] The crystal structures of Arp2 and Arp3 in the presence of the ATP or nucleotide analogs had the nucleotide-binding cleft more "closed" and thus, more similar to the filament favoring actin conformation.[24] However, there were no differences observed in the orientation of the Arp2 relative to Arp3 in the complexes, suggesting nucleotide-binding is important, but does not exclusively regulate the conformational changes in Arp2 and Arp3. Elimination of an exclusive nucleotide role in activating Arp2/3 complex suggests the VCA segment of WA family proteins likely plays a dominating role in activating the Arp2/3 complex compared to the contributions by other components such as interaction with existing "mother" actin filaments, nucleotide-binding, or the role of the complex's accessory proteins.

Here we assessed the role of V and C peptide of the VCA segment of WAVE protein in the activation of the complex through monitoring peptide effects on protein conformational changes. Actin, Arp2, and Arp3 were simulated in the presence and absence of nucleotide as well as the presence or absence of V or C domain peptides (six simulations per protein) for a period of 2ns. We chose monomers (actin, Arp2, and Arp3), rather than oligomers since the absence of quaternary structure limits will permit the largest degree of freedom for conformational space sampling, leading to a larger ensemble of all possible conformations of protein upon V or C domain binding. Each state was analyzed using parameters such as average conformational stability of an individual sub-domain, average interdomain distances, average distance between nucleotide-binding cleft residues, stability of V and C domain upon binding, stability and fluctuations in the nucleotide-binding cleft, and binding energies of the complexes.

RESULTS

2.1 Individual proteins were stable in different peptide bound states

The stabilities of actin, Arp2, and Arp3 in different peptide and nucleotide bound states were measured by calculating RMSD and RMSF of all atoms relative to the Energy minimized initial structure (hereafter post-min). Actin, Arp2, and Arp3 were stable over the 2ns period with RMSDs between 2.24 ± 0.09 Å and 4.07 ± 0.62 Å for all atoms conformations, suggesting none of the proteins were unfolding. One-way ANOVA was performed for each of the 18 simulations states. All means were significantly different ($p < 0.01$) by Tukey HSD post-hoc with N= 10,000. However, while significant (due to the

large N), each individual state was also assessed for large or meaningful conformational changes and fluctuations.

2.1.1 Actin:

Nucleotide bound actin had larger conformational changes in the V-bound state than the C-bound or peptide-free state. No major conformational changes were observed due to nucleotide-binding in actin when compared with nucleotide free states (Figure 2.3). The average RMSDs for all the states of actin was ≤ 3.01 Å while RMS fluctuations were ≤ ± 0.17 Å (Figure 2.3). All states varied ≤ 1.5 Å from the crystal structure (PDB ID: 1ATN, chain A). Comparisons between the crystal structure and the simulation centroid conformations of all the states suggest a tertiary structural change in SD2. A partial loss of the helical structure was observed in the SD4 (between residues 224-232) upon V peptide binding in the nucleotide bound actin. When compared to the crystal structure, the helical region moved away from where the central axis would be in a full filament. Hereafter, we will call the direction towards the putative filament central axis "proximal" and away from the central axis "distal."

V peptide had smaller conformational changes (2.64 ± 0.27 Å) than the C peptide (4.23 ± 0.29 Å) in the nucleotide bound actin (Figure 2.10). However, both the peptides were present in the hydrophobic groove between SD1 and 3 of the nucleotide bound actin.

2.1.2 Arp2:

Arp2 had larger conformational changes and fluctuations in nucleotide free states than the nucleotide bound states (Figure 2.3). No meaningful differences were observed

between the RMSDs of unbound V, or C bound Arp2 in either the presence or absence of nucleotide, though the absence of nucleotide did increase the mean RMSD by approximately 0.72 Å. This suggests peptide binding has no major effect on the structure of Arp2. The centroid conformation of nucleotide bound Arp2 had substantially larger conformational changes in SD1 and SD2. The larger conformational changes in SD2 reduced the IDD between SD2:SD4, resulted in closure of the nucleotide-binding cleft (compare Figure 2.S2 (i) and (iv)). The C-tail of Arp2 was displaced by the C peptide in the absence of the nucleotide, whereas both C-tail and the N-terminal helix of the C peptide moved away from the hydrophobic groove in nucleotide bound state (compare Figure 2.S2 (iii) and (vi)). The remainder of the C peptide did not shift. On the other hand, the N-terminal helix of the V peptide lost much its initial secondary structure (Figure 2.S2 (ii)) and was displaced by the C-tail of Arp2 irrespective of the nucleotide bound states (compare Figure 2.S2 (ii) and (v)). The nucleotide-binding cleft was widely open in all the nucleotide free states of Arp2, suggesting nucleotide stabilizes a closer interaction between SD1 and 3 (compare Figure 2.S2 (i), (ii), and (iii) with (iv), (v), and (vi) respectively).

Unlike actin, V and C peptide upon interacting with the nucleotide bound Arp2 had larger conformational changes (5.00 ± 0.89 Å) and (4.75 ± 0.49 Å), respectively (Figure 2.10). The peptide-binding site of Arp2 (4.07 ± 0.48 Å to 5.86 ± 0.57 Å) had larger conformational changes compared to the peptide-binding site of actin (1.59 ± 0.26 Å to 1.74 ± 0.38 Å), suggesting a diminished or even destabilizing effect due to the interaction between peptide and Arp2 (Figure 2.10).

2.1.3 Arp3:

In Arp3, large conformational changes were observed in the nucleotide free states irrespective of the peptide bound. These changes had relatively larger fluctuations than those observed in actin and Arp2 (Figure 2.3). Both RMSDs and fluctuations were reduced upon nucleotide-binding in the V, C, and free state (Figure 2.3). The C-tail of Arp3 that occupies the hydrophobic groove in SD1 and 3 was displaced by the C peptide in the nucleotide bound Arp3 centroid conformation and by the V peptide in the nucleotide free state. However, the V and C domains did not displace the C-tail of Arp3 in the nucleotide bound and free state, respectively. In addition to the C-tail displacement in nucleotide and C domain bound states, the DNase binding loop of the SD2 adopted different secondary conformations in different states. Unfortunately, as the DNase binding loop of Arp3 in all available crystal structures has unresolved residues, it is difficult to predict the most accurate/appropriate active state conformations. Sub-domains 1, 3, and 4 were relatively stable in all the states (RMSD ≤ 2.43 Å).

In Arp3, V peptide had larger conformational changes than the C peptide, irrespective of the nucleotide-binding state. The peptide-binding site of Arp3 had intermediate conformational changes (1.96 ± 0.14 Å to 3.10 ± 0.33 Å) when compared with actin and Arp2.

The V peptide of the nucleotide bound actin:V state that is a known crystal structure (PDB ID: 2A40) was more stable than the C peptide of the nucleotide bound actin:C state (Figure 2.10). On the contrary, the C peptide was more stable than the V

peptide in Arp2 and Arp3, irrespective of the nucleotide bound or free state, suggesting the strong likelihood of the C peptide preferentially binding to Arp2 and Arp3.

2.2 Sub-domains stabilities

We analyzed the stabilities of each individual SD to study its susceptibility to the conformational changes and fluctuations upon V and C domain binding. The stability of the sub-domains was measured by calculating RMSD and RMSF of all atoms for each of SD of every state, relative to the post minimization structure. One-way ANOVA was performed and all means were significantly different ($p < 0.01$) by Tukey HSD, with N= 10,000. We also compared centroid conformation of actin, Arp2, and Arp3 for important structural changes between the different states of the molecule and within the different states of the different molecule.

2.2.1 Actin:

In actin, sub-domains 2 (3.12 Å > RMSD > 2.67 Å) and 4 (3.90 Å > RMSD > 2.20 Å) had larger conformational changes than SD1 (2.29 Å > RMSD > 1.68 Å), and 3 (1.78 Å > RMSD > 1.61 Å), irrespective of the type of the peptide bound (Figure 2.4). In the crystal structure, a short segment of residues 224-232 in SD4 that forms a helix moved distally along with a partial loss of the secondary structure in the V and nucleotide actin (Ref: centroid conformation of actin:NTD_{ATP} PEP_{V} state). In addition to the helix movement, the DNase binding loop present in the SD2 adopts conformations that vary as a function of the nucleotide presence. However, the observed larger conformational changes and fluctuations in SD2 of actin (3.12 Å > RMSD > 2.67 Å) can be equally attributed to the absence of DNase I interaction and/or to actin:actin interaction required

for actin polymerization [20]. Similarly, larger conformational changes and fluctuations that were observed in the SD4 (3.90 Å > RMSD > 2.20 Å) could eventually lead to the required structural changes as mentioned by Rouiller and co-workers, the ~15 Å twisting of the SD3 and 4 relative to SD1 and 2 (Figure 2.4).[8]

No major effect was observed in the nucleotide-binding cleft region as a function of the nucleotide or peptide binding (Table 2.6).

2.2.2 Arp2:

In Arp2, SD1 (3.40 Å > RMSD > 2.45 Å) and 2 (5.61 Å > RMSD > 3.21 Å) had larger conformational changes than SD3 (1.96 Å > RMSD > 1.72 Å) and 4 (2.40 Å > RMSD > 1.69 Å), irrespective of the type of the peptide bound (Figure 2.5). SD2 of ATP: Arp2 in the peptide free state had the largest conformational change (RMSD ≤ 5.61 ± 0.29 Å), which was reduced upon peptide binding (for V: RMSD = 3.75 ± 0.37 Å, for C: RMSD = 4.28 ± 0.49 Å) (Figure 2.5). In the presence of V or C peptide, the DNase binding loop folds into a more stable β sheet and α helix structure instead of a coiled loop as present in the peptide free state. The nucleotide-binding cleft is more open in the nucleotide free states than the nucleotide bound state, irrespective of the type of the peptide bound (Table 2.6). The large conformational changes and widely open nucleotide-binding cleft suggest a nucleotide dependency and also explains the presence of unresolved residues in the crystal structure.

Sub-domains 1 and 2 of ATP:Arp2 were more dynamic than the SD1 and 2 of ATP:actin, whereas SD4 in ATP:actin had larger conformational changes than the ATP:Arp2 upon peptide binding (Figure 2.4 and 2.5). The relative order of the

conformational changes in the SD2 of ATP:Arp2 are V< C <<<<No V/C, suggesting the smallest conformational changes occur upon V binding. This also suggests a possible stabilization event due to peptide binding in the highly flexible region of Arp2 (Figure 2.4 and 2.5).

2.2.3 Arp3:

In Arp3, SD2 (5.32 Å > RMSD > 2.45 Å) had larger conformational changes and fluctuations than SD1 (2.43 Å > RMSD > 1.95 Å), 3 (1.71 Å > RMSD > 1.98 Å), and 4 (1.60 Å > RMSD > 1.90 Å) (Figure 2.6). Though SD2 of the nucleotide bound Arp3 had no major effect upon V or C binding when compared to *Arp3: NTD $_{ATP}$: PEP $_{ØV/ØC}$* (Figure 2.6), SD2 of Arp3:C, nucleotide bound state adopted similar conformations to the nucleotide bound actin:V state (Figure 2.S3 (v) and (vi)). Upon nucleotide-binding, conformational changes in Arp3: PEP_V state were reduced (compare *Arp3: NTD $_{ØATP}$: PEP $_V$* and *Arp3: NTD $_{ATP}$: PEP $_V$*), whereas a marginal increase was observed in the conformational changes in Arp3: PEP_C state (compare *Arp3: NTD $_{ØATP}$: PEP_C* and *Arp3: NTD $_{ATP}$: PEP_C*)(Figure 2.6). Thus, the nucleotide-binding stabilizes the SD2 of Arp3: PEP_V state whereas binding of the nucleotide as well as the C peptide destabilizes the SD2 of Arp3: PEP_C state, though not notably. In addition, the C-tail of Arp3 was displaced by the C peptide in the centroid conformation of nucleotide bound Arp3:C state whereas V peptide moved away from the hydrophobic cleft of Arp3. This suggests that the C peptide competes with the C-tail of Arp3. SD2 of the nucleotide bound Arp3:C adopted similar conformations to the nucleotide bound actin:V state (Figure 2.S3 (v) and (vi)).

As Arp2 shares greater sequence similarity with actin than Arp3, we expected Arp2 to exhibit fewer conformational fluctuations more like actin and expected Arp3 to be more dynamic. To the contrary, SD1, 3, and 4 of Arp3 maintained conformations and fluctuations like actin and were less dynamic than Arp2 (Figure 2.4, 2.5, and 2.6).

2.3 Inter-domain distance analysis and fluctuations

As mentioned earlier, Arp2 and Arp3 are thought to be in the "closed" conformations in an active state.[8, 14] Therefore, we assessed the compactness of the structures upon V and C peptide binding by measuring the center-to-center average inter-domain distances (IDD) and fluctuations between each pair of the sub-domains (Figure 2.7, 2.8, and 2.9). The change in IDD for each of the peptide binding states of actin, Arp2, and Arp3 was compared within the group and between the groups (Figure 2.7, 2.8, and 2.9). The change in IDDs serve as a measure of the librations of one of the sub-domains relative to other three sub-domains in the protein. The dynamic nature of these intra SDlibrations was determined by comparing fluctuations in the IDDs. The nucleotide free Arp2 and Arp3 illustrate the crystal structure in the "apo-state" (PDB ID: 1K8K) and served as a reference control for each of the peptide bound states. One-way ANOVA was performed and all means were found to be significantly different ($p < 0.01$) by Tukey HSD, with N= 10,000. However the individual states were assessed for large or meaningful conformational changes and fluctuations.

2.3.1 Actin:

No major effect of V or C peptide binding was observed on any of the inter-domain distances in actin. However, IDDs between SD2:SD4 were reduced upon

nucleotide-binding in both peptides bound states (Figure 2.7 (ii) and (v); (iii) and (vi)). The binding of C peptide compacts the nucleotide bound actin more than the V peptide binding by reducing the average IDD between SD1:SD4 and SD2:SD4. The IDDs between SD1:SD2, SD1:SD3, and SD3:SD4 had smaller fluctuations than the IDDs between SD1:SD4, SD3:SD2, and SD2:SD4. While the average IDDs between SD2:SD4 were reduced in the C bound and free peptide state, the IDD between SD2:SD4 in the V bound state was increased. Both the peptides states had compact conformations when compared with the peptide free state. However, the V bound actin adopts a lower energy conformation when compared with the C bound actin (Figure 2.12 (a)).

2.3.2 Arp2:

In the nucleotide free Arp2, the average IDDs between SD1:SD2, SD1:SD3, and SD3:SD4 had reduced fluctuations ($\leq \pm 0.3$ Å) when compared with the fluctuations in the IDDs ($\leq \pm 1.7$ Å) between SD1:SD4, SD3:SD2, and SD2:SD4 irrespective of the type of the peptide bound. These fluctuations in SD1:SD4, SD3:SD2, and SD2:SD4 IDDs were reduced upon nucleotide-binding (except in the C bound state (figure 2.8 (iii) and (vi))). In addition, the IDDs between SD2:SD4, SD1:SD4, and SD3:SD2 were reduced significantly in apo Arp2 (Figure 2.8 (i-iv)) and Arp2:V bound state (Figure (ii-v)), suggesting a possible nucleotide effect. However, the compactness of the Arp2:C nucleotide bound conformation could be attributed to the C binding (Figure 2.8 (iii and vi)). The nucleotide bound Arp2 adopts a more compact structure in the presence of V peptide than the apo or C peptide bound state. When compared with actin, Arp2 had a

less compact structure than actin irrespective of the peptide bound (Figure 2.7 (v): Figure 2.8(v); Figure 2.7 (vi): Figure 2.8 (vi)).

2.3.3 Arp3:

None of the nucleotide free states of Arp3 had large changes in the average IDD values, whereas SD1:SD2 and SD2:SD4 had greater fluctuations in the V bound state than the free and C bound state. The fluctuations were reduced in the V bound state upon nucleotide-binding, whereas the SD2:SD4 IDD value was reduced by approximately 5.0 Å, suggesting the closing of the nucleotide-binding cleft in Arp3. However, IDDs between SD1:SD3 and SD3:SD4 in nucleotide bound Arp3 (Figure 2.9 (iii)) were reduced significantly by 6.0 Å and 4.5 Å in the C bound state (Figure 2.9 (vi)), respectively. In addition to this compactness, the nucleotide effect was also observed in the C bound state resulting in the closure of the nucleotide-binding cleft. Overall, among the actin, Arp2, and Arp3 in V and C bound states, Arp3 had less compaction than Arp2 and actin (Figure 2.7 (v,vi), 2.8 (v,vi), and 2.9 (v,vi)). However, C bound Arp3 had a more compact conformation compared to the V bound Arp3 and V bound Arp2 in the nucleotide bound state.

2.4 Peptide, peptide binding site, and nucleotide-binding cleft stabilities

The global conformational changes such as total protein stabilities or individual SD stabilities may mask the effect of the peptide or nucleotide-binding on the respective site. Therefore, we assessed the stabilities of the V and C peptide as well as the local conformational changes at the peptide-binding site by calculating the average RMSD and fluctuations by measuring the RMSF in Å for all atoms in different peptides and

nucleotide bound states (Figure 2.10). In addition to this, we calculated the average conformational changes and fluctuations in the nucleotide-binding cleft in RMSD and RMSF (Å), respectively (Table 2.6). All means were significantly different ($p<0.01$) by ANOVA with Tukey HSD, with N= 10,000. The individual states were assessed for large conformational changes and fluctuations.

2.4.1 Actin:

V peptide had reduced conformational changes and fluctuations in the nucleotide bound actin state relative to the nucleotide free actin state, whereas C peptide had larger conformational changes in the nucleotide bound actin state than the nucleotide free state (Figure 2.10). The peptide-binding site had no major conformational change arising from binding of either V or C peptide however, higher fluctuations were observed in the nucleotide free states. We also used centroid conformations of different states to compare the orientation and position of the V peptide relative to the C peptide. Both V and C peptide consist of an amphipathic helix (~13 residues) followed by a stretch of a linker region (~ 10 residues). The amphipathic helix of V peptide moved slightly away from the hydrophobic groove (Figure 2.S1:v). Similarly, the linker region (R451 to E454) also lost a few contacts with the nucleotide bound actin. The C peptide occupied the hydrophobic groove in the nucleotide bound and free actin, but the linker moved away from the nucleotide bound actin. The V peptide had smaller conformational change (RMSD: 0.72 Å) from the crystal structure. Other peptide bound states had substantial conformational changes (RMSD: < 3.26 Å), when compared to the crystal structure. Unlike Arps, actin lacks the extended C-tail region, which occupies the hydrophobic groove.

2.4.2 Arp2:

In Arp2, both V and C peptides undergo larger conformational changes and greater fluctuations compared to any of the states in actin and Arp3 (Figure 2.10). V and C peptide had larger conformational changes in the nucleotide bound state than the nucleotide free state. However, the fluctuations were increased in the V peptide in the nucleotide bound state, whereas nucleotide bound Arp3:C state, C peptide had reduced fluctuations. The peptide-binding site had greater fluctuations and more substantial conformational changes than that of the peptide-binding site in actin and Arp3. The C-tail of the nucleotide bound Arp2 occupied the hydrophobic groove, whereas the C-tail moved away from the groove in the nucleotide free Arp2. The C peptide displaced the C-tail of Arp2 irrespective of the nucleotide bound states, whereas the C-tail moved proximally but still occupied the groove in the presence of the V peptide. The alpha helix of the C peptide was moved away proximally in the nucleotide bound state (RMSD from crystal structure: 1.03 Å) than the nucleotide free state (RMSD from crystal structure: 3.2 Å), but had a small bend that reduces the distance between the turns of the alpha helix. The linker region of the C peptide moved away from proximal plane of the protein, when compared with the linker segment of the V peptide.

As the hydrophobic groove was more fully occupied by the C peptide than the V peptide in Arp2, we suggest that the C peptide has more specific binding than the V peptide to Arp2.

2.4.3 Arp3:

The C peptide had smaller conformational changes than the V peptide in the nucleotide bound Arp3, whereas there were no significant differences in the fluctuations due to nucleotide-binding (Figure 2.10). The peptide-binding site had increased fluctuations in the nucleotide bound states than the free states. Unlike the partial displacement of the C-tail of Arp2, we observed a complete proximal displacement of the C-tail in Arp3, suggesting a competition between the C-tail region and the peptides for the binding site. The partial displacement of the C-tail of Arp2 compared to Arp3 by the C peptide suggests the C-tail of Arp3 has more specific binding than the C-tail of Arp2.

2.5 Nucleotide-binding clefts distances

We did not observe any significant nucleotide effect in actin, but the nucleotide-binding site in Arp2, and Arp3 had substantially reduced conformational changes and fluctuations upon nucleotide-binding (Figure 2.11). Overall, all nucleotide bound states had ≤ 1.54 Å average RMSD irrespective of the type of peptide bound, but nucleotide bound actin had higher fluctuations compared to Arp2 and Arp3. One-way ANOVA was performed and all means were significantly different ($p < 0.01$) by Tukey HSD, with N= 10,000, however the individual states were assessed for the meaningful conformational changes and fluctuations.

We calculated the nucleotide-binding cleft distances (NBCD) (distance 1, 2, and 3) using Pollard's definition for the nucleotide-binding cleft distances (Table 2.2).[24] The NBCDs in actin had no major conformational changes or increases in fluctuations as a function of the peptide or nucleotide-binding (Table 2.6). However, nucleotide-binding

clefts of Arp2 and Arp3 had a significant effect as a function of the peptide as well as nucleotide-binding (Table 2.7, 2.8). The nucleotide-binding clefts were much more open in nucleotide free Arp2 and Arp3 however, the nucleotide-binding cleft in the C bound Arp3 was more closed than the C bound Arp2 (Table 2.7, 2.8).

2.6 Binding energy

To test the stability and to determine the relative order of the conformations produced by our simulations, we assessed the average binding energies of the complexes over the 2ns time period (Figure 2.12a). Binding energy is defined as the interaction energy of the protein: peptide in the complex (Interaction energy = Internal energy of the complex – (internal energy of the protein + internal energy of the peptide)). Overall, actin, Arp2, and Arp3 preferentially bind V peptide relative to C peptide, irrespective of the nucleotide-binding state. V bound actin (-208.99 ± 29.37 kcal/mol) was energetically more stable than Arp2:V (-188.49 ± 27.87 kcal/mol)or Arp3:V (-131.03 ± 24.23 kcal/mol) in the nucleotide bound state, whereas Arp2:C (-108.01 ± 30.95 kcal/mol) was more stable than Arp3:C (-104.63 ± 29.47). The nucleotide free Arp2:V state (-258.70 ± 25.14 kcal/mol) had the lowest energy conformation among all the states; however, it is very unlikely to have Arp2 devoid of nucleotide in an active cell during actin polymerization (Figure 12 (b)). The nucleotide bound actin:V state is the next most likely low energy conformation. This is consistent with the role of V peptides interacting with ATP:actin and in agreement with the crystal structure of V bound actin (PDB ID: 2A40).[10] The V bound actin is thought to the growing end of the actin filament at the barbed end of Arp2 and Arp3.[10, 13, 35] However, the possibility of nucleotide bound Arp2:V

(-188.49 ± 27.87 kcal/mol), and Arp3:V (-131.03 ± 24.23) cannot be ruled out in the population of nucleotide bound actin:V conformations. As the binding energies of V bound actin and Arp3 are -181.73 ± 18.73 kcal/mol and Arp3 -131.74 ± 18.24 kcal/mol in the "apo" state (nucleotide free state), the possibility of V peptide to bind actin and Arp3 in the presence of the nucleotide is less likely. In the presence of C peptide, nucleotide bound Arp2 is more stable than that of the Arp3. Actin bound to the C peptide states had lower stability than rest of the states, irrespective of the nucleotide-binding state.

DISCUSSION

Arps share great sequence similarity with actin and fold like actin. However, there are major structural dissimilarities in actin and Arps such as, the presence of an extended C-tail that occupies the hydrophobic groove between SD1 and 3 at the carboxy terminus of Arps relative to actin.[14, 20, 38] The C-tail is absent in actin, renders the hydrophobic groove available for binding of the V and C peptides without any competition. In addition to the C-tail, Arp2 and Arp3 have an extended helix (residues T342 to K361 in Arp3, and residues Y325 to K335 in Arp2) in the SD3.The actin was crystalized in the presence of DNase I that interacts with the SD2 of actin at the pointed end.[20] Though the DNase I prevents the self-polymerization of globular actin into filamentous actin during crystallization, the possibility of influencing the conformation of SD2 cannot be ruled out. The SD2 of actin is the smallest SD and consists of three stranded anti-parallel beta sheet and a helix.

Therefore, we expect a differential conformational response of actin and Arps as a function of the V or C peptide binding. We performed 18 MD simulations with monomeric actin, Arp2, and Arp3 in the presence of V, or C, or in the absence of the peptide, in the nucleotide bound or free states. All 18 simulations were stable and proteins were not unfolding over the period of 2ns. Different parameters such as conformational compactness of the molecule, average individual SD stability, average interdomain distances, and binding energy were analyzed to understand the tertiary and quaternary conformational changes for activating the Arp2/3 complex. Understanding the conformational changes at the monomeric level will help in designing the oligomeric MD simulations experiments that may include the two actin subunits from the existing actin filament, Arp2 and Arp3 subunits, and VCA domain of the WAVE Regulatory complex in the future.

Actin, Arp2, and Arp3 have different conformational changes

In the absence of V and C peptide, no significant difference was observed due to the nucleotide-binding in actin (compare actin:$NTD_{(ATP)}$:$PEP_{(\emptyset V/\emptyset C)}$ and actin:$NTD_{(\emptyset ATP)}$:$PEP_{(\emptyset V/\emptyset C)}$) (Figure 2.3). However, binding of the C peptide had reduced conformational changes than that of binding of the V peptide in the nucleotide bound state (Figure 2.3). The larger conformational changes were observed in Arp2: $NTD_{(ATP)}$: $PEP_{(\emptyset V/\emptyset C)}$ than the actin:$NTD_{(ATP)}$:$PEP_{(\emptyset V/\emptyset C)}$ and Arp3:$NTD_{(ATP)}$:$PEP_{(\emptyset V/\emptyset C)}$, suggesting a strong destabilization effect due to the binding of nucleotide in Arp2 (Figure 2.3). These conformational changes were reduced upon V or C peptide binding in the Arp2: $NTD_{(ATP)}$ suggesting a stabilizing effect due to peptide binding (Figure 2.3). No meaningful

difference was observed between the RMSD of the Arp3: NTD_{ATP} upon V and C peptide binding, suggesting the conformation of Arp3 was least affected due to the binding of V or C peptide (Figure 2.3).

In addition to the stabilization effect due to the peptide binding, a major nucleotide effect was observed in Arps (Figure 2.3). Nucleotide free Arps had larger conformational changes and fluctuations than the nucleotide free actin states, irrespective of the type of the peptide bound (Figure 2.3). The nucleotide free Arp3 show a stronger destabilization effect due to V peptide binding than the C peptide (Figure 2.3). On the contrary, no significant difference in the RMSD's of the nucleotide free Arp2 was observed upon V or C binding. Thus, we observed the effect of the nucleotide presence, in addition to the peptide stabilization in Arp2 and Arp3, as stated by Nolen and Pollard earlier.[24] Therefore, the stability of the molecule at the global level is dependent on the stability of nucleotide-binding site, peptide binding site and stability of the individual sub-domain.

Conformational changes in actin, Arp2, and Arp3 upon peptide and nucleotide-binding at the SD level

Along with Arp2 and Arp3, other accessory subunits of the Arp2/3 complex (ArpC2-C3) interact with the side of the preexisting actin filament to stabilize the complex.[8] The pointed end of Arp2 and Arp3 subunit (SD4 and 2) interacts with the monomeric actin subunits of the preexisting filament whereas, the barbed end of both Arps (SD1 and 3) provide a template surface for the incoming actin molecule to polymerize into daughter filament. Together, Arp2 and Arp3 form a short pitch dimer

like actin, where the SD1 and 3 of Arp3 interacts with the SD2 and 4 of Arp2, respectively. Thus, each of the sub-domains of Arp2 and Arp3 is involved in different sets of atomic interactions.

On the other hand, SD1 and 3 of actin interacts with the SD2 and 4 of the next actin subunit in the filament in a repeated manner. Also unlike Arps, actin lacks the C-tail and an extended helix (residues T342 to K361 in Arp3, and residues Y325 to K335 in Arp2) in the SD3. SD2 is the smallest SD of actin and it interacts with DNase I in the crystal structure. Therefore, the possibility of the influence of DNase I interaction on the conformation of the SD2 cannot be ruled out. In light of that, the observed larger conformational changes and fluctuations in the SD2 of actin (3.12 Å > RMSD > 2.67 Å) can be equally attributed to the absence of DNase I interaction whereas, the larger conformational changes and fluctuations in the SD4 (3.90 Å > RMSD > 2.20 Å) suggest stabilizing atomic interactions between the SD3 of the lower actin molecule that would constitute the longitudinal actin dimer (Figure 2.4).

In Arp2, SD1 and 2 were more dynamic than the SD3 and 4. The conformational changes in the SD1 of the nucleotide bound Arp2 were reduced upon peptide binding (V or C peptide) when compared with the counter nucleotide free Arp2 states and suggest an effect of the peptide on the binding site. In addition to this, the DNase binding loop adopts more stable secondary structures instead of a coiled coil structure suggesting a long distance longitudinal effect due to peptide binding in Arp2.

Unlike Arp2, SD2 of Arp3 had larger conformational changes when compared with all other domains of Arp3. In the V bound state, presence of the nucleotide reduces

the conformational changes in the SD2 of Arp3 and is similar to the nucleotide bound and peptide free Arp3 state, whereas the conformational changes in SD2 were reduced upon nucleotide-binding in the C bound state of Arp3. However, the conformational changes in the SD2 of the nucleotide bound Arp3 were not significantly different due to the type of the peptide bound (free, V, or C bound).

In all the three molecules, SD2 was more dynamic than the sub-domains 1,3, and 4. Sub-domains 3 and 4 of Arp3 and Arp2 were more stable than the SD3 and 4 of actin.

Conformational changes at the SD level affect the inter-domain distances and compactness of the monomeric actin, Arp2, and Arp3

Actin:

We did not observe a large difference in the compactness of the actin as a function of the peptide or nucleotide-binding individually. However, the reduced average IDD between SD2:SD4 in the presence of V or C peptide and nucleotide bound actin suggest a synergistic effect of the peptide and nucleotide-binding in closing the nucleotide cleft that may compact the molecule at the pointed end. The nucleotide and V peptide bound actin that represented the known crystal structure of actin:v (PDB ID: 2A40) had lowest energy conformation among all the nucleotide bound states of actin, Arp2, and Arp3 (Figure 12b).

Arp2:

In the absence of the nucleotide, Arp2 had less compact conformation, irrespective of the type of the peptide bound. The nucleotide cleft was widely open (> 7.0 Å) in all the three states (Figure 2.8 (i), (ii), (iii)), suggesting a significant effect of the

nucleotide-binding in Arp2. In the nucleotide bound state, V peptide bound Arp2 (Figure 2.8 (v)) had more compact structure than that of C peptide bound Arp2 (Figure 2.8(vi)), and adopted the low energy conformation as well. However, the V peptide had weak affinity for the hydrophobic groove as the C-tail of Arp2 was present in the grove and the V peptide was moved away from the center of the axis.

On the other hand, in the C bound state (Figure 2.8 (iii)), the average IDDs between SD2:SD4 and SD1:SD4 were reduced by ~ 5.7 ± 0.4 Å and ~2.2 ± 0.3 Å, respectively, when compared with the nucleotide and peptide free state (Figure 2.8 (i)), suggesting an exclusive role of the C peptide in closing the nucleotide-binding cleft by reducing the IDD between SD2:SD4. Additionally, the C peptide competes with the C-tail of Arp2 for the hydrophobic groove. The C-tail of Arp2 moved away from the hydrophobic groove, in an upward direction, and the C peptide occupied the groove. Therefore, C peptide is more likely to bind in the hydrophobic groove of Arp2, despite Arp2: V bound state being the most compact and low energy conformation (Centroid conformations were used to compare).

Arp3:

Unlike Arp2, we did not observe the "exclusive" C peptide binding effect in Arp3 that compacts the molecule in the absence of the nucleotide. Also, Arp3 had no significant changes in the average IDDs due to the nucleotide-binding only. Like actin, a synergistic effect was observed in Arp3 where the presence of the nucleotide and peptide reduced the average IDDs between SD2:SD3 and SD1:SD4 in Arp3 by ~2.5 ± 0.4 Å and ~8.2 ± 0.2 Å, respectively. Specifically, in the C peptide and nucleotide bound Arp3

state, the average IDD between SD1:SD3 and SD3:SD4 were reduced significantly by ~6.3 Å and ~4.4 ± 0.1 Å, respectively. Thus, the nucleotide bound Arp3 in the presence of C peptide (Figure 2.9 (iv)) is the most compact conformation among all the states of actin, Arp2, and Arp3. In the nucleotide bound Arp3, C peptide competes with the C-tail of Arp3 and occupies the hydrophobic groove by replacing the C tail of Arp3 proximally away, whereas the C-tail displaces the V peptide away from the groove, suggesting that the C peptide has stronger affinity for Arp3 than the V peptide.

Peptide, peptide binding site, nucleotide-binding site, and binding energy

Unlike Arps, actin lacks the extended C-tail region that competes with the V and C peptide to occupy the hydrophobic groove. Thus in actin, the hydrophobic groove is accessible for the binding the V or C peptide. That the hydrophobic groove was stable irrespective of the type of the peptide bound or the presence or absence of the nucleotide suggests no local effect of the V or C peptide binding on the conformation of actin. However, the C peptide was more dynamic compared to the V peptide in the nucleotide bound actin state, suggesting actin:NTD_{ATP}:PEP_V is more stable conformation than the actin:NTD_{ATP}:PEP_C. Since the actin:NTD_{ATP}:PEP_V state adopts the lowest energy conformation among all the nucleotide bound states of actin, Arp2, and Arp3, the actin:NTD_{ATP}:PEP_V state is the most stable state among all the states. (Figure 12(a) and 12(b)). Irrespective of the type of peptide or nucleotide bound, the NBC in actin had reduced RMSD (≤ 1.5 Å), shows no nucleotide dependency in actin. The average distances (B1 and B2) of the width of the nucleotide-binding cleft were less than 6.0 Å except nucleotide free actin in the C peptide bound state (6.46 ± 0.86 Å) suggesting actin

favors closed conformations irrespective of the type of the peptide and nucleotide bound (Table 2.6).

In Arp2 and Arp3, C-tail occupies the hydrophobic groove is thought to act like intrinsic profilin that binds the hydrophobic grove at the barbed end of actin and promotes the open conformation of the nucleotide cleft.[38] Thus, Arps favor open conformations and render the complex "inactive" or in the "OFF" state. The V and C peptide competes with the C-tail of Arp2 and Arp3 for the hydrophobic groove and thought to promote the closing of the nucleotide-binding cleft upon binding. In Arp2, the hydrophobic groove was occupied by the C peptide, whereas the V peptide was moved away from the grove. The peptide-binding site of Arp2 had larger fluctuations and more conformational changes than that of the peptide-binding site in actin and Arp3, suggesting a local conformational perturbation upon peptide binding in Arp2 (Figure 2.10).

In Arp3, the V peptide was more dynamic than the C peptide irrespective of the nucleotide-binding status. The peptide-binding site had intermediate conformational changes and fluctuations when compared to actin and Arp2, suggesting SD1 of Arp3 is less perturbed due to the peptide binding than the Arp2.

The average width of the nucleotide-binding site (distance B1 and B2) of Arp2 and Arp3 is less than 6.0 Å in the presence of the nucleotide, whereas it is greater than 7.0Å suggesting a strong nucleotide effect that promotes the closed conformation in the nucleotide bound state. In addition to the conformational changes due to the peptide and nucleotide-binding, the nucleotide bound Arp2:C and Arp3:C adopts lower energy

conformations than that of the nucleotide free Arp2 and Arp3, C bound states (Figure 12(b)).

CONCLUSIONS

Here we assessed the conformational changes in actin, Arp2, and Arp3 due to V or C peptide binding that may lead to the structural rearrangement of Arp2 and Arp3 during activation of the Arp2/3 complex. One of the predictions is that the V peptide bound actin adopts the lowest energy conformation among the pool (Figure 2.13 (a)). Therefore, we predict that during actin branching, V peptide binds to available actin. We further propose that the dimer, V bound actin may get delivered to one of the Arps (Arp2 or Arp3) site followed by the delivery of the second V bound actin dimer to another Arp site (Figure 2.13 (b)). Thus, the sequence of the delivery to the Arp site is not important; however the binding of the C peptide to Arp3 is significant. Binding of the C peptide to Arp3 induces a conformational shift that compacts Arp3 by rearranging the SD3. Rearrangement of the SD3 leads to the destabilization of the Arp3:Arp2 inactive interface (Figure 2.13 (c)). The rearrangement of Arp2 relative to Arp3 from inactive state into an active state leads to polymerization.

In light of the conformational changes occurring in the SD3 of Arp3, we strongly believe that the Arp2:Arp3 dimer interface is crucial in regulating the quaternary interactions required for the destabilization of the inactive Arp2/3 complex. In Chapter 3, we have identified the important amino acid residues that modulate the stability of the inactive state of the Arp2/3 complex. We have computationally designed mutants that

destabilize the interface. Our predictions were validated using site-directed mutagenesis and transient transfection of B35 rat neuroblastoma cells. All together, our conformational data and computational mutant study (from Chapter 3) provide much needed mechanistic clues as to how the Arp2/3 complex is regulated *in vivo*.

METHODS

2.1 Initial crystal structures

2.1.1 Arp2 and Arp3:

The crystal structure of Arp2/3 complex was obtained from the Brookhaven Protein Data Bank (PDB) in two different conformations: "active-like" (PDB ID: 2P9K at 2.59 Å resolution) and "inactive" (PDB ID: 1K8K at 2.0 Å resolution).[14, 24, 39] Arp3 and Arp2 (PDB ID: 2P9K: A and B chains respectively) had a well-defined nucleotide-binding site with the nucleotide substrate (ATP) present with bound Ca^{2+}. During the refinement of the co-crystalized structures of the 2P9* group of Arp2/3 proteins, the 2P9K structure had smaller average B-factors than the other members of the family. In addition to this, the 2P9K structure had more resolved intra-crystalline water molecules and protein atoms than other members of the family. Use of these structures provides more active-like and refined conditions than other structures and is thus more likely to provide accurate starting conformations for further modeling.

2.1.2 Actin:

Initial coordinates of actin monomer were obtained from the PDB database (PDB ID: 1ATN, chain A, at 2.8 Å resolution). All residues in the X-ray crystal structure were

well defined with Ca^{2+}bound at the highest binding affinity site in the nucleotide cleft region.[20]

2.1.3 V and C domain of WAVE:

The V domain coordinates were extracted from the ternary complex of the WH2 domain of WAVE with actin-DNAse I (PDB ID: 2A40 at 1.80Å resolution) using PyMOL.[10, 40] The relative positions of V with respect to actin, Arp2, or Arp3 were found from superposition of the actin of 2A40 structure on the relevant actin, Arp2, or Arp3 structure. As C peptide is thought to form an amphipathic helix similar to V peptide when it binds to the Arp2/3 complex, we used the atomic coordinates of the V peptide backbone to model the structure of the C peptide (see below).[28]

2.2 Model building

2.2.1 Actin, Arp2, and Arp3:

Unlike actin, Arp3 had 18 missing residues (#1,2,40-50,355-358), whereas 117 residues of the total 394 residues (#1-8,35-71,77-81,87-107,121-138,365-394) of Arp2 were unresolved in the crystal structure.[14] Available crystal structure coordinates (PDB ID: 1K8K: A chain) were used to model the missing coordinates in 2P9K structures for Arp2 (Chain:B) and Arp3 (Chain:A). The molecular modeling software suite CHARMM v34.b4 with the CHARMM 27 force field was used to build the hydrogen atoms in actin, Arp2 and Arp3. In addition to the hydrogen atoms, missing residues in Arp3 (#1,2,40-50,355-358) were also built using CHARMM. The carboxy terminal of Arp2 and Arp3 from 2P9K also has 5 and 7 unresolved residues, respectively. The positions of these C-terminal residues were taken from the 1K8K structure after superposition of 1K8K chain

A and B on 2P9K chain A and B, individually. This modeled carboxy terminal segment in Arp2 and Arp3 is referred as the "C-tail" in the rest of the document. Arp2 (2P9K, chain B) lacks 117 amino acid residues out of 394 total amino acid residues, approximately 30% of the total structure. Homology modeling was used to predict the missing 117 residue atomic coordinates of Arp2.

2.3 Homology modeling (HM)

The software package Modeller was used to predict the missing coordinates of the Arp2 subunit.[41,42] The prediction accuracy was improved by using the multiple template approach. Different scripts *(build_profile.py, salign.py, align2d_mult.py, model_mult.py)* included with Modeller were used to build the Arp2 model in a stepwise manner.

2.3.1 Template identification:

The *build_profile.py* script reads a text format file, *pdb_95.pir* that contains non-redundant PDB sequences (available at https://salilab.org/modeller/tutorial/basic.html) at 95% sequence identity into the sdb database.[41] The script removes any non-standard residues in the sequences as well as sequences that had fewer than 30 or more than 4000 amino acid residues to improve the sequence profile database. Table 2.1 lists the final resultant PDB structures used as templates.

2.3.2 Multiple sequence alignment of the identified templates:

The *salign.py* script reads all the sequences from PDB files and generates an initial rough alignment. The alignment is then improved by using parameters such as gap penalties and gap scores.

2.3.3 Alignment of the target sequence to the template structures:

The *align2d_mult.py* script aligns the query sequence to the template structures by requesting a pair-wise alignment. The align block parameter was set to equal the number of structures in the template alignment to avoid the change in existing alignment between the templates.

2.3.4 Model building:

The *model_mult.py* script models the target Arp2 sequence based on the alignment against the multiple templates.

2.4 Missing/resolved atoms

In the final model, available crystal coordinates of Arp2 (PDB ID: 2P9K, chain B, residues #9-34,72-76,82-86,108-120,139-364) were utilized. The missing coordinates were extracted from the predicted Modeller homology model after superposition of the two structures using PyMOL. Any of the remaining missing atoms after all the combined methods, such as hydrogen atoms, were built using the modeling suite, CHARMM v34.b4.[44] Similarly, residues #1, 2, 40-50, 355-358 in Arp3 as well as the hydrogen atoms in both actin and Arp3 were built using CHARMM. The carboxy terminal of Arp3 from 2P9K also has unresolved residues. The crystal structure of open state Arp2/3 complex (PDB ID: 1K8K) was used as a template and superposed with the 2P9K to procure the orientation of the carboxy terminal of Arp3 in the closed state. Later, the missing residues in the carboxy terminal of Arp3 were built using CHARMM in the presence of C or V peptide.

2.5 Structure modeling of C peptide

The crystal structure coordinates of the V peptide of WAVE were used as a template to build a C peptide model, as the crystal structure of the C peptide has not been determined. The C peptide is a shorter sequence (only 20 amino acid residues) that cannot be modeled using Modeller but is too long to trivially build using CHARMM. Sequence similarities between V and C peptides have been identified by others.[10, 28] PyMOL was used to convert the V peptide structure to the C peptide sequence using the default Dunbrack rotamer library and the most likely rotamer.[45]

2.6 Solvation, ions, and periodic boundaries

Each of the modeled proteins was individually solvated using TIP3P water molecules in a rectangular prism box, with dimensions 18 Å larger than the dimensions of that protein, thus providing approximately 3 layers of solvent. TIP3P water molecules were randomly replaced with Na^+ and Cl^- counter ions based on the number of ionizable groups being modeled or a molarity of 150 mM, whichever was greater, such that electrostatic neutrality was achieved. Periodic boundary conditions were applied to eliminate surface tension effects on the bulk properties of the molecules.

2.7 Pre-simulation: Energy minimization

Three sets of energy minimization were performed in a stepwise manner for each of the proteins that were simulated in order to obtain a low energy initial conformation and reduce the atomic strain between protein, solvent, and counter-ions. The Steepest Descent method was used for minimization.[46] The first round had 50 steps of Steepest Descent performed only on the solvent and counter-ions with remaining atoms fixed.

This was followed by a second round of 50 steps of Steepest Descent on only the protein with fixed solvent and counter ions. In the final round, the entire system was minimized to a lower energy conformation over 50 steps. This incremental method was chosen to minimize protein coordinate changes from the crystal structure values.

2.8 Equilibration of the system

A constant pressure-temperature (isobaric-isothermal) ensemble (NpT) was simulated using CHARMM, similar to previous *in silico* experiments on actin.[34, 47] The CHARMM27 force field parameters were used for all atoms in conjunction with the particle-mesh Ewald sum method to calculate long-range electrostatic interactions in the system.[44, 48] All intermolecular hydrogen bonds were constrained using the SHAKE algorithm, allowing for an integration time step of 2fs.[49] Each system was assigned a temperature of 300 K at the outset (instantaneous heating) and the temperature was kept constant using a Nosé-Hoover thermostat.[50-52] Every system was equilibrated until energy and pressure terms fluctuated around a consistent mean for at least 50 ps (approximately 300-400 ps total equilibration per system).

2.9 Production MD

Each equilibrated system was simulated for an additional 2ns. Conformations were sampled and analyzed every 0.2 ps during the production run.

2.10 Analysis

The collected trajectories for all 18 states were analyzed for conformational and energetic stability and fluctuations. We assessed the average conformational changes in ATP:actin, ATP:Arp2, and ATP:Arp3 in V peptide and C peptide bound and free states

by calculating RMSD and RMSF as a function of the peptide binding. The corresponding nucleotide free state was used as a reference state for comparison. The center-to-center average inter domain distances were also measured to assess the compactness of the conformations as a function of the peptide binding (Table 2.3 - 2.5).

We assessed conformational changes in the nucleotide-binding site, peptide, and peptide-binding site in different nucleotide states by measuring the RMSD and RMSF relative to the energy minimized initial structure (Figure 2.10 and 2.11). Such measurements were used to characterize changes to the vibrations and librations in Arp2 and Arp3 compared to actin due to the binding of V and C peptides. We used the centroid conformation (conformation with smallest RMSD from the mean trajectory conformation) of each individual state to compare the structural changes between the different states of the molecule and within the different states of the different molecule.

ACKNOWLEDGMENTS

We thank the Texas Advanced Computing Center and Texas Womans University Office of Technology for high performance computing resources. We thank Dr. Lynda Uphouse for advice regarding statistical analysis and Dr. DiAnna Hynds for thoughtful discussion and inputs in this paper. This project was also supported by internal funding from TWU (Research Enhancement Program, Multidisciplinary Research Program, and Art & Sciences Research Development Fund).

REFERENCES

1. Pantaloni D, Le Clainche C, Carlier MF. Mechanism of actin-based motility. Science 2001 May 25;292(5521):1502-6.
2. Svitkina TM, Borisy GG. Arp2/3 complex and actin depolymerizing factor/cofilin in dendritic organization and treadmilling of actin filament array in lamellipodia. J Cell Biol 1999 May 31;145(5):1009-26.
3. Welch MD, Mullins RD. Cellular control of actin nucleation. Annu Rev Cell Dev Biol 2002;18:247-88.
4. Pollard TD, Borisy GG. Cellular motility driven by assembly and disassembly of actin filaments. Cell 2003;112(4).
5. Abercrombie M, Heaysman JEM, Pegrum SM. The locomotion of fibroblasts in culture. Exp Cell Res 1970;62(2-3).
6. Lodish, H. F., A. Berk, C. Kaiser, M. Krieger, A. Bretscher, H. Ploegh, A. Amon, and M. Scott, Matsudaira.'. Molecular cell biology. 7th ed. ed. W. H. Freeman and Company, N. Y.; (2012).
7. May RC. The Arp2/3 complex: A central regulator of the actin cytoskeleton. Cell Mol Life Sci 2001 Oct;58(11):1607-26.
8. Rouiller I, Xu XP, Amann KJ, Egile C, Nickell S, Nicastro D, Li R, Pollard TD, Volkmann N, Hanein D. The structural basis of actin filament branching by the Arp2/3 complex. J Cell Biol 2008 Mar 10;180(5):887-95.

9. Padrick SB, Cheng HC, Ismail AM, Panchal SC, Doolittle LK, Kim S, Skehan BM, Umetani J, Brautigam CA, Leong JM, Rosen MK. Hierarchical regulation of WASP/WAVE proteins. Mol Cell 2008 Nov 7;32(3):426-38.

10. Chereau D, Kerff F, Graceffa P, Grabarek Z, Langsetmo K, Dominguez R. Actin-bound structures of wiskott-aldrich syndrome protein (WASP)-homology domain 2 and the implications for filament assembly. Proc Natl Acad Sci U S A 2005 Nov 15;102(46):16644-9.

11. Chen Z, Borek D, Padrick SB, Gomez TS, Metlagel Z, Ismail AM, Umetani J, Billadeau DD, Otwinowski Z, Rosen MK. Structure and control of the actin regulatory WAVE complex. Nature 2010;468(7323).

12. Ismail AM, Padrick SB, Chen B, Umetani J, Rosen MK. The WAVE regulatory complex is inhibited. Nat Struct Mol Biol 2009 May;16(5):561-3.

13. Padrick SB, Doolittle LK, Brautigam CA, King DS, Rosen MK. Arp2/3 complex is bound and activated by two WASP proteins. Proc Natl Acad Sci U S A 2011 Aug 16;108(33):E472-9.

14. Robinson RC, Turbedsky K, Kaiser DA, Marchand JB, Higgs HN, Choe S, Pollard TD. Crystal structure of Arp2/3 complex. Science 2001 Nov 23;294(5547):1679-84.

15. Ti SC, Jurgenson CT, Nolen BJ, Pollard TD. Structural and biochemical characterization of two binding sites for nucleation-promoting factor WASp-VCA on Arp2/3 complex. Proc Natl Acad Sci U S A 2011 Aug 16;108(33):E463-71.

16. Dominguez R. Actin filament nucleation and elongation factors--structure-function relationships. Crit Rev Biochem Mol Biol 2009 Nov-Dec;44(6):351-66.

17. Volkmann N, Amann KJ, Stoilova-McPhie S, Egile C, Winter DC, Hazelwood L, Heuser JE, Li R, Pollard TD, Hanein D. Structure of Arp2/3 complex in its activated state and in actin filament branch junctions. Science 2001 Sep 28;293(5539):2456-9.

18. Schutt CE, Myslik JC, Rozycki MD, Goonesekere NC, Lindberg U. The structure of crystalline profilin-beta-actin. Nature 1993 Oct 28;365(6449):810-6.

19. Sheterline P, Clayton J, Sparrow J. Actin. Protein Profile 1995;2(1):1-103.

20. Kabsch WW. Atomic structure of the actin:DNase I complex. Nature (London) 1990;347(6288):37-44.

21. Kurisu S, Takenawa T. The WASP and WAVE family proteins. Genome Biol 2009;10(6):226,2009-10-6-226. Epub 2009 Jun 15.

22. Goley ED, Rammohan A, Znameroski EA, Firat-Karalar EN, Sept D, Welch MD. An actin-filament-binding interface on the Arp2/3 complex is critical for nucleation and branch stability. Proc Natl Acad Sci U S A 2010 May 4;107(18):8159-64.

23. Rodal AA, Sokolova O, Robins DB, Daugherty KM, Hippenmeyer S, Riezman H, Grigorieff N, Goode BL. Conformational changes in the Arp2/3 complex leading to actin nucleation. Nat Struct Mol Biol 2005 Jan;12(1):26-31.

24. Nolen BJ, Pollard TD. Insights into the influence of nucleotides on actin family proteins from seven structures of Arp2/3 complex. Mol Cell 2007 May 11;26(3):449-57.

25. Kelleher JF, Atkinson SJ, Pollard TD. Sequences, structural models, and cellular localization of the actin-related proteins Arp2 and Arp3 from acanthamoeba. J Cell Biol 1995 Oct;131(2):385-97.

26. Rodal AA, Sokolova O, Robins DB, Daugherty KM, Hippenmeyer S, Riezman H, Grigorieff N, Goode BL. Conformational changes in the Arp2/3 complex leading to actin nucleation. Nat Struct Mol Biol 2005 Jan;12(1):26-31.

27. Nolen BJ, Littlefield RS, Pollard TD. Crystal structures of actin-related protein 2/3 complex with bound ATP or ADP. Proc Natl Acad Sci U S A 2004 Nov 2;101(44):15627-32.

28. Panchal SC, Kaiser DA, Torres E, Pollard TD, Rosen MK. A conserved amphipathic helix in WASP/scar proteins is essential for activation of Arp2/3 complex. Nat Struct Biol 2003 Aug;10(8):591-8.

29. Chen Z, Borek D, Padrick SB, Gomez TS, Metlagel Z, Ismail AM, Umetani J, Billadeau DD, Otwinowski Z, Rosen MK. Structure and control of the actin regulatory WAVE complex. Nature 2010;468(7323):533- 538.

30. Higgs HN, Blanchoin L, Pollard TD. Influence of the C terminus of wiskott-aldrich syndrome protein (WASp) and the Arp2/3 complex on actin polymerization. Biochemistry 1999 Nov 16;38(46):15212-22.

31. Lee SH, Kerff F, Chereau D, Ferron F, Klug A, Dominguez R. Structural basis for the actin-binding function of missing-in-metastasis. Structure 2007 Feb;15(2):145-55.

32. Marchand JB, Kaiser DA, Pollard TD, Higgs HN. Interaction of WASP/scar proteins with actin and vertebrate Arp2/3 complex. Nat Cell Biol 2001 Jan;3(1):76-82.

33. Abraham VC, Krishnamurthi V, Taylor DL, Lanni F. The actin-based nanomachine at the leading edge of migrating cells. Biophys J 1999 Sep;77(3):1721-32.

34. Dalhaimer P, Pollard TD. Molecular dynamics simulations of Arp2/3 complex activation. Biophys J 2010 Oct 20;99(8):2568-76.

35. Boczkowska M, Rebowski G, Kast DJ, Dominguez R. Structural analysis of the transitional state of Arp2/3 complex activation by two actin-bound WCAs. Nature Communications 2014;5.

36. Dayel MJ, Holleran EA, Mullins RD. Arp2/3 complex requires hydrolyzable ATP for nucleation of new actin filaments. Proc Natl Acad Sci U S A 2001 Dec 18;98(26):14871-6.

37. Nolen BJ, Littlefield RS, Pollard TD. Crystal structures of actin-related protein 2/3 complex with bound ATP or ADP. Proc Natl Acad Sci U S A 2004 Nov 2;101(44):15627-32.

38. Dalhaimer P, Pollard TD, Nolen BJ. Nucleotide-mediated conformational changes of monomeric actin and Arp3 studied by molecular dynamics simulations. J Mol Biol 2008 Feb 8;376(1):166-83.

39. Berman HM, Battistuz T, Bhat TN, Bluhm WF, Bourne PE, Burkhardt K, Feng Z, Gilliland GL, Iype L, Jain S, Fagan P, Marvin J, Padilla D, Ravichandran V, Schneider B, Thanki N, Weissig H, Westbrook JD, Zardecki C. The protein data bank. Acta Crystallogr D Biol Crystallogr 2002 Jun;58(Pt 6 No 1):899-907.

40. Schrödinger. The PyMOL Molecular Graphics System, Version 1.5.04 Schrodinger, LLC .

41. Sali A, Blundell TL. Comparative protein modelling by satisfaction of spatial restraints. J Mol Biol 1993 Dec 5;234(3):779-815.

42. Eswar N, Webb B, Marti-Renom MA, Madhusudhan MS, Eramian D, Shen MY, Pieper U, Sali A. Comparative protein structure modeling using MODELLER. Curr Protoc Protein Sci 2007 Nov;Chapter 2:Unit 2.9.

43. Sali A. *salign.py* : A script for multiple sequence alignment using modeller. <http://salilab.org/modeller/tutorial/advanced.html>. .

44. Brooks BR, Bruccoleri RE, Olafson BD, States DJ, Swaminathan S, Karplus M. CHARMM: A program for macromolecular energy, minimization, and dynamics calculations. Journal of Computational Chemistry 1983;4(2).

45. Dunbrack RL,Jr, Karplus M. Conformational analysis of the backbone-dependent rotamer preferences of protein sidechains. Nat Struct Biol 1994 May;1(5):334-40.

46. Choi C, Elber R. Reaction path study of helix formation in tetrapeptides: Effect of side chains. J Chem Phys 1991;94(1):751.

47. Pfaendtner J, Volkmann N, Hanein D, Dalhaimer P, Pollard TD, Voth GA. Key structural features of the actin filament Arp2/3 complex branch junction revealed by molecular simulation. J Mol Biol 2012 Feb 10;416(1):148-61.

48. Kolafa J, Perram JW. Cutoff errors in the ewald summation formulae for point charge systems. Molecular Simulation 1992;9(5):351.

49. Ryckaert J, Ciccotti G, Berendsen HJC. Numerical integration of the cartesian equations of motion of a system with constraints: Molecular dynamics of n-alkanes. Journal of Computational Physics 1977;23(3):327- 341.

50. Nose´ S. A unified formulation of the constant temperature molecular dynamics methods. J Chem Phys 1984;81(1):511.

51. Hoover W. Canonical dynamics: Equilibrium phase-space distributions. Physical Review A 1985;31(3):1695-1697.

52. Ryckaert J, Ciccotti G, Berendsen HJC. Numerical integration of the cartesian equations of motion of a system with constraints: Molecular dynamics of n-alkanes. Journal of Computational Physics 1977;23(3):327- 341.

TABLES

PDB ID	Resolution	Type of the molecule
1QZ5	1.45 Å	Actin
1D4X	2.00 Å	Actin
1K8K	2.00 Å	Arp3
1YAG	1.90 Å	Actin
1ATN*	2.80 Å	Actin
1J6Z*	1.54 Å	Actin
1C0G	1.60 Å	Actin

Table 2.1: *Template structures used to develop the Arp2 homology model.*
Structures identified by the homology modeling software program Modeller as templates for Arp2. *: 1ATN and 1J6Z. These structures were added manually to improve the accuracy of the model. All of the residues were resolved in the 1ATN structure, providing a fully folded template. 1J6Z is an uncomplexed actin and thus provides a less quaternary-structure influenced representative of the position of surface loops in monomeric states.

Region	Actin	Arp2	Arp3
Sub-domain 1	1-32,70-144, and 338-372	1-33,73-148, and 353-394	1-32,77-151, and 376-418
Sub-domain 2	33-69	34-72	33-76
Sub-domain 3	145-180 and 270-337	149-184, and 274-352	152-195 and 291-375
Sub-domain 4	181-269	185-273	196-290
Peptide Binding site	A22, G23, D24, D25, A26, Y143, A144, G146, T148, E167, G168, Y169, I341, S344, I345, S348, L349, and M355	M1, K7, Y22, A23, G24, S25, N26, F27, E29, Y147, Q149, G150, L151, L152, E171, G172, F173, R349, L356, V360, D363, I364, M365, D367, F371, G390, V391, T392, V393, and R394	P6, Y21, A22, G23, N24, T25, E26, P27, Q28, A150, W153, E160, R161, T162, L163, E182, G183, Y184, F379, S382, M383, L384, S386, T387, E389, P412, V413, F414, G415, V416, and M417
Nucleotide Binding Site	S14, G15, H73, G158, D157, V159	T15, G16, N76, G162, D161, V163	T14, G15, H80, G173, D172, V174
Nucleotide cleft distance 1: B1	S14:G158	T15:G162	T14:G173
Nucleotide cleft distance 2: B2	G15:D157	G16:D161	G15:D172
Nucleotide cleft distance 3: B3	H73:V159	N76:V163	H80:V174

Table 2.2: *List of amino acid residues defining sub-domains, V or C peptide binding site, nucleotide-binding site, nucleotide-binding cleft distances for actin, Arp2, and Arp3*. B3 and B2 are at the proximal end, whereas B1 is at the distal end of the molecules.

Average Inter Domain Distances (IDDs) ± RMSF (Å) in Actin							
		SD1:SD2	SD3:SD4	SD1:SD3	SD2:SD4	SD1:SD4	SD3:SD2
No Peptide	ATP free	26.06 ± 0.34	25.72 ± 0.22	25.88 ± 0.23	31.14 ± 0.86	36.51 ± 0.39	39.54 ± 0.52
	ATP bound	25.19 ± 0.35	25.78 ± 0.20	25.71 ± 0.19	31.16 ± 0.47	36.15 ± 0.23	39.37 ± 0.39
V-domain Bound	ATP free	26.02 ± 0.38	25.04 ± 0.24	26.15 ± 0.20	31.07 ± 0.64	36.30 ± 0.46	39.65 ± 0.53
	ATP bound	25.86 ± 0.41	25.64 ± 0.20	25.72 ± 0.17	30.27 ± 0.82	36.03 ± 0.44	38.96 ± 0.42
C-domain Bound	ATP free	26.78 ± 0.25	26.37 ± 0.28	25.78 ± 0.31	30.56 ± 0.93	37.28 ± 0.40	39.26 ± 0.62
	ATP bound	25.73 ± 0.42	26.12 ± 0.20	25.87 ± 0.18	29.41 ± 0.52	35.91 ± 0.36	39.00 ± 0.38

Table 2.3: *Average Inter-Domain Distances (IDD) ± RMSF (Å) for 6 inter-domain distances of actin in the peptide free, V and C peptide bound forms.*

Average Inter Domain Distances (IDDs) ± RMSF (Å) in Arp2							
		SD1:SD2	SD3:SD4	SD1:SD3	SD2:SD4	SD1:SD4	SD3:SD2
No Peptide	ATP free	27.38 ± 0.25	25.86 ± 0.20	29.23 ± 0.32	39.67 ± 1.42	40.89 ± 0.56	44.80 ± 0.80
	ATP bound	26.05 ± 0.47	26.19 ± 0.18	28.07 ± 0.22	32.18 ± 0.57	36.87 ± 0.33	41.58 ± 0.29
V-domain Bound	ATP free	28.93 ± 0.48	25.27 ± 0.17	28.59 ± 0.25	39.49 ± 1.77	39.13 ± 0.84	46.06 ± 0.70
	ATP bound	28.35 ± 0.36	25.65 ± 0.18	27.98 ± 0.21	31.58 ± 0.64	37.19 ± 0.28	42.18 ± 0.37
C-domain Bound	ATP free	27.95 ± 0.33	25.38 ± 0.19	31.41 ± 0.39	33.93 ± 1.03	38.64 ± 0.81	44.68 ± 0.73
	ATP bound	27.58 ± 0.48	25.86 ± 0.20	28.16 ± 0.23	33.31 ± 1.30	37.24 ± 0.47	42.99 ± 0.69

Table 2.4: *Average Inter Domain Distances (IDD) ± RMSF in (Å) for Arp2 in the peptide free, V, and C peptide bound forms*.

Average Inter Domain Distances (IDDs) ± RMSF (Å) in Arp3							
		SD1:SD2	SD3:SD4	SD1:SD3	SD2:SD4	SD1:SD4	SD3:SD2
No Peptide	ATP free	26.51 ± 0.38	27.72 ± 0.24	29.25 ± 0.32	40.30 ± 1.24	39.28 ± 0.60	45.27 ± 0.93
	ATP bound	26.93 ± 0.56	28.04 ± 0.28	29.17 ± 0.31	35.76 ± 0.91	37.45 ± 0.32	45.06 ± 0.60
V-domain Bound	ATP free	26.45 ± 1.77	28.20 ± 0.20	28.92 ± 0.25	40.78 ± 1.82	38.61 ± 0.66	46.53 ± 1.43
	ATP bound	25.46 ± 0.77	27.93 ± 0.19	28.53 ± 0.21	35.28 ± 0.97	37.76 ± 0.32	42.88 ± 0.99
C-domain Bound	ATP free	26.85 ± 0.49	27.93 ± 0.27	29.54 ± 0.34	40.10 ± 1.47	39.39 ± 0.61	46.17 ± 1.33
	ATP bound	28.58 ± 1.02	23.57 ± 0.18	23.24 ± 0.15	35.33 ± 0.78	31.18 ± 0.45	43.63 ± 0.99

Table 2.5: *Average Inter Domain Distances (IDDs) ± RMSF in (Å) for Arp3 in the peptide free, V, and C peptide bound forms*.

Average Nucleotide Binding Cleft Distance (NBCD) ± RMSF (Å)				
Actin		B1	B2	B3
No Peptide	ATP free	5.31 ± 0.41	5.15 ± 0.33	6.46 ± 0.50
	ATP bound	4.66 ± 0.16	4.83 ± 0.17	6.02 ± 0.59
V-domain Bound	ATP free	4.96 ± 0.31	5.07 ± 0.37	5.53 ± 0.44
	ATP bound	4.81 ± 0.27	4.76 ± 0.17	5.72 ± 0.69
C-domain Bound	ATP free	6.46 ± 0.86	5.43 ± 0.43	5.31 ± 0.36
	ATP bound	4.98 ± 0.21	4.60 ± 0.15	5.40 ± 0.41
Arp2		B1	B2	B3
No Peptide	ATP free	9.98 ± 1.09	10.57 ±1.15	7.95 ± 1.02
	ATP bound	5.06 ± 0.59	4.55 ± 0.19	5.47 ± 0.29
V-domain Bound	ATP free	9.50 ± 1.30	10.22 ±1.20	8.12 ± 1.17
	ATP bound	6.63 ± 0.44	5.70 ± 0.59	4.61 ± 0.18
C-domain Bound	ATP free	8.51 ± 0.81	8.74 ± 0.56	9.25 ± 1.32
	ATP bound	5.12 ± 0.28	4.60 ± 0.18	5.63 ± 0.33
Arp3		B1	B2	B3
No Peptide	ATP free	7.90 ± 0.62	10.05 ± 1.08	9.43 ± 1.40
	ATP bound	4.77 ± 0.20	4.89 ± 0.21	5.54 ± 0.28
V-domain Bound	ATP free	8.28 ± 1.24	5.85 ± 0.80	10.62 ± 1.74
	ATP bound	4.76 ± 0.22	4.72 ± 0.17	5.77 ± 0.56
C-domain Bound	ATP free	10.56 ± 0.85	9.28 ± 0.86	10.46 ± 1.42
	ATP bound	4.96 ± 0.22	4.65 ± 0.16	4.97 ± 0.30

Table 2.6: *Average nucleotide-binding cleft distances and root mean square fluctuations (RMSF) in Å for actin, Arp2, and Arp3 in different peptide and nucleotide bound states*. Distances are between the non-hydrogen mean atomic positions of residues defining the cleft [24]. Residues are listed in Table 2.

FIGURES

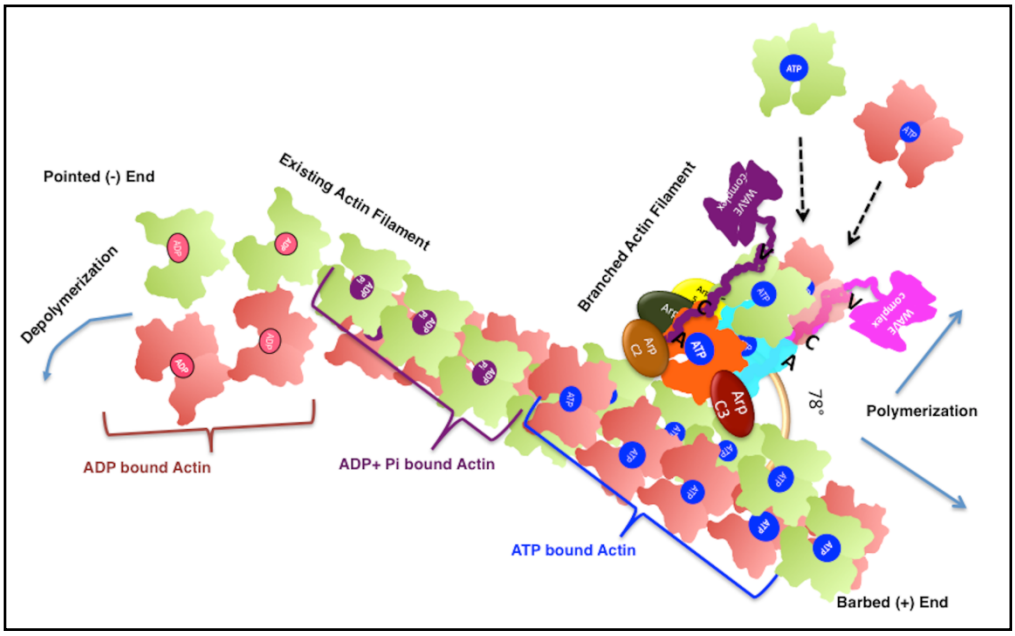

Figure 2.1: *Model Representation of Branched Actin Filament*.

Proteins and protein regions involved in polymerization/depolymerization of a branched actin filament are represented. Blue solid circle: ATP; Purple solid circle: ADP+Pi; Red solid circle: ADP; Orange subunit: Arp3; Cyan subunit: Arp2; Faded Green or Faded Red subunit: actin; Purple or pink units: Wiskott-Aldrich complex with VCA domains; Brown/yellow/dark red/dark green: accessory proteins of Arp2/3 complex. (Concepts from: Padrick and Rosen et al., 2011; Ti and Pollard et al., 2011; Rouiller and Hanein et al., 2008.)

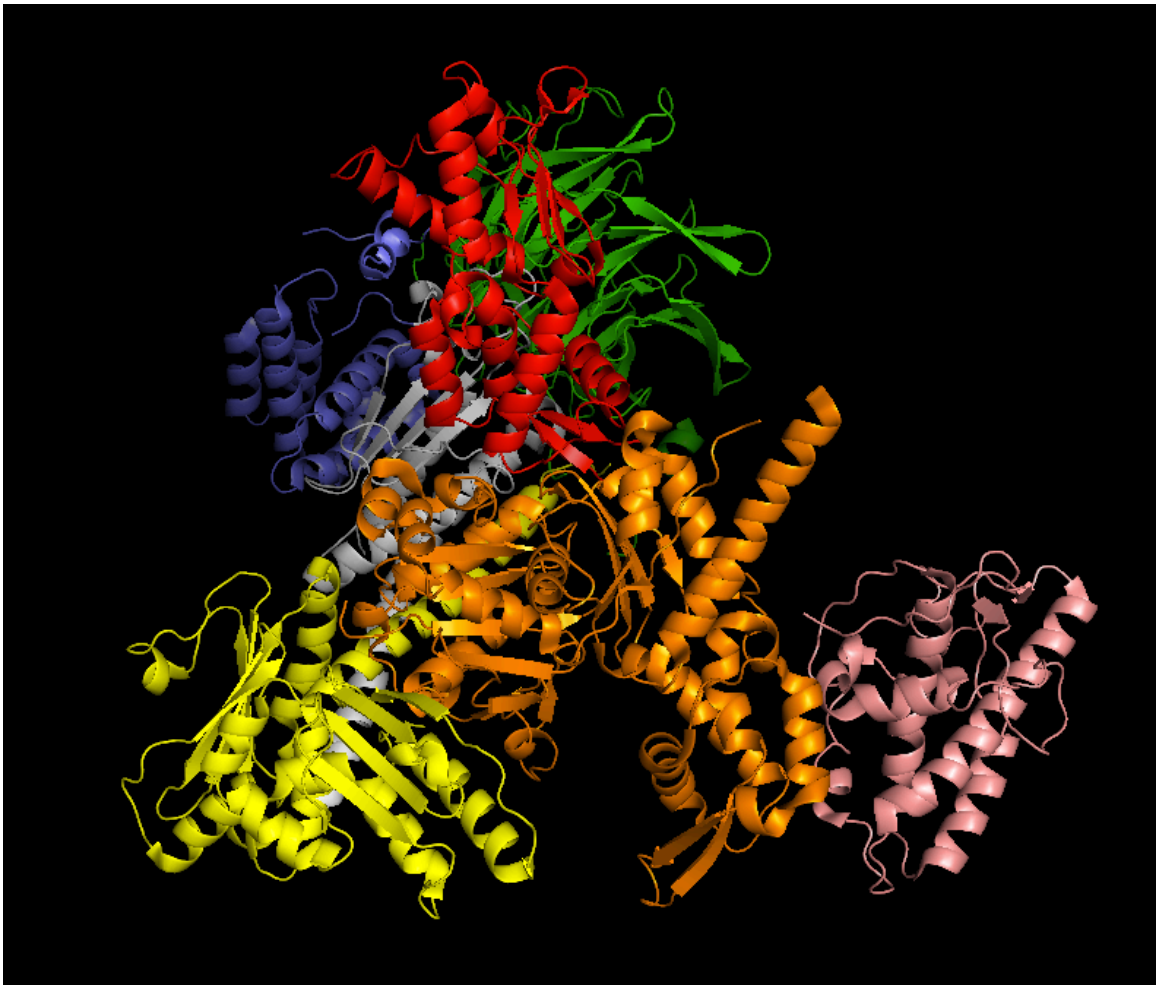

Figure 2.2: *Cartoon Representation of Arp2/3 complex using PyMOL (PDB ID: 1K8K).* Green:ArpC1;Yellow:ArpC2;Lightpink:ArpC3;White:ArpC4;Blue:ArpC5;Red:Arp2;Orange:Arp3.

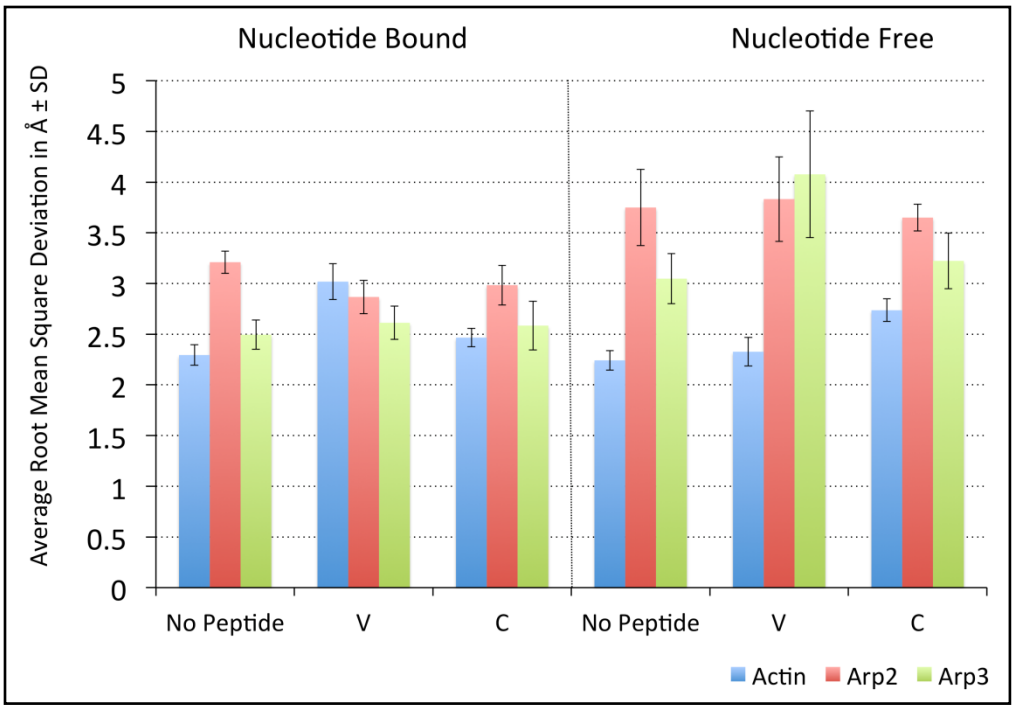

Figure 2.3: *Average protein-only RMSD from the minimized initial structure over the 2ns time period*. The error bars represent the RMSF (Å) values. Blue: Actin, Red: Arp2, and Green: Arp3. "No Peptide", "V", and "C" indicate apo-protein, protein bound to V peptide, or protein bound to C peptide, respectively.

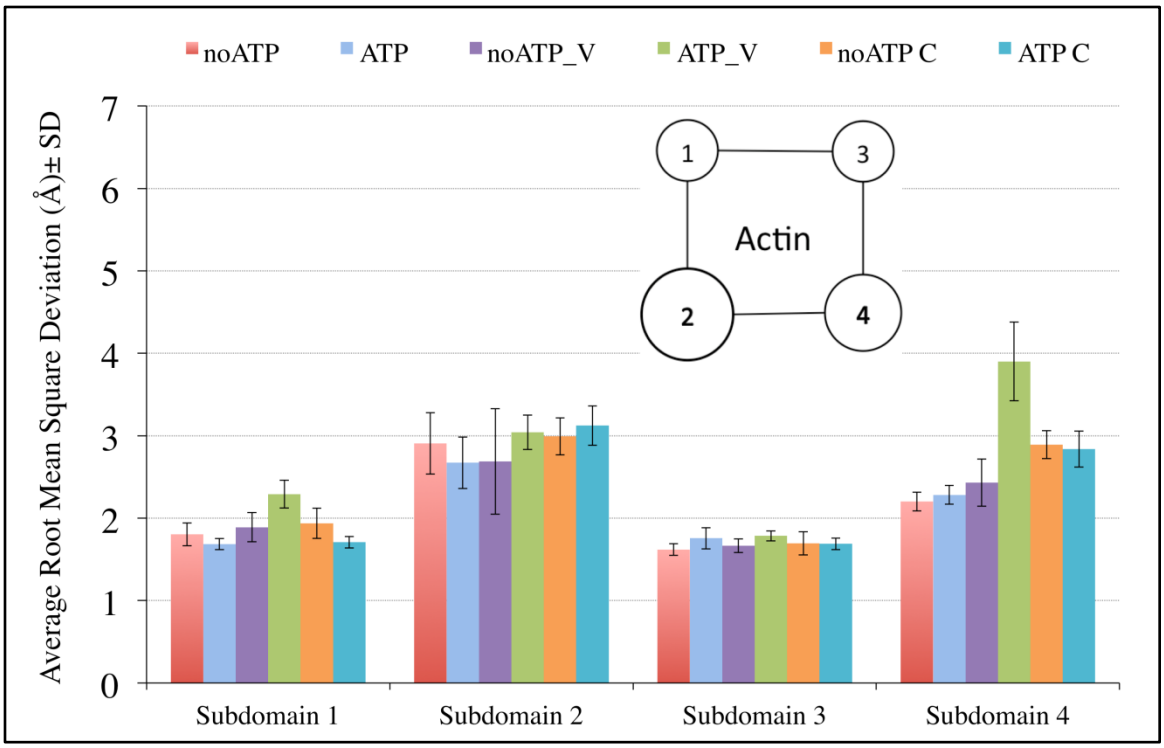

Figure 2.4: *Average all-atom RMSDs (Å) for the 4 sub-domains of actin.*

Red: protein with no ATP and no peptide. Cyan: protein with ATP and no peptide. Purple: protein with no ATP and V peptide. Green: protein with ATP and V peptide. Orange: protein with no ATP and C peptide. Teal: protein with ATP and C peptide. The error bars represent RMSF (Å) values for the same. The inset shows the conformational changes in each sub-domain, where a circle radius represents the group mean of all the states for the respective sub-domain. In this figure, the width and length of the edge lines have no meaning except to suggest the sub-domains are interacting.

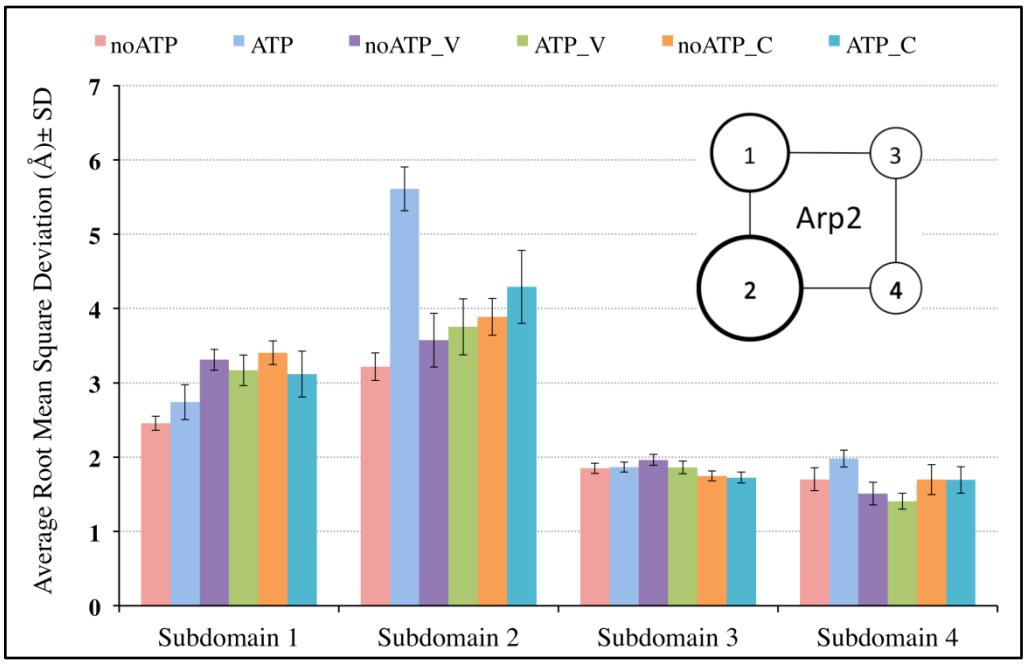

Figure 2.5: *Average all-atom RMSDs (Å) for the 4 sub-domains of Arp2.*

Red: protein with no ATP and no peptide. Cyan: protein with ATP and no peptide. Purple: protein with no ATP and V peptide. Green: protein with ATP and V peptide. Orange: protein with no ATP and C peptide. Teal: protein with ATP and C peptide. The error bars represent RMSF (Å) values for the same. The inset shows the conformational changes in each sub-domain, where a circle radius represents the group mean of all the states for the respective sub-domain. In this figure, the width and length of the edge lines have no meaning except to suggest the sub-domains are interacting.

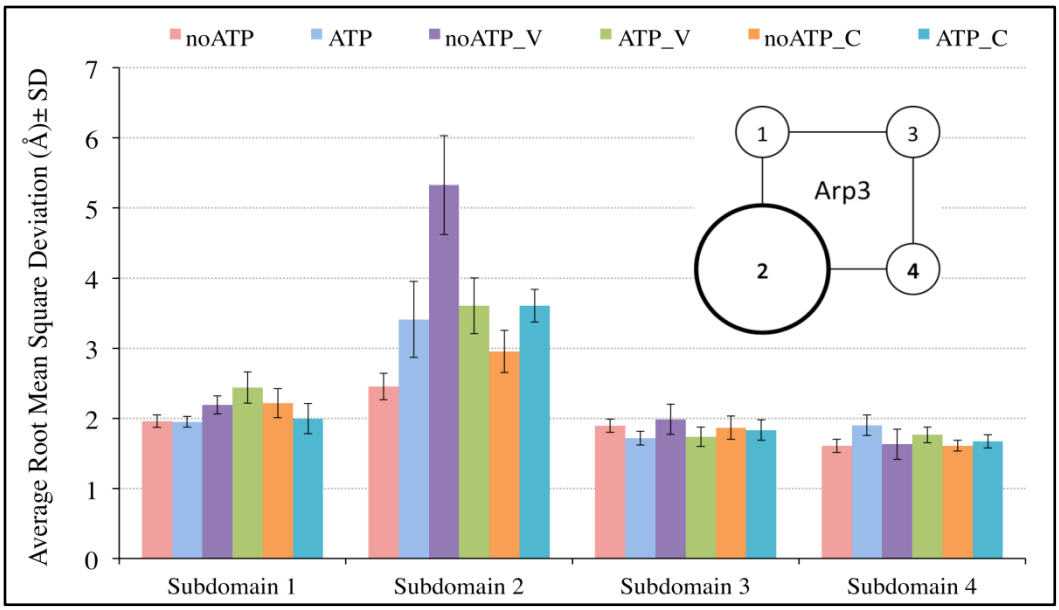

Figure 2.6: *Average all-atom RMSDs (Å) for the 4 sub-domains of Arp3.*

Red: protein with no ATP and no peptide. Cyan: protein with ATP and no peptide. Purple: protein with no ATP and V peptide. Green: protein with ATP and V peptide. Orange: protein with no ATP and C peptide. Teal: protein with ATP and C peptide. The error bars represent RMSF (Å) values for the same. The inset shows the conformational changes in each sub-domain, where a circle radius represents the group mean of all the states for the respective sub-domain. In this figure, the width and length of the edge lines have no meaning except to suggest the sub-domains are interacting.

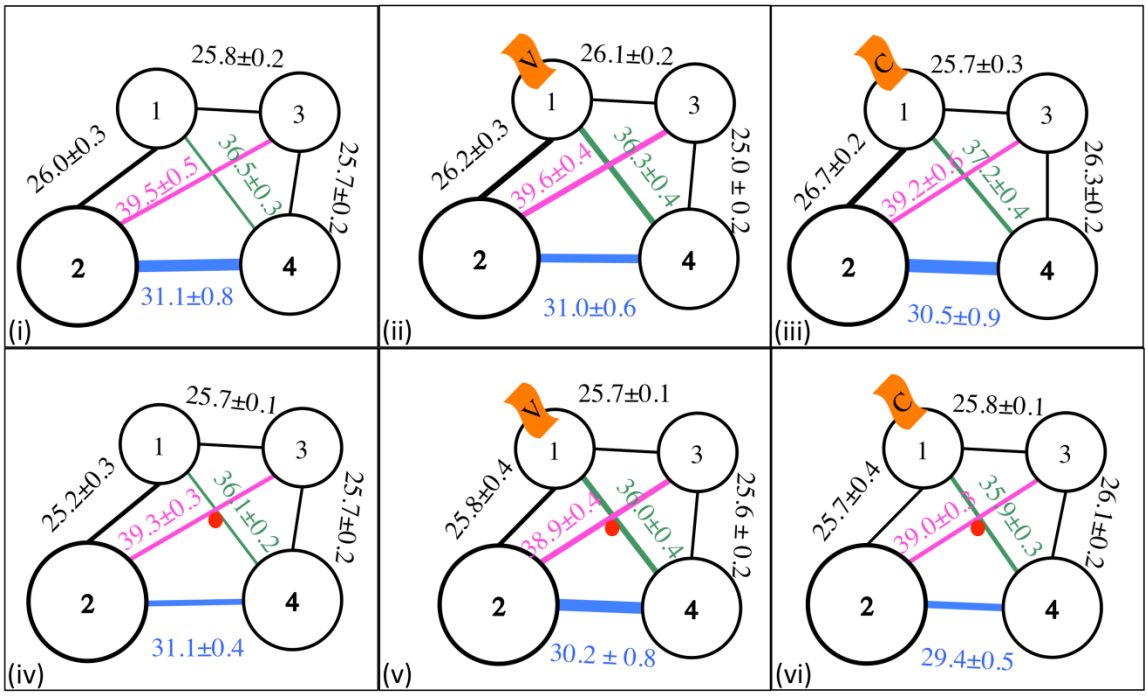

Figure 2.7: *Cartoon representation of the average inter-domain distances (IDD) (Å) for the 6 SDinteractions of actin in the absence of V or C peptide, V peptide bound, and C peptide bound states*. Key: circle: sub-domain; radius of the circle: RMSD of the SD in Å; connecting lines: inter-domain distance in Å; length of the line: average distance between the sub-domains in Å; width of both circle and lines: average fluctuations in Å (SD).

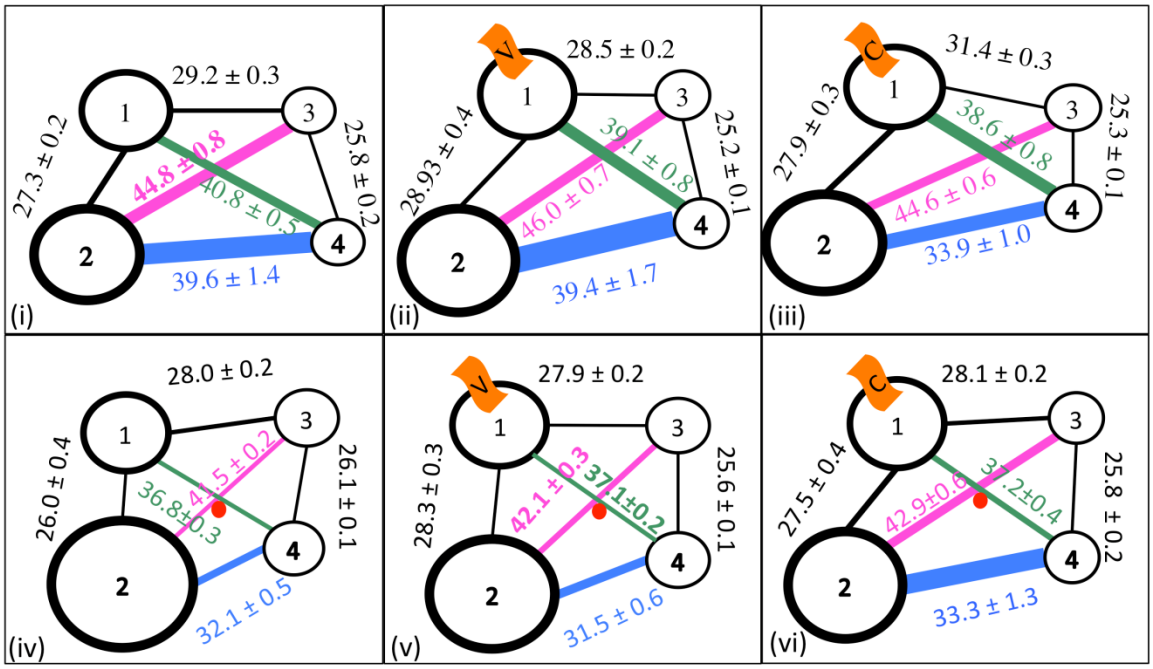

Figure 2.8: *Cartoon representation of the average inter-domain distances (IDD) (Å) for 6 SDinteractions of Arp2 in the absence of V or C peptide, V peptide bound, and C peptide bound states*. Key: circle: sub-domain; radius of the circle: RMSD of the SD in Å; connecting lines: inter-domain distance in Å; length of the line: average distance between the sub-domains in Å; width of both circle and lines: average fluctuations in Å (SD).

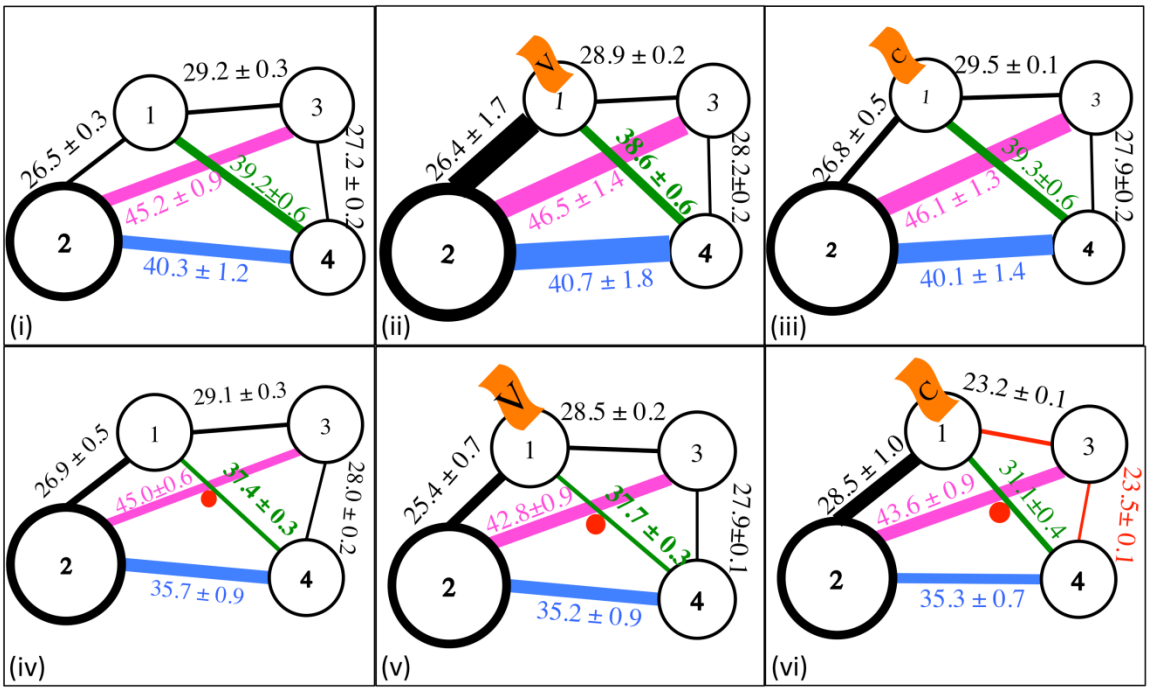

Figure 2.9: *Cartoon representation of the average inter-domain distances (IDD) (Å) for 6 SDinteractions of Arp3 in the absence of V or C peptide, V peptide bound, and C peptide bound states*. Key: circle: sub-domain; radius of the circle: RMSD of the SD in Å; connecting lines: inter-domain distance in Å; length of the line: average distance between the sub-domains in Å; width of both circle and lines: average fluctuations in Å (SD).

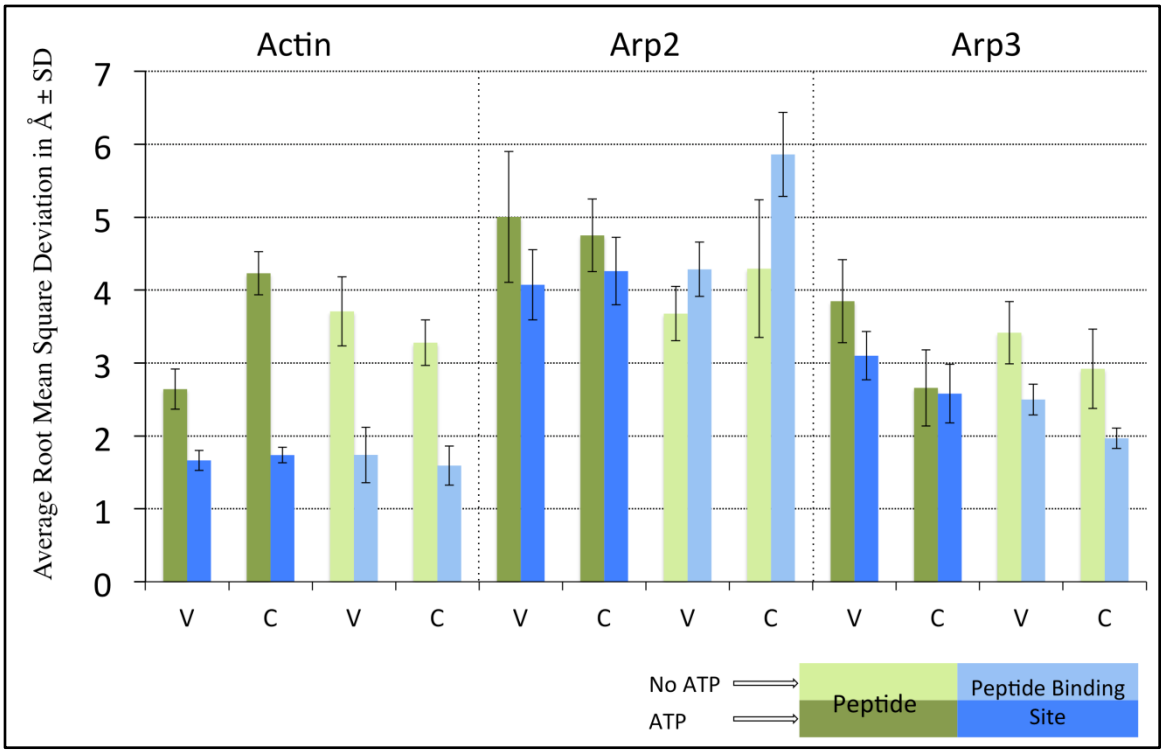

Figure 2.10: *The average RMSD (Å) of peptide (V and C peptide) and peptide binding site for actin, Arp2, and Arp3 in different peptide bound states for 2ns time period*. The error bars represent the RMSF (Å) values for the same.

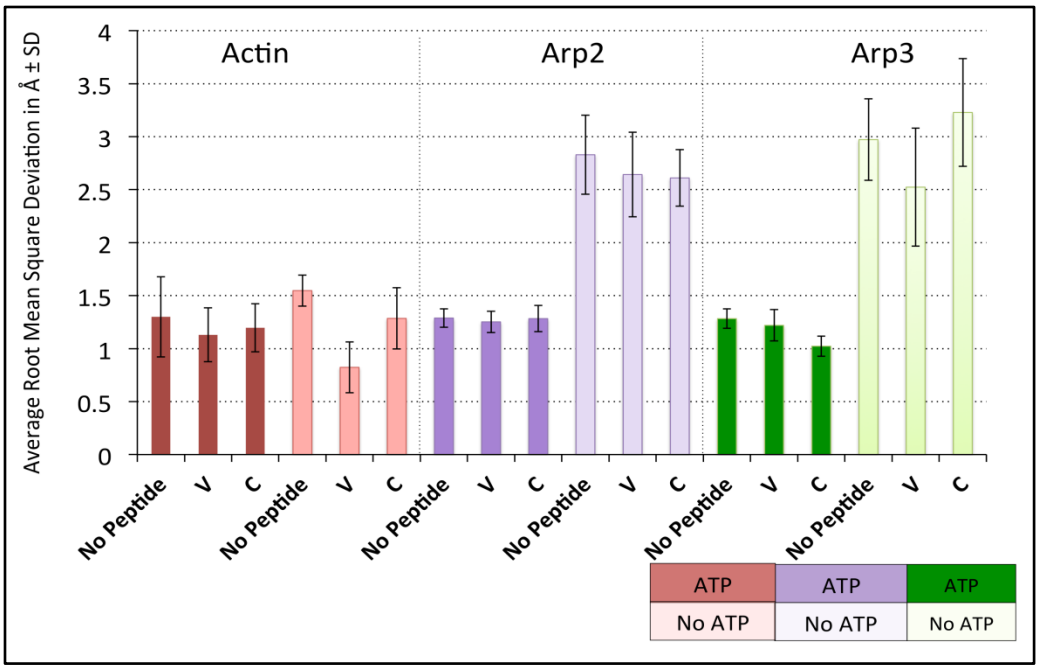

Figure 2.11: *The average RMSD (Å) of the nucleotide-binding site for actin, Arp2, and Arp3 in different peptide bound states for 2ns time period*. The error bars represent the RMSF (Å) values for the same.

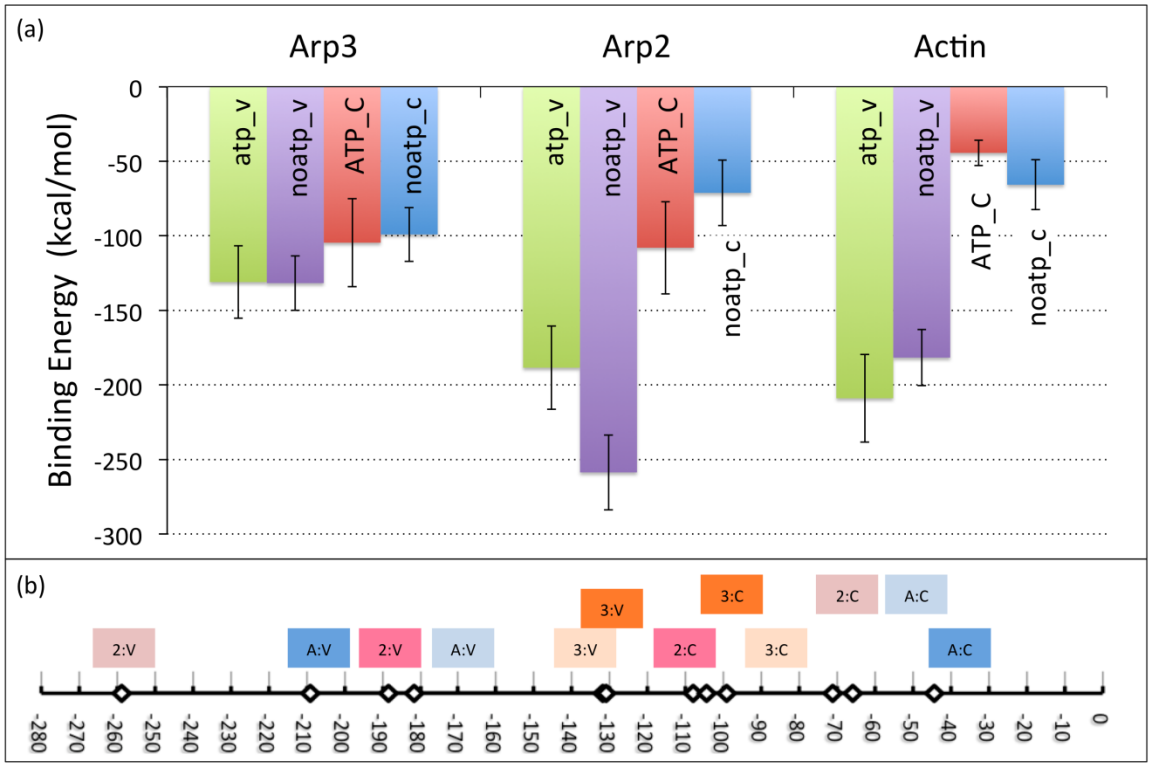

Figure 2.12: *Protein:Peptide Binding Energies*

(a) Binding energy of the complexes (actin:V, actin:C, Arp2:V, Arp2:C, Arp3:V, and Arp3:C);(b) All states are arranged in terms of their binding energy order, lowest energy conformation (2:V) is on the left, whereas the less stable complex (A:C) is on the right of the binding energy number line. Key: '2':Arp2; '3':Arp3; 'A': actin; 'V': V peptide; 'C': C peptide. Values are in kcal/mol.

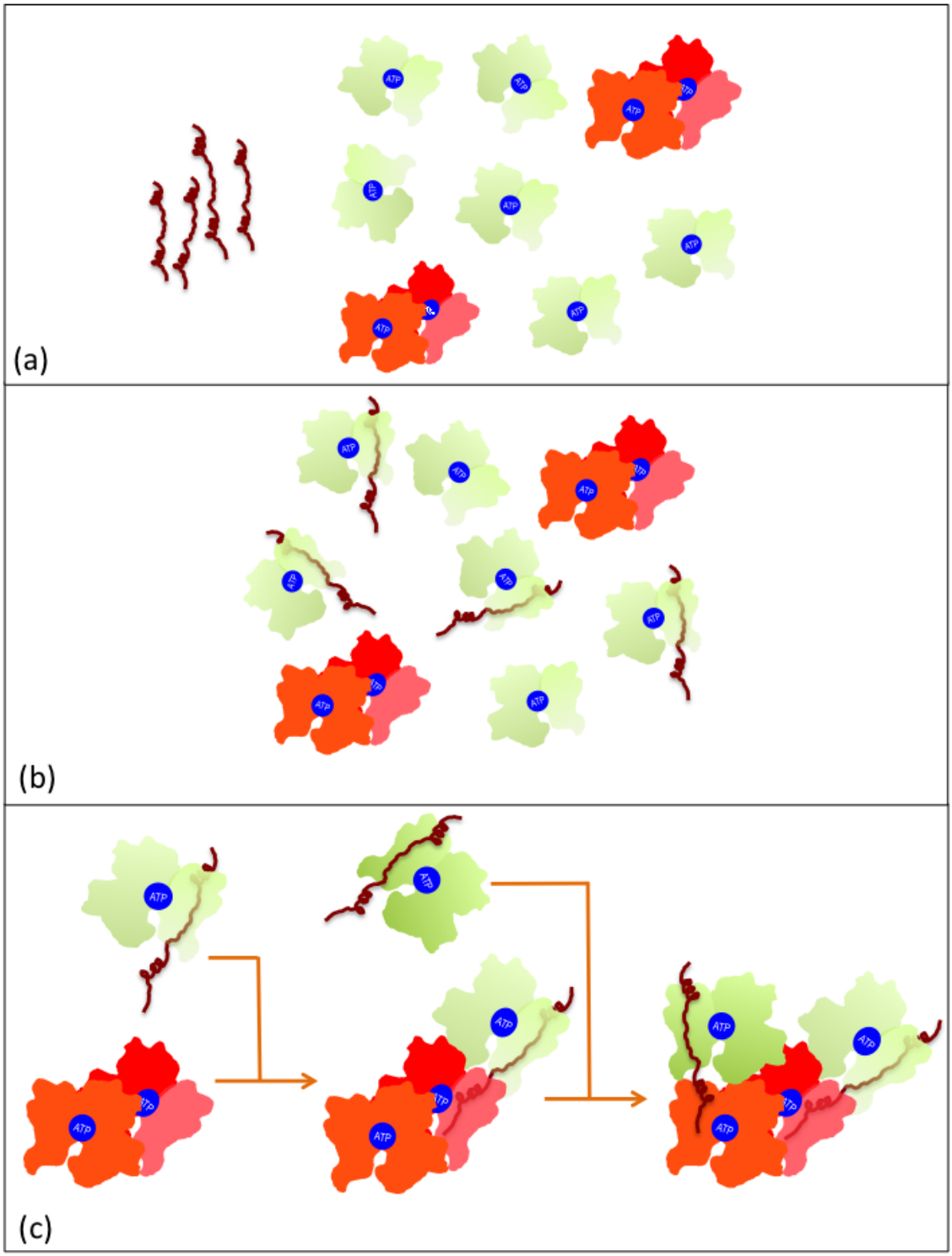
(a)
(b)
(c)

Figure 2.13: *Hypothetical Model for the conformational rearrangement between Arp2:Arp3 dimer*. (A) Pool of V peptide, monomeric actin and Arp2/3 complex. (B) V peptide is bound to the monomeric actin (C) V peptide bound actin is delivered at one of the Arp binding site, followed by the delivery of another V peptide bound actin at the second Arp binding site.

Key: ATP (blue solid circles), Arp3 (orange subunit), Rearranged Arp2 (red subunit), Arp2 with unresolved sub-domain 1 and 2 (red and salmon subunit); actin (Green subunit); VCA region of Wiskott-Aldrich complex (brown helical structure), R161A, S226Q, R447W mutants in Arp3 (✖), CK-66 inhibitors (x), (Some concepts from: Padrick and Rosen et al., 2011; Ti and Pollard et al., 2011; Rouiller and Hanein et al., 2008.)

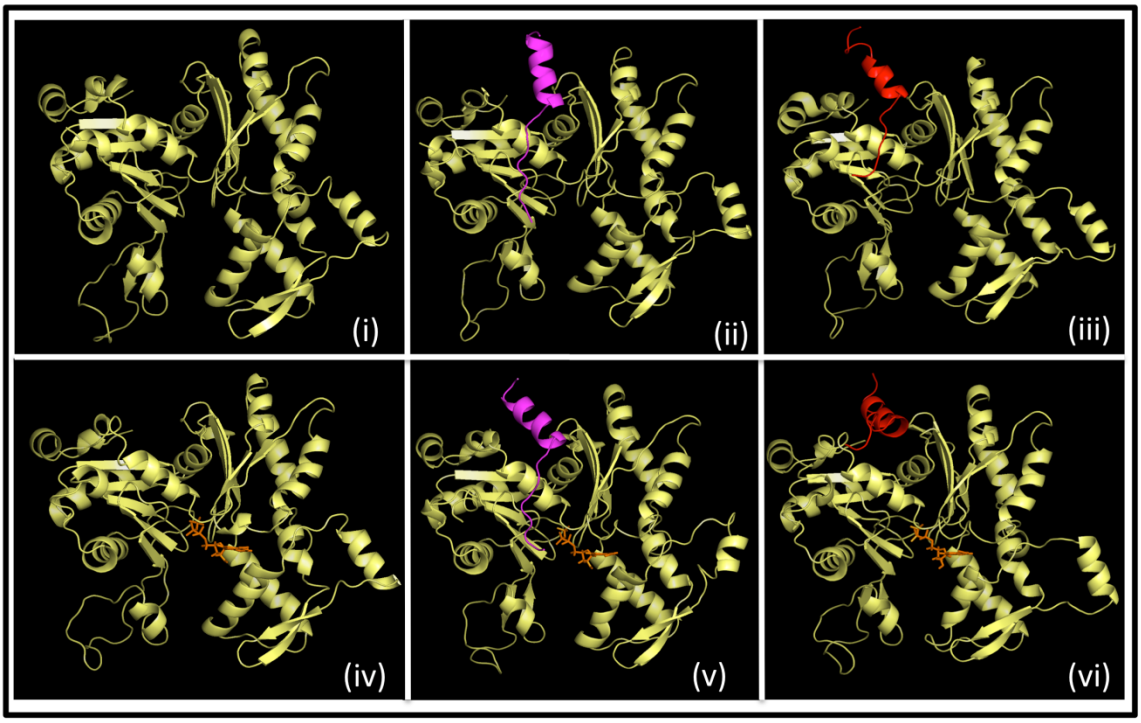

Figure 2.S1: *Cartoon representation of the centroid conformation of actin over the period of 2ns*. Key: Actin (Yellow cartoon), ATP (Orange sticks), V peptide (Magenta cartoon), C peptide (Red cartoon)

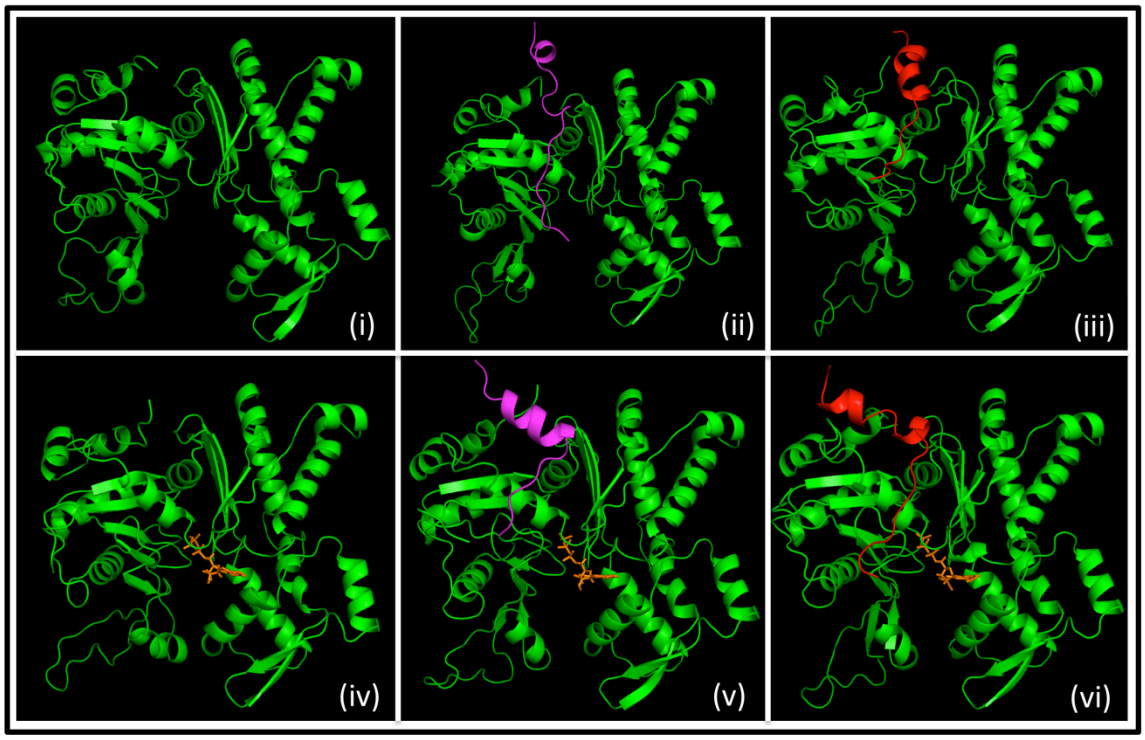

Figure 2.S2: *Cartoon representation of the centroid conformation of Arp2 over the period of 2ns*. Key: Arp2 (Green cartoon), ATP (Orange sticks), V peptide (Magenta cartoon), C peptide (Red cartoon)

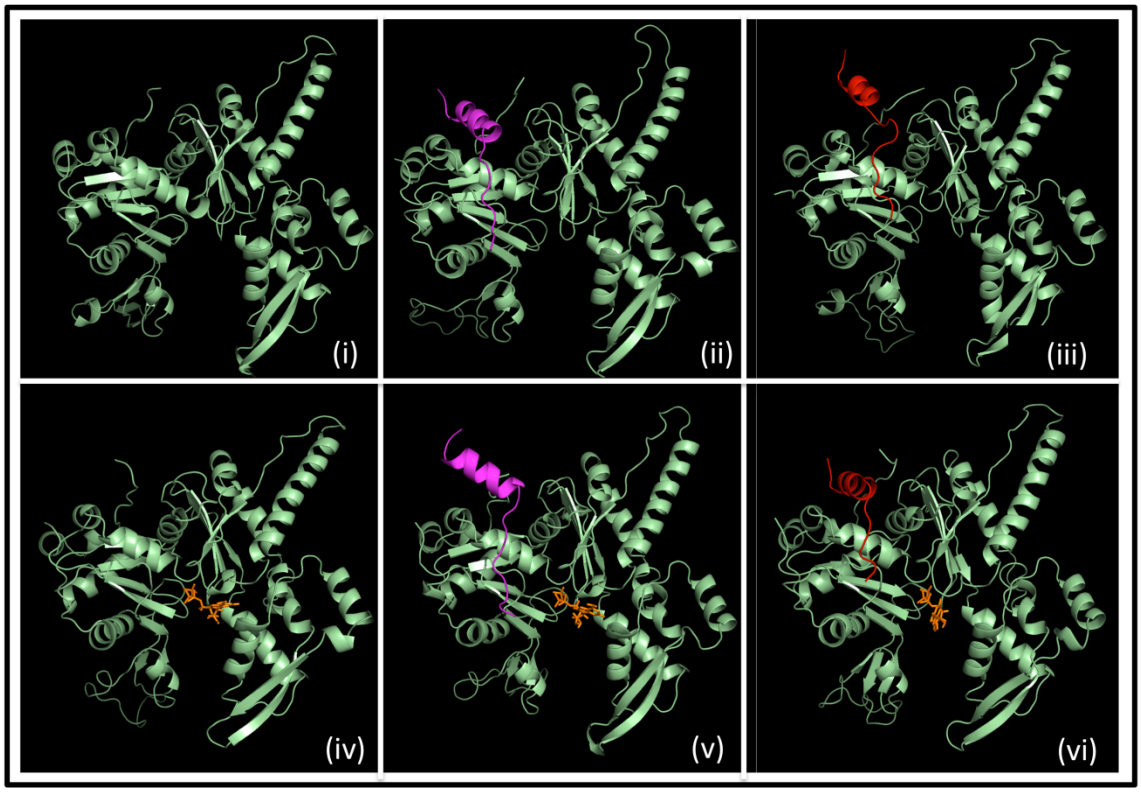

Figure 2.S3: *Cartoon representation of the centroid conformation of Arp3 over the period of 2ns*. Key: Arp3 (Pale green cartoon), ATP (Orange sticks), Vpeptide (Magenta cartoon), C peptide (Red cartoon).

CHAPTER III

SPECIFIC INTERFACIAL RESIDUES CONTROL REARRANGEMENT OF THE ARP2:ARP3 DIMER DURING ACTIVATION OF THE ARP2/3 COMPLEX.

Amruta C. Mahadik[1], Sounick Haldar[1], DiAnna Hynds[1], Brian W. Beck[2,†]

1 Department of Biology, Texas Woman's University, Denton, Texas, United States of America

2 Texas Advanced Computing Center, University of Texas at Austin, Austin, Texas, United States of America

†Author to whom correspondence should be addressed: bbeck@tacc.utexas.edu

Running title: “Mutant Control of Arp2:3 Interface”

Manuscript pages: 30, supplementary material pages: 0, tables: 4, figures: 11

ABSTRACT

The Arp2/3 complex is the key component in the branching of actin filaments, a process essential for cellular responses to the environment. Arp2 and Arp3, the major subunits of the Arp2/3 complex nucleate to form the first short pitch dimer of the daughter actin filament. Nucleation promoting factors like WASP/WAVE family proteins activate the Arp2/3 complex and promote the elongation process by delivering the first actin monomer to the daughter actin filament. Recent studies have shown that Arp3 and Arp2 subunits undergo conformational changes that activate the complex. Crystal structures are available, but mechanisms controlling quaternary interactions are still not well understood. Here, we use computational alanine scanning methods to identify "hot spot" residues that stabilize the Arp2:Arp3 dimer interface in the inactive state and propose mutations that will destabilize the inactive state, favoring the activate state (R123A, S188Q, and R409W). We validated these predications with mutagenesis and transient transfection of GFP-tagged R123A Arp3 expressed in B35 neuroblastoma cells. Cells changed morphology to more spherical structures with altered neurite growth and excess cortical actin while preserving the Arp2/3 complex, suggesting that Arp3:R123A successfully altered the quaternary interactions, making the Arp2/3 complex constitutively active.

KEYWORDS

Arp2/3 complex, actin branching, molecular modeling, computational alanine scanning, mutagenesis, microscopy, immunocytochemistry

IMPORTANCE/IMPACT

The Arp2/3 complex is responsible for allowing actin filaments to branch. Here we use molecular modeling to identify mutations in Arp3 predicted to promote Arp2/3 activation. We then construct these mutants and show they promote actin filaments in neurite cells.

ABBREVIATIONS AND SYMBOLS

A-domain: Acidic domain

Arp: Actin Related Protein

Arp 2/3 Complex: Actin Related Protein 2/3 Complex

CAS: Computational Alanine Scanning

C-domain: Central domain

DIC : Differential Inference Contrast

FRET : Fluorescence Resonance Energy Transfer

ITC : Isothermal Titration Calorimetry

NPF: Nucleation Promoting Factors

PDB: Protein Data Bank

RMSD: Root Mean Square Deviation

V-domain: Verprolin domain

WA Family: Wiskott-Aldrich Family

WASP: Wiskott-Aldrich Syndrome Protein

WAVE Wiskott-Aldrich syndrome VErprolin homolog

INTRODUCTION

Actin cytoskeleton is at the heart of various cellular processes such as cell locomotion, migration, adhesion, division, phagocytosis, and intracellular motility of vesicles, organelles, and certain pathogens.[1-3] These extracellular and intracellular processes are characterized by the rapid transition of globular actin (G-actin) into filamentous actin (F-actin) that polymerizes (oligomerizes) into filaments at the "barbed" or "+" filament end.[4] It is often convenient to classify actin filaments into two types: linear and branched [5]. Linear filaments are thought to support cellular structures like filopodia (β-actin) and stress fibers (γ-actin), whereas branched filaments are enriched in lamellipodia in eukaryotic cells.[6, 7] Actin Binding Proteins (ABP) such as Nucleation Promoting Factors (NPF) tightly regulate the polymerization and depolymerization of F-actin, while ABPs such as the Actin Related Protein 2/3 complex (Arp2/3 complex), initiates the branching of actin filaments.[8-14] (Figure 3.1)

Arp2/3 complex is composed of two major subunits (Arp2 and Arp3) along with five accessory subunits (ArpC1, ArpC2, ArpC3, ArpC4, ArpC5)[13, 15, 16] (Figure 3.2(A)). Like actin, Arp2 and Arp3 are members of the actin family (PFAM PF00022) and the actin-like ATPase superfamily (PFAM CL0108) that includes amongst its 29 members the Arps, actins, several sugar kinases, and the HSP70s. [17, 18] The accessory subunits, ArpC1-5, facilitate the binding of the Arp2/3 complex to existing actin filaments by mediating quaternary interactions between cofactors and the existing mother filament (Figure 3.1).[19] Nucleation promoting factors, such as WASP, N-WASP, WAVE, and

WHAMM, are all oligomeric protein complexes, each of which contain a C-terminal VCA region in common.[8, 11] The VCA region regulates nucleation and branching, whereas other domains in Wiskott-Alrich (WA) complexes facilitate cellular localization [8-10, 20] (Figure 3.1). The VCA region consists of V (verprolin), C (central), and A (acidic) domains that modulate interactions with actin (V domain) and the Arp2/3 complex (CA domain) at actin branch points.[12, 14, 21]

The structure of the Arp2/3 complex has been determined experimentally at different resolutions and in a number of conformations thought to represent both active (filament favoring) and inactive conformations.[13, 19, 22, 23] The Arps maintain substantial structural similarity with actin, but the complex is thought to undergo conformational rearrangements that allow Arp2 and Arp3 to form an active "short-pitch" F-actin-like dimer. This short-pitch Arp2:Arp3 dimer provides a template surface from which a daughter actin filament branch will polymerize.[13, 19, 22, 23]

While similar in structure, detailed comparison of Arp2/3 complex crystal structures to structures derived from electron microscopy/tomography (EM), as well as to x-ray structures of actin filaments suggests that the Arp3 and Arp2 subunits are not arranged in the actin filament-like conformation in the Arp2/3 crystal structure but rather are in an inactive state.[19, 22, 23] Indeed, while a handful of Arp2/3 structures have more active-like conformations [such as the seven 2P9* structures of Nolen and Pollard which have open, intermediate, or closed nucleotide-binding clefts], there are no structures currently available that represent the active-state quaternary conformation.[22] The lack of

such structures greatly increases the difficulty of characterizing quaternary conformational changes during the activation of the Arp2/3 complex.

In addition, available Arp2/3 crystal structures, such as PDBid 1K8K, are often incompletely specified.[13] Many of the residues in sub-domains 1 and 2 of Arp2 are not reported/resolved, suggesting that either a) these residues lack well-defined structures or b) the structured domains librate around more mobile elements[13, 22] (Figure 3.2(A)). As the sequence similarity of Arp2 and Arp3 with actin is high (>69% and >61%, respectively), the structural similarity of the unresolved domains is also likely to be high, consistent with mobile but structured domains.[24]

Both actin tertiary and quaternary structure are known to be nucleotide-binding state dependent.[22, 25] However the Arps are known to have less nucleotide-binding affinity.[26] The nucleotide-binding clefts of both Arp3 and Arp2 in the crystal structures are more open than that of actin (approximately 12° and 18°, respectively) and both lack nucleotide.[13] The previously mentioned lack of active Arp2/3 complex structures also hampers characterization of the impact of nucleotide-binding on complex activation. However, Nolen and colleagues have been able to crystallize the Arp2/3 complex in the presence and absence of ATP or nucleotide analogs.[22] In these crystal structures, Arp2 and Arp3 have nucleotide-binding clefts more "closed" and thus more similar to F-actin, but the relative orientation of Arp2 to Arp3 remains in the inactive conformation.[22] Arp2/3 quaternary structure shows limited nucleotide-binding dependency, reinforcing the importance of NPFs in branch activation.

As mentioned earlier, the V and CA domains of the VCA region of NPFs are known to interact with actin (V) and Arp 2 and 3 subunits (CA), respectively.[8] In cells, the concentration of actin monomers is high (>100 μM).[27, 28] Actin monomers are therefore the preferred binding sites for V-domains of NPFs, with relatively high affinity (Kd <1.0 μM).[8, 29-31] Padrick and co-workers proposed a model for the affinity of V-domain bound actin relative to C-domain bound Arp2 and Arp3, where V-domain bound actin has strong affinity and is delivered to Arp2, but activates the Arp2/3 complex weakly. On the other hand, V-domain bound actin has lower affinity towards Arp3, but results in strong activation of the complex.[12] However, ITC and FRET studies have shown that V-domain bound actin binds first to Arp2 and ArpC1 that in turn produces a partial conformational change at the barbed end of Arp3.[32] Thus, both models differ in the proposed V-domain bound actin binding to Arp2 and Arp3, but confirm that conformational changes in Arp3 are involved in activating the Arp2/3 complex.

Electron microscopy and single-particle analysis have confirmed that the Arp2/3 complex exists in several conformations in equilibrium, with major motions including nucleotide-binding-cleft opening and closing, quaternary changes corresponding to filament favoring and disfavoring states, and combinations thereof.[23] The transition from inactive to active mainly involves the movement of Arp2 relative to Arp3, closing of the nucleotide cleft favoring binding of nucleotides, and a ~15° rotation of sub-domains 3 and 4 relative to sub-domains 1 and 2.[19] The composition of quaternary interactions of Apr2 and Arp3 with other subunits of the complex such as ArpC1 and ArpC2 are different in active conformations than in inactive conformations. Upon rearrangement,

new contacts bury a surface area that is 1700 Å^2 larger than the contacts in the inactive complex.[19] A stall in the motion of sub-domains 3 and 4 of Arp2 was observed in a restrained MD simulations studies at forces lower than 120 kcal/mol Å^2 where the domains were further than 2 Å distance from the target conformation (Arp2:3 short-pitch helix).[33] This stall indicates an energy barrier that must be overcome during branch formation, possible by conformational changes associated with Arp2/3 binding of NPFs and/or the mother filament. Dalhaimer and Pollard's simulations did not reproduce the known nucleotide cleft closures or the ~15° rotation of the two halves of both Arps, suggesting that interactions with NPFs or the mother filament are most likely required for these conformational changes to take place during branch formation.[33]

In addition to these conformational studies using MD and single-particle analysis, Hetrick and Nolen used two small organic heterocycles, CK-666 and CK-869, to probe the role of Arp2/3 complex in actin remodeling processes. CK-869 is representative of a class of Arp2/3 inhibitors that destabilize the short pitch interface of Arp2 and Arp3.[34] Unlike the classical mode of action for PPI inhibitors[35], CK-869 binds to a pocket near the Arp2:Arp3 interface in sub-domain 1 of Arp3 and locks the sensor loop in an open conformation. CK-666 functions as an allosteric effector, stabilizing the inactive-state.[34] These inhibitors stabilize the Arp2/3 complex in an inactive conformation even in the presence of NPFs such as VCA fragments, WASP, and existing filaments of actin.[34] Thus, in addition to external regulatory interactions playing a role, inherent quaternary interactions at the Arp2:Arp3 interface, if altered, may affect the activation of the complex. This is especially interesting as both CK inhibitors bind in domain 1, not far

from where NPFs are thought to bind.[8] It is not inconceivable that NPFs may be destabilizing the inactive state in order to activate Arp2/3. As the surface loops and interface residues in this region are not disordered in the crystal structures, computational methods such as molecular modeling may prove useful.

Therefore, we propose that the quaternary interaction of specific interfacial residues, present at the Arp2:Arp3 interface, dominate the stability of the Arp2/3 complex in the inactive state. Mutations of these specific residues would destabilize the inactive state of the complex, perhaps mimicking the interactions of NPFs. It is likely that the active conformation is similar to the short-pitch dimer structure of F-actin (PDB id: 1M8Q). Thus destabilizing the inactive state should thus have limited impact on active-state stability and may shift the Arp2/3 equilibrium towards active, promoting constitutive activation and the branching of actin filaments.

Here we used computational alanine scanning (CAS) to identify residues in the wild-type quaternary interactions at the Arp2:3 interface that may contribute to the stability of the inactive-state of the complex (Figure 3.2(B)). In addition, we designed point mutations in the identified Arp3 residues that are predicted to alter the quaternary interactions and result in the disruption of the Arp2:3 interface. While this could result in the disruption of the complex altogether it is more likely to shift the equilibrium towards the active state. We validated our modeling predictions by creating the proposed substitutions in GFP-labeled *Homo sapiens* Arp3 using mutagenesis and using B35 neuroblastoma cells as a transient transfection expression system. The mutated cells were

assessed for the alteration in cell morphology, actin filament arrangement, and change in the neurite outgrowth.

RESULTS

3.1 Identification of the important residues of the Arp2: Arp3 interface

Results from computational alanine scanning (CAS) of the Arp2:3 interface of the Arp2/3 complex in the inactive state (based on PDBid 1K8K) are shown in Table 3.1. Calculations yielded three "strong" hot spots (free energy change upon alanine substitution, $\Delta\Delta G_{ala} \geq 2$ kcal/mol): Arp3:R123, Arp2:N205, and Arp2:E248. Four "moderate" hot spots (2 kcal/mol $\leq \Delta\Delta G_{ala} \geq 1$ kcal/mol) were also identified: Arp3: S188, Arp3:R409, Arp2:D209, and Arp2:R250. The $\Delta\Delta G_{ala}$ for Arp3 R123, S188, and R409 residues were 3.98, 1.78, and 1.32 kcal/mol (Table 3.1).

Side chain orientation and local quaternary packing of both arginine residues (R123 and R409) in sub-domain 1 and S188 in sub-domain 3 were examined. The charged R123 interacts with the carbonyl oxygen of G201 of Arp2 within hydrogen-bonding distance. The terminal amine of R409 likely donates a hydrogen to the carbonyl oxygen of Arp2:R200. In addition to these hydrogen bonds, S188 forms a third hydrogen bond with Arp2:D209 (Figure 3.5). These interactions anchor sub-domain 4 of Arp2 to sub-domain 1 of Arp3 and help maintain Arp2/3 in the inactive conformation. These stabilizing interactions likely serve to restrain the subunits from rearranging prior to activation.

Repetition of these calculations on different conformations of nucleotide bound Arp2/3 structures (2P9I: Intermediately-Open, 2P9K: Closed) both indicated that R123 and S188 in Arp3, and N205, E248, and R250 in Arp2 were energetically important ($\Delta\Delta G_{ala}$ > 1 kcal/mol, a common definition of "hotspot") across multiple conformations. R409 was energetically important in the 1K8K and 2P9I conformations, but not in the 2P9K conformation.[36] The consistently large magnitude R123 $\Delta\Delta G_{ala}$ across multiple conformational states suggests R123 is the most likely to be important for the conformational stability of Arp2 and Arp3 subunits prior to activation and thus is the prime target for mutagenesis validation. S188 is also "hot" across multiple conformations and would also be a suitable target, though it's potential presence in the active interface may increase the complexity of interpretation of mutation results.

While alanine substitution at positions R123, S188, and R409 is predicted to destabilize the Arp2:Arp3 interface, single alanine mutations may not be sufficiently disruptive such that quaternary structure alters. Mutations to more destabilizing residues would promote more complete dissociation of particular conformations of Arp2/3.

3.2 Design of "improved" destabilizing mutations

The 3 identified hotspot residues were systematically substituted for all other amino acid residues except glycine and proline using PyMol's mutagenesis module and re-analyzed by CAS to identify more destabilizing mutants. Substitution to arbitrary conformations of amino acids is not likely to produce physically meaningful targets as all residues can be artificially oriented into destabilizing conformations. PyMol provides the Dunbrack & Karplus backbone dependent rotamer library for all 20 amino acids.[37] These

were used to create the least physically unrealistic conformations for substitution mutants for all three hot spots. The rotamers are ordered according to their frequencies of occurrence in proteins (%Mutation). PyMOL also indicates the strain associated from Van der Waals (VdW) overlap. Rotamers were selected based on two criteria: (1) The orientation of the rotamer should be the mostly probable from the Dunbrack set and (2) The strain should be minimal. Rotamers should not induce steric clash with the backbone or buried side chains in the protein containing them.

These designed point mutants were subjected to a second round of CAS (Table 3.2). Unlike the initial CAS round, a negative change in the $\Delta\Delta G_{ala}$ suggests alanine substitution stabilizes the interface and therefore that the substituted amino acid residue is more disruptive than alanine (Figure 3.3). To test the mutant rotamer selection protocol, self-mutations were made at S188S and R409R and analyzed by CAS (Table 3.3). At position S188, rotamer 1 was selected and essentially returned the crystal structure results. At position R409, 2 rotamers (4 and 8) had the lowest strain, but rotamer 4 was chosen, as it was the more probable rotamer. The $\Delta\Delta G_{ala}$ of these conformations (0.49 and 0.87 kcal/mol) were in qualitative agreement with crystal structure results though at about half the effect. All other rotamers produced substantially lower $\Delta\Delta G_{ala}$ compared to the crystal structure.

CAS is by definition mutation to alanine, so the $\Delta\Delta G_{ala}$ of any Ala mutant is 0.00. For R123, 16 of 17 other amino acid residue substitutions produced no $\Delta\Delta G_{ala}$ at that position as only the terminal amines of R123 are at the interface. All other amino acids essentially retract from the interface. Lys produced a stabilizing result and was rejected in

favor of the original alanine. As nearly of the side chains of substituted amino acid residues were unable to reach the interface and therefore lost stabilizing interactions relative to Arg, we predict any amino acid with a short side chain such as serine or glycine would destabilize the interface. However, we choose alanine over all other amino acid residues, as it would have minimum steric clash with the Arp3 backbone.

At position S188, only Glu and Gln produced large negative $\Delta\Delta G_{ala}$ ($\Delta\Delta G_{ala}$ =-1.04 and -1.07 kcal/mol, respectively) with most residues predicted to be stabilizing. Gln was selected as the target. The Gln side chain extends towards the carbonyl oxygen of Arp2:D209 and may induce a conformational change in the helical region of Arp2:sub-domain 4 (Figure 3.6).

Similar to S188, only substitution to Trp at R409 produced a large negative $\Delta\Delta G_{ala}$ ($\Delta\Delta G_{ala}$ = -1.63 kcal/mol) and was selected as a target. The Trp CD1 potentially clashes with the backbones of Arp2:R200 and Arp2:G201 while losing the terminal amine hydrogen bond to R200.

All 3 of these positions are entirely (R123, R409) or substantially within only the inactive interface. Therefore, we predict these point mutants will destabilize the inactive-state and result in the activation of the Arp2/3 complex.

Comparison of these residues to homologous positions in other members of the Arp3 gene family (Gene:ACTR3, HomoloGene:68483) and in members of the actin gene family (Gene:ACTA1, HomoloGene:121702) reveals that not only is *Bos taurus* Arp3 R123, S188, and R409 completely conserved with *Homo sapiens* Arp3 (R161, S226, and R447), but that the Arg positions are conserved between Arp3 and actin, and Arp3:S188

is homologous with a conserved His in actin, H173.[38] In this work, we continue to use *Bos taurus* residue numbering for consistency with models.

3.3 Confirm the predicted altered properties of Arp2:Arp3 dimer

CAS predicted R123A as the most likely disruptive mutant in Arp3. We assessed the effects of R123A point mutation on neurite initiation and outgrowth in B35 rat neuroblastoma cells. B35 cells are commonly used to study axonal growth cone guidance and cell motility.[39] During development, neurons produce motile sensory cellular extensions, the tip of which is a fan-shaped structure known as the growth cone.[40] The tips of the growth cone continue to extend and develop into an axon or a dendrite, a process known as "neurite outgrowth". Neurite outgrowth is an actin-dependent process and involves a complex coordination of signaling pathways that regulate the polymerization of actin into filaments.[40, 41] Filopodia and lamellipodia cellular structures play important roles in neurite outgrowth and growth cone motility and are dependent on the formation of linear and branched actin filament meshworks.[42] Because of this sensitivity to actin branching, the morphology of B35 cells was used to gauge the impact of Arp3 mutation.

3.4 Generation of Arp3 expression vectors

We synthesized the N-terminally GFP-tagged and C-terminally V5 epitope-tagged wild type and mutated Arp3 (R123A) recombinant construct by homologous recombination (Figure 3.4). We assessed the efficiency of the recombination process by performing a restriction digestion of GFP-Arp3 WT recombinant vector with BgII restriction enzyme. The presence of approximately 4000kb, 1800kb, and 1200kb size

fragments (sites (needed for a total of three fragments) was within the insert. Figure 3.7) suggest that the homologous recombination generated the appropriate recombinant DNA as one of the restriction

3.5 Transfected B35 Neuroblastoma cells

Immunocytochemistry was used to assess the cell morphology of GFP-Arp3 transfected B35 neuroblastoma cells by using anti-GFP and anti-Arp3 antibodies. The cells were viable in all groups 3 days post-transfection, indicating minimal toxicity due to the transfection method and protocol. Differential Interference Constrast (DIC) and Fluorescence images indicate nearly 100% of cells were transfected with either empty vector (GFP only) or GFP-Arp3. The cell morphology of both was normal, showing neurites (Figure 3.8).

In western-blot analysis, anti-GFP immunoreactive bands were found at 75 kDa (the expected molecular weight of the fusion protein) in transfected cells, but not in untransfected cells (Figure 3.9(A)). Furthermore, anti-Arp3 western blots had immunoreactive bands at 50 kDa in both transfected and untransfected cells, corresponding to the expected molecular weight of endogenous Arp3 (Figure 3.9(B)). An additional Arp3 immunoreactive band was also evident at approximately 75 kDa (the expected size of the fusion protein) in transfected, but not in untransfected cells (Figure 3.9(B)).

3.6 Effect of GFP-Arp3 and GFP-Arp3-R123A on Arp2/3 complex formation

The mutation in the Arp3:123 position was predicted to destabilize the Arp2:3 interface resulting in either continued binding with an altered conformation or complete

disruption. Extracts of cells transfected with either wild type or mutant GFP-Arp3 were co-immunoprecipitated (co-IP) with anti-Arp2 antibodies (Figure 3.10). Input blots show the 75 kDa GFP-Arp3 fusion band in R123A mutated and wild-type cells, while empty vector (EV, GFP only) does not (Figure 3.10(B)). After Co-IP, blotting with anti-GFP antibodies also showed the presence of 75kDa band in mutated and wild type cells, whereas untransfected and cells transfected with GFP did not show any band (Figure 3.10(B)). This analysis suggests that Arp3:R123A continues to be able to bind members of the Arp2/3complex.

3.7 Arp3-R123A alters actin filament arrangement and cell morphology

GFP-Arp3 expressing B35 neuroblastoma cells were assessed for cell morphology with phalloidin staining. The florescent images reveal no change in the cellular morphology of untransfected, transfected with the empty vector, or wild type GFP-Arp3 expressing cells (Figure 3.11(A-C)). The Arp3:R123A mutant had a substantial effect on the cell morphology, elaborating few, if any, neurites and generally presenting in clusters of spherical forms (Figure 3.11(D)). The mutated cells also show increased cortical phalloidin staining, suggesting the accumulation of filamentous actin at the cell periphery.

DISCUSSION

Characterization of the interfacial region

Table 3.1 and Figure 3.5 indicate that while the interface is somewhat packed, burying 553 $Å^2$ over 23 residues (15 primarily polar or charged), only 3 of the residues

appear to contribute the bulk of the stabilization: R123, S188, R409.[43] The $\Delta\Delta G_{ala}$ for S188, and R409 residues of Arp3 is 3.98, 1.78, and 1.32 kcal/mol. R123 and R409 in the sub-domain 1 both have interactions within the 4.0 Å of Arp2 but only in the inactive state, while S188 in the sub-domain 3 of Arp3 potentially has interactions in both inactive and active conformations. These energetically important hotspots not only stabilize the inactive dimer interface but also are important to the integrity of the complex in several different conformations. The side chains of these 3 residues project towards sub-domain 2 of Arp2, anchoring it with 3-4 hydrogen bonds, a number of weak electrostatic interactions, and VdW packing of the interface. We predict that these hot spots if mutated, together or individually, will destabilize the inactive Arp2:Arp3 dimer interface.

Design and rotamer selection of destabilizing mutants

Alanine substitution is a classical approach used to scan the interface as it eliminates the side chain beyond β-carbon, without changing the main-chain conformation or imposing extreme electrostatic or steric effects. Here, we systematically assessed the possibility of substituting all other amino acid residues for the hot spots with the goal of altering the interface properties such that the quaternary equilibrium would shift. Selecting amino acid targets with more physically reasonable rotamers that had the highest conformational probabilities but no steric clash with the backbone limited the effects on tertiary changes. Somewhat unexpectedly, at all three positions, out of 17 possible substitutions, only 1 or 2 amino acid substitutions produced mutants more destabilizing than wild type to alanine substitution (Table 3.2). R123A, S188Q, and R409W were all identified as potentially disruptive quaternary mutations. Interestingly,

all R123 mutants except for lysine retracted from the interface entirely, suggesting that R123 may act as a lynch pin, stabilizing a pivot in a particular state. This idea of a lynch pin is consistent with the restrained molecular dynamics simulations of Dailhammer, Pollard, and Nolen showing a barrier to movement towards the active conformation. "Shrinking" the arginine to an alanine at 123 with the concomitant loss of stabilizing interactions suggests R123A may be the best possible target for mutatgenesis.[25]

R123A point mutant rendered Arp2/3 complex constitutively active

GFP tagged Arp3:R123A point mutant, when expressed in B35 neuroblastoma cells, altered cell morphology from long, slender individual cells with developing neurites to clusters of spherical cells with effectively no neurites (Figure 3.11). While this might arise if the Arp2/3 complex were completely dissociated, thus preventing the formation of filamentous and branched actin meshworks necessary for neurite development, co-IP studies demonstrate Arp3:R123A continues to bind Arp2 (or at least a complex containing Arp2)[42]. Furthermore, loss of activity would lead to diminished nucleation. Our results show that R123A mutants have enhanced cortical phalloidin staining, implying more filamentous actin is present, not less.

If, on the other hand, only the inactive were destabilized, then the equilibrium would shift, resulting in a constitutively active complex. This in turn would increase the number of nucleation starting points for actin polymerization and lead to the types of elevated actin polymerization and accumulation seen in Figure 11D. The apparent increased rate of actin polymerization did not increase the level of neurites but rather eliminated it. One possible reason for this is that the unusually high concentration of actin

filament could be hindering the formation of regular cytoskeletal scaffold thus producing spherical globular structures instead of normal neurite morphology. It is interesting to note that while our Arp3 constructs were regulated by the constitutive CMV promoter, the expression of Arp2 and the other Arp2/3 complex subunits necessary for actin nucleation remained under the control of the endogenous promoters.

Future implications of the mutants

CK-666 and CK-869, small organic heterocycles developed by Hetrick et. al. both inhibit activation of the Arp2/3 complex by trapping the complex in the "OFF" state.[34] CK-666 is a classical allosteric effector, stabilizing the inactive state of the complex, while CK-869 directly disrupts key protein-protein interfaces in the short pitch Arp2-Arp3 active dimer. Nolen's work (PDBid 3UKU, 3UKR, 3ULE) reveals that the CK-869 binding site is in close proximity to both the nucleotide-binding cleft as well as being near the Arp2:3 dimer interface (Figure 3.5). CK-869 binding locks the sensor loop in an open conformation and moves the B7/αC loop toward the sub-domain 2. This movement creates a steric clash with the αE/αF loop of Arp2 in the short pitch position. Similarly, CK-666 binds to the interface of Arp2:Arp3 in the inactive conformation. As shown in Figure 5, CK-869 is directly adjacent to R123. This implies that not only does CK-869 destabilize the active state, but it may also stabilize R123, thus promoting the inactive state. Similarly, CK-666 binds adjacent to S188 and is a known inactive state stabilizer. Both compounds have been shown to inhibit filament formation even in the presence of NPF activation.[34]

Our R123A mutational studies demonstrated that the interfacial R123 mutation "rescues" the complex from inactive to a constitutive active, resulting in substantial accumulation of actin filaments in B35 neuroblastoma cells. It would be interesting to test the effect of CK-869 and CK-666 inhibitors on our Arp3:R123A mutant as they should have diminished effect.

CONCLUSIONS

Here we have identified residues critical to the stability of the native inactive state of the Arp2/3 complex. We have computationally designed mutants that destabilize the interface and have validated these predications with site-directed mutagenesis and transient transfection of B35 rat neuroblastoma cells. While wild-type transfections show normal cell morphology, Arp3:R123A mutants simultaneously demonstrate stable Arp2/3 complex formation, increased cortical actin, but reduced neurite outgrowth, suggesting a constitutively active Arp2/3 complex. Taken together our results provide much needed mechanistic clues as to how theArp2/3 complex is regulated *in vivo*.

METHODS

3.1 Computational alanine scanning (CAS)

We used the computational alanine scanning (CAS) method developed by Kortemme and Baker and available at the ROBETTA server to identify the energetically important residues at the Arp2:Arp3 dimer.[44-46] CAS modeling uses simple energy functions to measure the change in the pseudo-free energy (conformational energy with a

free-energy of solvation term, $\Delta\Delta G_{ala}$) due to substitution of alanine for individual interfacial wild-type (w.t.) amino acid residue.[44] In this CAS algorithm, an interface amino acid residue is defined as (i) a residue that has at least one atom within a sphere with a 4 Å radius of an atom belonging to the other partner in the protein complex, or (ii) a residue that becomes significantly buried upon complex formation, as measured by an increase in the number of Cβ atoms within a sphere with a radius of 8 Å around the Cβ atom of the residue of interest.[44] A positive change in the $\Delta\Delta G_{ala}$ indicates a destabilizing effect on the interface upon substitution, whereas a negative value indicates a stabilizing effect (Figure 3.3(A)). Identified amino acid residues with $\Delta\Delta G_{ala} \geq 1$ kcal/mol are termed "hot spots." Positions at which alanine stabilizes the model ($\Delta\Delta G_{ala} \leq -1$ kcal/mol) are termed "cold spots."

For a static model, thermodynamic cycle arguments show that the energy of an alanine-substituted model (ΔG_{ala}) is the same regardless of whether the original structure was a hot or cold spot. i.e.

$$\Delta G_{ala} = \Delta\Delta G_{ala}^{hot} - \Delta G_{native}^{hot} = \Delta\Delta G_{ala}^{cold} - \Delta G_{native}^{cold}$$

Rearrangement indicates that the difference in two substitutions to alanine describes their relative stability:

$$\Delta\Delta G_{ala}^{hot} - \Delta\Delta G_{ala}^{cold} = \Delta G_{native}^{hot} - \Delta G_{native}^{cold}$$

As such, we propose that one could crudely identify destabilizing or stabilizing mutations by comparing the differences in $\Delta\Delta G_{ala}$ (Figure 3.3). Destabilizing mutations

would produce $\Delta\Delta G_{mut>ala} < \Delta\Delta G_{wt>ala}$ and < -1 kcal/mol (Figure 3.3(B)), while stabilizing mutations would produce $\Delta\Delta G_{mut>ala} > \Delta\Delta G_{wt>ala} > 1$ kcal/mol (Figure 3.3(C)). CAS analysis was performed on the Arp2:Arp3 interaction of the 1K8K, 2P9I, and 2P9K Arp2/3 complex structures available from the Protein Data Bank (PDB) and results are shown in Table 3.1.[13, 22, 47] Three Arp2/3 structures were evaluated in order to assess the conformational sensitivity and variation of hotspots.

3.2 Extended CAS

Identified w.t. "hot spots" were substituted with all other amino acid residues (except proline and glycine) and re-analyzed by CAS to determine the most disruptive amino acid residue other than alanine that would highly destabilize the interface and potentially disrupt the complex. Only the 1K8K structure was analyzed for disruptive mutants and results are shown in Table 3.2. The mutagenesis function of PyMOL, a modeling and visualization software package, was used to create point mutants by substituting the "hot spots" in sub-domains 1 and 3 of Arp3.[48] The mutagenesis process includes selection of a rotamer of the amino acid residue from the supplied Dunbrack backbone-dependent rotamer library.[37] The selection is dependent on the frequency of occurrence of the rotamer at that position (%Mutation) and the type of the quaternary interactions that rotamer renders. Thus, rotamer substitution may develop new quaternary interactions or loose wild-type interactions at the interface. We selected rotamers that produced the lowest Van der Waals steric clash using the *show_bumps.py* and *mutate.py* PyMol code of and which had also the largest %Mutation.[49] We further limited mutant targets to substitutions with best rotamers and lowest $\Delta\Delta G_{ala}$ that also had no steric clash

with the backbone atoms of Arp3 in order to limit tertiary changes. CAS values for each rotamer are shown in Table 3.4.

3.3 Validation of computational mutant prediction

The effects of point mutation of Arp3 were validated by creating the mutants using site-directed mutagenesis (SDM) followed by transient transfection in B35 rat neuroblastoma cells. B35 cells are commonly used to study axonal growth and cell motility (actin dependent processes) and offer substantial advantages such as ease of culture, efficiency of transfection (for transient or stable expression), and ability to establish stable cell lines.[39]

3.4 Generation of green fluorescent protein (GFP) tagged Arp3

Arp3 subunit was tagged with GFP (717 bp). An entry vector containing the complete open reading frame (ORF) of human Arp3 (1371bp) and a destination vector containing GFP (717 bp) and V5 epitope (42 bp) were amplified in One Shot Top 10 cells (E. coli) cultured in Lysogeny broth with appropriate selection markers, specitnomycin and chloramphenicol, respectively.[50] In addition to the GFP and V5 epitope, the destination plasmid vector had chloramphenicol ($Chlor^r$) and ampicillin resistance ($Ampr^r$) genes (N-EmGFP-DEST, Invitrogen) too. Plasmid DNA was isolated using Qiagen Miniprep and Midiprep kits. The Arp3 ORF was transferred into the destination vector by homologous recombination with LR Clonase II (Invitrogen, Carlsbad, CA) in Tris/EDTA. The site-specific digestion by Clonase II of the Arp3 construct was followed by the exchange of Arp3 to the destination vector.

In the final construct, the Arp3 gene had two flanking regions, a GFP gene, and V5 epitope separated by linkers of 15bp and 7bp, respectively. Transformation of *E. coli* with the final recombinant product was followed by the selection of transformed cells based on ampicillin (demonstrates presence of the plasmid) and chloramphenicol sensitivity (confirms successful recombination). The transformation efficiencies were calculated using the control plasmid pUC19. Restriction digestion with BgII and sequencing were used to confirm correct recombination.

3.5 Site directed mutagenesis (SDM)

Site directed mutagenesis was performed to generate Arp3 mutants (b.t. R123A/ h.s. R161A) using a double-primer PCR method. The primers used to mutate wild type arginine to alanine were:

Sense:

5'-CTCCACTCAATACACCAGAAAAC**GCA**GAGTATCTTGCAGAAATTATGT -3'

Antisense:

5'-ACATAATTTCTGCAAGATACTC**TGC**GTTTTCTGGTGTATTGAGTGGAG- 3’

Quick Change II Site-Directed Mutagenesis Kit (Invitrogen, Carlsbad, CA) was used following the kit protocol without any modifications. This protocol employs both forward and reverse primers in the same PCR reaction for 12-18 cycles. The PCR products are denatured and reannealed. The non-mutated methylated parental plasmid is digested with DpnI and the remaining plasmids are transformed into *E.coli* cells. Mutation was verified by sequencing (Biosynthesis).

3.6 Gel electrophoresis

We confirmed the DNA digestion by gel electrophoresis. Samples were mixed 1:1 with loading buffer (bromophenol blue) and electrophoresed through 1.5% agarose gels in Tris-Acetate-EDTA (TAE) buffer for 1 hour at 130 V. DNA was labeled with 25 mg/ml ethidium bromide for 30 min and the size of DNA fragments was compared to a standard DNA ladder.

3.7 Transfection in B35 neuroblastoma cells

B35 rat neuroblastoma cells were used for the expression of the wild type and mutant Arp3. These cells were routinely cultured in 10% fetal bovine serum (FBS)-containing medium and incubated at 37°C until 90% confluent. For splitting cells, 0.25% trypsin in phosphate buffered saline (PBS) was used. For biochemical experiments (co-immunoprecipitation and western blot), cells were seeded in 6-well plates at a density of 20,000 cells/cm2. LipofectamineTM 2000 was used to transfect cells without any modification in the instructions from the manufacturers.

3.8 Immunocytochemistry

Transfection efficiencies were estimated using immunocytochemistry for GFP. For immunocytochemistry experiments, cells were seeded in 6-well plates at a density of 10,000 cells/cm^2. Controls included untransfected and cells transfected with empty vector (vector with GFP but no Arp3). Two days after transfection, the cells were fixed in 4% paraformaldehyde and immunolabeled with mouse anti-V5 (1:200; Invitrogen, Carlsbad, CA) and rabbit anti-GFP (1:200; Invitrogen, Carlsbad, CA) antibodies. Immunolabeling was visualized using appropriate secondary antibodies including Alexafluor 488-

conjugated goat anti- mouse and Alexafluor-555 conjugated donkey anti-rabbit antibodies (Invitrogen, Carlsbad, CA). Actin was stained with Texas Red-phalloidin (165 nM; Invitrogen, Carlsbad, CA). One image per replicate (3 per condition) was captured with 40X and 100X objectives. Transfection efficiencies were estimated by comparing the number of cells expressing GFP to the total number of cells in each image.

3.9 Co-Immunoprecipitation

Co-immunoprecipitation and western blot studies were performed to determine the association between WAVE1 and Arp3 in B35 neuroblastoma cells in different conditions such as untransfected cells, cells transfected with empty vector (EV; GFP alone), GFP-wild type (WT) Arp3 and GFP-R161A Arp3. Cell lysates (400 μg total protein) were precipitated overnight at 4ºC with rabbit anti-WAVE1 antibodies (10 μg) and incubated with protein A agarose beads for 2 hrs at room temperature. Electrophoresis was performed using immunoprecipitates and lysates through 12% sodium dodecyl sulfate polyacrylamide gels (SDS-PAGE) and transferred to nitrocellulose. Nitrocellulose was blocked in 5% nonfat dry milk in Tris buffered saline containing 0.1% Tween-20 (TBST). Blots were probed with rabbit anti-GFP antibodies (1:1000) overnight followed by goat anti-rabbit antibodies-horse radish peroxidase (1:5000) for 2 hours and immunoreactive bands were visualized by enhanced chemiluminescence and quantified using scanning densitometry readings. The nitrocellulose was stripped and re-probed with anti-Arp3 (to confirm the complex formation of WAVE1/Arp3), anti-Arp2 (to determine the influence of Arp3-R161A on association of Arp2 and Arp3 in the complex) and anti-WAVE1 antibodies (to evaluate

the efficiency of the immunoprecipitation). The experimental controls were anti-WAVE1 antibody precipitates of lysates from untransfected and GFP-only cultures; and the negative control for immunoprecipitation was normal rabbit serum precipitates. In addition, reverse immunoprecipitations with anti-GFP or anti-Arp3 antibodies were performed.

ACKNOWLEDGMENTS

We thank Texas Womans University Office of Technology for high performance computing resources. We thank Jairus Reddy and Alexandra Wright for useful discussions. The work of ACM and SH for specific portions of this project were supported by internal funding from TWU (Research Enhancement Program, Multidisciplinary Research Program, and Arts & Sciences Research Development Fund).

REFERENCES

1. Pantaloni D, Le Clainche C, Carlier MF. Mechanism of actin-based motility. Science 2001 May 25;292(5521):1502-6.
2. Svitkina TM, Borisy GG. Arp2/3 complex and actin depolymerizing factor/cofilin in dendritic organization and treadmilling of actin filament array in lamellipodia. J Cell Biol 1999 May 31;145(5):1009-26.
3. Welch MD, Mullins RD. Cellular control of actin nucleation. Annu Rev Cell Dev Biol 2002;18:247-88.
4. Hanson J, Lowy J. The structure of F-actin and of actin filaments isolated from muscle. J Mol Biol 1963;6(1).
5. Pollard TD, Borisy GG. Cellular motility driven by assembly and disassembly of actin filaments. Cell 2003;112(4).
6. Abercrombie M, Heaysman JEM, Pegrum SM. The locomotion of fibroblasts in culture. Exp Cell Res 1970;62(2-3).
7. Lodish, H. F., A. Berk, C. Kaiser, M. Krieger, A. Bretscher, H. Ploegh, A. Amon, and M. Scott, Matsudaira.'. Molecular cell biology. 7th ed. ed. W. H. Freeman and Company, N. Y.; (2012).
8. Chereau D, Kerff F, Graceffa P, Grabarek Z, Langsetmo K, Dominguez R. Actin-bound structures of wiskott-aldrich syndrome protein (WASP)-homology domain 2 and the implications for filament assembly. Proc Natl Acad Sci U S A 2005 Nov 15;102(46):16644-9.

9. Chen Z, Borek D, Padrick SB, Gomez TS, Metlagel Z, Ismail AM, Umetani J, Billadeau DD, Otwinowski Z, Rosen MK. Structure and control of the actin regulatory WAVE complex. Nature 2010;468(7323).

10. Ismail AM, Padrick SB, Chen B, Umetani J, Rosen MK. The WAVE regulatory complex is inhibited. Nat Struct Mol Biol 2009 May;16(5):561-3.

11. Padrick SB, Cheng HC, Ismail AM, Panchal SC, Doolittle LK, Kim S, Skehan BM, Umetani J, Brautigam CA, Leong JM, Rosen MK. Hierarchical regulation of WASP/WAVE proteins. Mol Cell 2008 Nov 7;32(3):426-38.

12. Padrick SB, Doolittle LK, Brautigam CA, King DS, Rosen MK. Arp2/3 complex is bound and activated by two WASP proteins. Proc Natl Acad Sci U S A 2011 Aug 16;108(33):E472-9.

13. Robinson RC, Turbedsky K, Kaiser DA, Marchand JB, Higgs HN, Choe S, Pollard TD. Crystal structure of Arp2/3 complex. Science 2001 Nov 23;294(5547):1679-84.

14. Ti SC, Jurgenson CT, Nolen BJ, Pollard TD. Structural and biochemical characterization of two binding sites for nucleation-promoting factor WASp-VCA on Arp2/3 complex. Proc Natl Acad Sci U S A 2011 Aug 16;108(33):E463-71.

15. May RC. The Arp2/3 complex: A central regulator of the actin cytoskeleton. Cell Mol Life Sci 2001 Oct;58(11):1607-26.

16. Volkmann N, Amann KJ, Stoilova-McPhie S, Egile C, Winter DC, Hazelwood L, Heuser JE, Li R, Pollard TD, Hanein D. Structure of Arp2/3 complex in its

activated state and in actin filament branch junctions. Science 2001 Sep 28;293(5539):2456-9.

17. Schutt CE, Myslik JC, Rozycki MD, Goonesekere NC, Lindberg U. The structure of crystalline profilin-beta-actin. Nature 1993 Oct 28;365(6449):810-6.

18. Sheterline P, Clayton J, Sparrow J. Actin. Protein Profile 1995;2(1):1-103.

19. Rouiller I, Xu XP, Amann KJ, Egile C, Nickell S, Nicastro D, Li R, Pollard TD, Volkmann N, Hanein D. The structural basis of actin filament branching by the Arp2/3 complex. J Cell Biol 2008 Mar 10;180(5):887-95.

20. Dominguez R. Actin filament nucleation and elongation factors--structure-function relationships. Crit Rev Biochem Mol Biol 2009 Nov-Dec;44(6):351-66.

21. Machesky LM, Mullins RD, Higgs HN, Kaiser DA, Blanchoin L, May RC, Hall ME, Pollard TD. Scar, a WASp-related protein, activates nucleation of actin filaments by the Arp2/3 complex. Proc Natl Acad Sci U S A 1999 Mar 30;96(7):3739-44.

22. Nolen BJ, Pollard TD. Insights into the influence of nucleotides on actin family proteins from seven structures of Arp2/3 complex. Mol Cell 2007 May 11;26(3):449-57.

23. Rodal AA, Sokolova O, Robins DB, Daugherty KM, Hippenmeyer S, Riezman H, Grigorieff N, Goode BL. Conformational changes in the Arp2/3 complex leading to actin nucleation. Nat Struct Mol Biol 2005 Jan;12(1):26-31.

24. Kelleher JF, Atkinson SJ, Pollard TD. Sequences, structural models, and cellular localization of the actin-related proteins Arp2 and Arp3 from acanthamoeba. J Cell Biol 1995 Oct;131(2):385-97.

25. Dalhaimer P, Pollard TD, Nolen BJ. Nucleotide-mediated conformational changes of monomeric actin and Arp3 studied by molecular dynamics simulations. J Mol Biol 2008 Feb 8;376(1):166-83.

26. Nolen BJ. Crystal structures of actin-related protein 2/3 complex with bound ATP or ADP. Proceedings of the National Academy of Sciences 2004;101(44).

27. Abraham VC, Krishnamurthi V, Taylor DL, Lanni F. The actin-based nanomachine at the leading edge of migrating cells. Biophys J 1999 Sep;77(3):1721-32.

28. Koestler SA, Rottner K, Lai F, Block J, Vinzenz M, Small JV. F- and G-actin concentrations in lamellipodia of moving cells. PLoS One 2009;4(3):e4810.

29. Higgs HN, Blanchoin L, Pollard TD. Influence of the C terminus of wiskott-aldrich syndrome protein (WASp) and the Arp2/3 complex on actin polymerization. Biochemistry 1999 Nov 16;38(46):15212-22.

30. Lee SH, Kerff F, Chereau D, Ferron F, Klug A, Dominguez R. Structural basis for the actin-binding function of missing-in-metastasis. Structure 2007 Feb;15(2):145-55.

31. Marchand JB, Kaiser DA, Pollard TD, Higgs HN. Interaction of WASP/scar proteins with actin and vertebrate Arp2/3 complex. Nat Cell Biol 2001 Jan;3(1):76-82.

32. Boczkowska M, Rebowski G, Kast DJ, Dominguez R. Structural analysis of the transitional state of Arp2/3 complex activation by two actin-bound WCAs. Nature Communications 2014;5.

33. Dalhaimer P, Pollard TD. Molecular dynamics simulations of Arp2/3 complex activation. Biophys J 2010 Oct 20;99(8):2568-76.

34. Hetrick B, Han MS, Helgeson LA, Nolen BJ. Small molecules CK-666 and CK-869 inhibit actin-related protein 2/3 complex by blocking an activating conformational change. Chem Biol 2013;20(5).

35. Wilson AJ. Inhibition of protein-protein interactions using designed molecules. Chem Soc Rev 2009 Dec;38(12):3289-300.

36. Clackson T, Wells JA. A hot spot of binding energy in a hormone-receptor interface. Science 1995 Jan 20;267(5196):383-6.

37. Dunbrack RL,Jr, Cohen FE. Bayesian statistical analysis of protein side-chain rotamer preferences. Protein Sci 1997 Aug;6(8):1661-81.

38. Homologene. <http://www.ncbi.nlm.nih.gov/homologene>. .

39. Otey,C.A.,Boukhelifa,M., Maness,P. B35 neuroblastoma cells: An easily transfected, cultured cell model of central nervous system neurons. In: Hollenbeck,P., Bamburg,J., editor. Neurons: Methods and applications for the cell biologist. ; 2003.

40. Dent EW, Gupton SL, Gertler FB. The growth cone cytoskeleton in axon outgrowth and guidance. Cold Spring Harb Perspect Biol 2011 Mar 1;3(3):10.1101/cshperspect.a001800.

41. Schaefer AW, Schoonderwoert VTG, Ji L, Mederios N, Danuser G, Forscher P. Coordination of actin filament and microtubule dynamics during neurite outgrowth. Developmental Cell 2008;15(1).

42. Korobova F, Svitkina T. Arp2/3 complex is important for filopodia formation, growth cone motility, and neuritogenesis in neuronal cells. Mol Biol Cell 2008 Apr;19(4):1561-74.

43. Krissinel,E.,Henrick,K. Detection of protein assemblies in crystals. 2005.

44. Kortemme T, Kim DE, Baker D. Computational alanine scanning of protein-protein interfaces. Sci STKE 2004 Feb 3;2004(219):pl2.

45. Kortemme T, Baker D. A simple physical model for binding energy hot spots in protein-protein complexes. October 29, 2002;99(22):14116.

46. Baker D. Robetta: Full-chain protein structure prediction server. <http://robetta.bakerlab.org/>. .

47. Berman HM, Battistuz T, Bhat TN, Bluhm WF, Bourne PE, Burkhardt K, Feng Z, Gilliland GL, Iype L, Jain S, Fagan P, Marvin J, Padilla D, Ravichandran V, Schneider B, Thanki N, Weissig H, Westbrook JD, Zardecki C. The protein data bank. Acta Crystallogr D Biol Crystallogr 2002 Jun;58(Pt 6 No 1):899-907.

48. Schrödinger. The PyMOL Molecular Graphics System, Version 1.5.04 Schrodinger, LLC.

49. Holder T. 2011 <https://raw.githubusercontent.com/Pymol-Scripts/Pymol-script-repo/master/show_bumps.py>. .

50. BERTANI G. Sensitivities of different bacteriophage species to ionizing radiations. J Bacteriol 1960 Mar;79:387-93.

TABLES

	PDB id : 1K8K		PDB id: 2P9I		PDB id: 2P9K	
	Residue #	$\Delta\Delta G_{ala}$	Residue #	$\Delta\Delta G_{ala}$	Residue #	$\Delta\Delta G_{ala}$
Arp3	L117	0.15	L177	0.32	L117	0.32
	T119	0.02	T119	0.04	T119	0.04
			E121	0.18		
	R123	3.98	R123	1.17	R123	6.27
	Y184	0.77	Y184	0.49	Y184	0.61
			V185	0.1		
	I186	0.66	I186	0.64	I186	0.72
	S188	1.78	S188	0.97	S188	0.83
	C189	-0.01	C189	-0.01	C189	-0.01
	D310	0.41				
			C307	-0.01	C307	0.00
	V311	0.02			V311	0.02
	S406	-0.02				
	R409	1.32	R409	1.82	R409	0.49
	H410	0.94	H410	0.51	H410	0.8
Arp2	L198	0.81			L199	0.21
	L199	0.25				
	R200	0.24	R200	0.03	R200	0.94
	Y202	0.56	Y202	0.62	Y202	0.52
	F204	0.02	F204	0.05	F204	0.05
	N205	2.14	N205	2.16	N205	1.56
	H206	-0.01	H206	0.01	H206	0.01
	S207	0.39	S207	-0.09	S207	0.01
	D209	1.35	D209	0.76	D209	0.57
	E248	2.29	E248	1.87	E248	1.68
	R250	1.69	R250	1.52	R250	1.27
			K253	0.29	K253	-0.09

Table 3.1: *Computational alanine scan output for different conformations of Arp2/3 complex*. Values are in kcal/mol. Greyed cells represent energetically important hot spots at the interface ($\Delta\Delta G_{ala} \geq 1.0$ kcal/mol).

	$\Delta\Delta G_{ala}$ (kcal/mol)		
	1K8KA:R123	1K8K:S188	1K8K:R409
1 ALA (A)	A*	0.00†	0.00†
2 CYS (C)	A	-0.18	-0.15
3 ASP (D)	A	-0.34	-0.15
4 GLU (E)	A	**-1.04**	0.26
5 PHE (F)	A	-0.31	0.67
6 GLY (G)	NP	NP	NP
7 HIS (H)	A	-0.1	0.28
8 ILE (I)	A	0.46	0.5
9 LYS (K)	0.28	0.6	0.19
10 LEU (L)	A	1.03	0.62
11 MET (M)	A	0.34	0.17
12 ASN (N)	A	0.62	0.18
13 PRO (P)	NP	NP	NP
14 GLN (Q)	A	**-1.07***	0.57
15 ARG (R)	Self	0.17	Self
16 SER (S)	A	Self	-0.12
17 THR (T)	A	1.77	0.42
18 VAL (V)	A	0.29	0.15
19 TRP (W)	A	1.85	**-1.63***
20 TYR (Y)	A	1.18	0.63

Table 3.2: *CAS output for substituted amino acid residues of Arp3 at positions R123, S188, and R409*. **A**: residue leaves quaternary interaction upon substitution. **Self**: wild type residues. **NP**: CAS not performed due to limits in the methodology. * Chosen for mutation. † Substitution to alanine followed by CAS yields $\Delta\Delta G_{ala} = 0.0$ by definition.

Position	Rotamer	%Mutation	Strain	$\Delta\Delta G_{ala}$ (kcal/mol)
S188	**Ser_r1**	83.1	149	1.76
	Ser_r2	15.8	182	1.57
	Ser_r3	1.1	159	0.65
R409	Arg_r1	16.6	498	-2.25
	Arg_r2	10.5	301	-0.55
	Arg_r3	7.3	520	-4.07
	Arg_r4	7	181	0.49
	Arg_r5	5.3	601	-4.1
	Arg_r6	4.7	402	0.61
	Arg_r7	4.5	479	-5.34
	Arg_r8	3.6	182	0.87
	Arg_r9	2.5	972	-12.25
	Arg_r10	2.4	524	-5.35
	Arg_r11	2.4	656	-7.02
	Arg_r12	2.3	867	0.18
	Arg_r13	2.1	763	0.23
	Arg_r14	2.1	406	-0.37
	Arg_r15	1.7	882	-4.23
	Arg_r16	1.7	773	-8.6
	Arg_r17	1.7	589	-3.85
	Arg_r18	1.7	558	-4.05
	Arg_r19	1.6	1045	1.37
	Arg_r20	1.5	434	-0.48
	Arg_r21	1.4	306	0.91
	Arg_r22	1.3	306	-0.84
	Arg_r23	1.3	632	0.2
	Arg_r24	1.2	335	0.12
	Arg_r25	1.2	335	0.32
	Arg_r26	1	887	-8.92
	Arg_r27	1	201	0.16

Table 3.3: *Rotamer selection for self-substitution of S188S and R409R*.

Dunbrack rotamers ranked by likelihood (%Mutation) for Ser and Arg. VDW strain generated by PyMol culpt due to rotamer orientation and atomic packing. $\Delta\Delta G_{ala}$ from computational alanine scanning of structure 1K8K after rotamer substitution for original conformation. Bold Letters represents the selected "best" rotamer frame based on the strain number.

	R123A		*S188Q*		*R409W*	
	Residue #	$\Delta\Delta G_{ala}$	***Residue #***	$\Delta\Delta G_{ala}$	***Residue #***	$\Delta\Delta G_{ala}$
Arp3	L117	0.15	L117	0.15	L117	0.15
	T119	0.02	T119	0.02	T119	0.02
	A123		R123	3.98	R123	3.98
	Y184	0.76	Y184	0.77	Y184	0.77
	I186	0.66	I186	0.66	I186	0.66
	S188	1.78	Q188	-1.07	S188	1.78
	C189	-0.01	C189	-0.01	C189	-0.01
	D310	0.41	D310	0.41	D310	0.41
	V311	0.02	V311	0.02	V311	0.02
	S406	-0.02	S406	-0.02	S406	-0.02
	R409	1.32	R409	1.32	W409	-1.63
	H410	0.94	H410	0.94	H410	0.94
Arp2	L198	0.8	L198	0.81	L198	0.81
	L199	0.25	L199	0.25	L199	0.32
	R200	0.24	R200	0.24	R200	0
	Y202	0.62	Y202	0.56	Y202	0.57
	F204	0.02	F204	0.05	F204	0.02
	N205	2.14	N205	2.14	N205	2.14
	H206	-0.01	H206	-0.01	H206	-0.01
	S207	0.39	S207	0.39	S207	0.39
	D209	1.35	D209	-1.59	D209	1.35
	E248	2.29	E248	2.28	E248	2.29
	R250	1.69	R250	1.69	R250	1.69

Table 3.4: *Computational alanine scan for R123A, S188Q, and R409W mutant conformations of Arp2/3 complex*. All structures are based on PDBid 1K8K. Values are in kcal/mol. Greyed cells represent energetically important hot spots at the interface (ΔGala $\geq$ 1.0 kcal/mol). Black cells are predicted to be destabilizing interactions upon mutation.

FIGURES

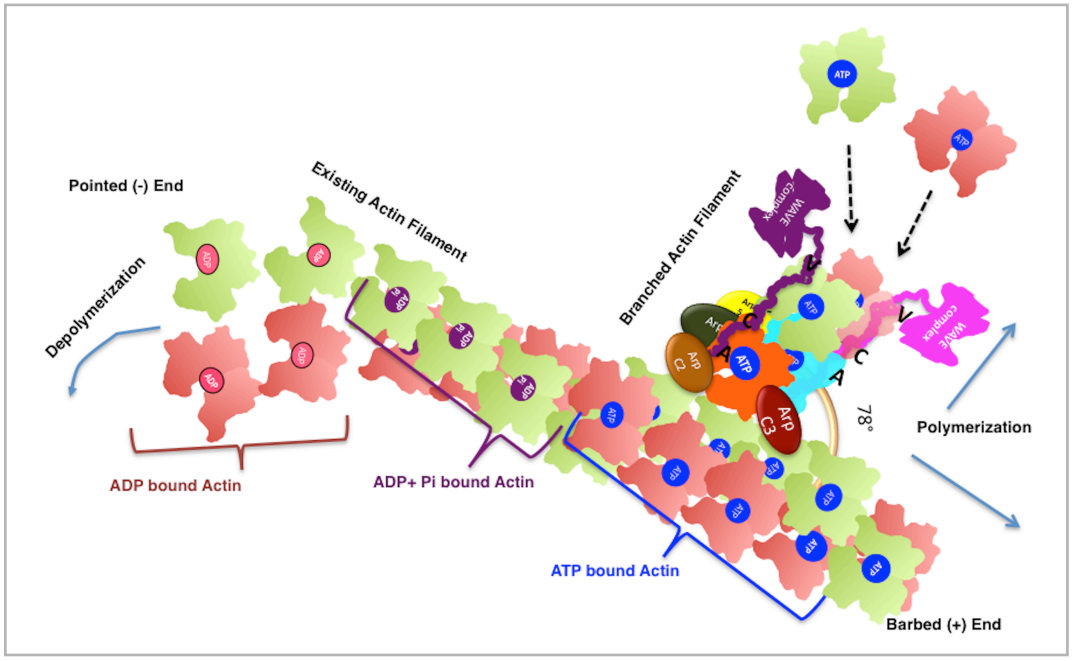

Figure 3.1: *Model Representation of Branched Actin Filament.*

Orange subunit with blue solid circle: ATP bound Arp3; Cyan subunit with Blue solid circle: ATP-bound Arp2; Green or light orange with blue solid circle: ATP-bound actin; Green or light orange with orange solid circle: ADP-bound actin; Green or light orange with purple solid circle: ADP+Pi bound actin; Purple and pink units: Wiskott-Aldrich complex with VCA domain; Brown/yellow/dark red/dark green: accessory proteins of Arp2/3 complex [12, 14, 19].

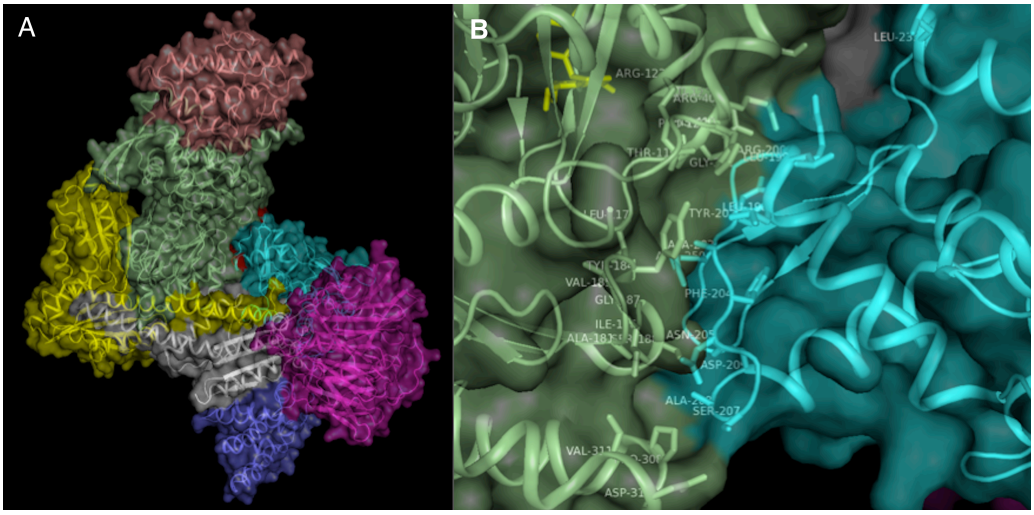

Figure 3.2: ***(****A) Cartoon representation of Arp2/3 complex (PDB id: 1K8K).* Pale green: Arp3; Cyan:Arp2, Magenta:ArpC1; Yellow:ArpC2; Salmon:ArpC3; White:ArpC4;Blue:ArpC5. Red colored surface represents interfacial residues of Arp2:Arp3 dimer. (B) Close view of Arp2:Arp3 interface (PDB id: 1K8K). Pale green: Arp3; Cyan: Arp2; Sticks represent the side chains of amino acid residues of Arp2 and Arp3 at the interface within 4.0 Å of each other, respectively; Yellow sticks represent the Arp2/3 complex inhibitor CK-869 PDB id: 3UKU [34] after superposition of Arp3.

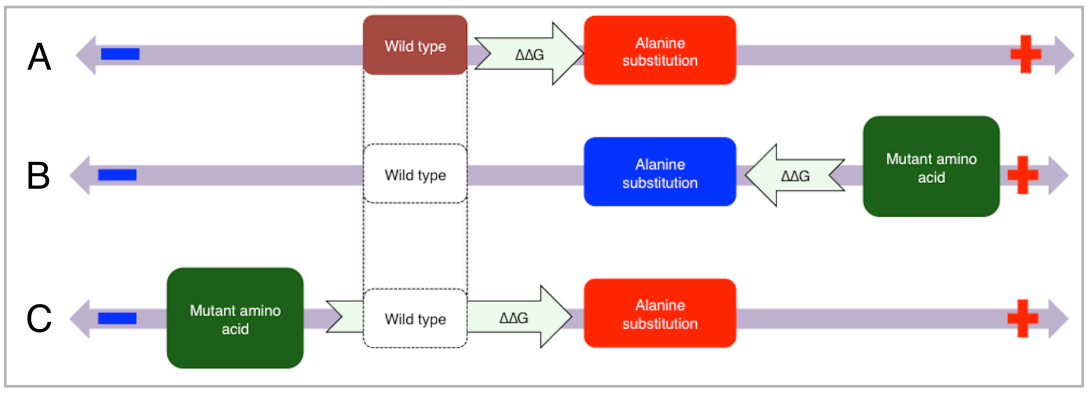

Figure 3.3: *Interpretation of the free energy change due to alanine substitution in the wild type and mutant amino acid of Arp3 at Arp2:Arp3 dimer interface.* (A) Identification of the energetically important residue: $\Delta\Delta G_{ala} \geq 1$ kcal/mol, alanine destabilization indicates the w.t. stabilizes the interface. Designing the mutant: (B) $\Delta\Delta G_{mut>ala} \leq -1$ kcal/mol, indicates mutant amino acid destabilizes the interface. (C) $\Delta\Delta G_{mut>ala} \geq \Delta\Delta G_{wt>ala} \geq 1$kcal/mol indicates mutant amino acid had more stabilization effect than the wild type residue. Negative and positive signs represent the directional negative and positive change in the pseudo-free energy change upon alanine substitution, respectively.

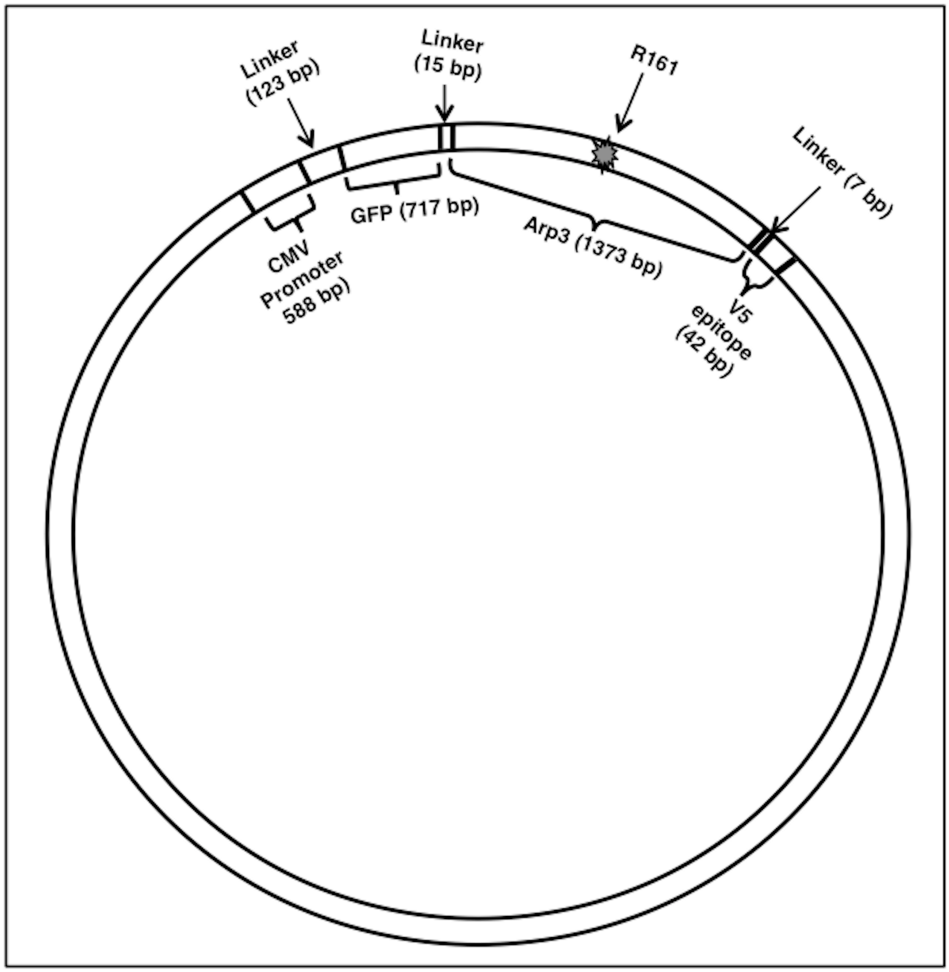

Figure 3.4: *Plasmid map for the GFP-Arp3 construct.*

The positions for the mutation site for R123A (R161A in *Homo sapiens*) in the Arp3 gene, the GFP tag, and V5 epitope tag are shown. Both GFP and V5 epitope are separated by 15 bp and 7 bp linkers, respectively. The CMV promoter is 123 bp upstream of this construct.

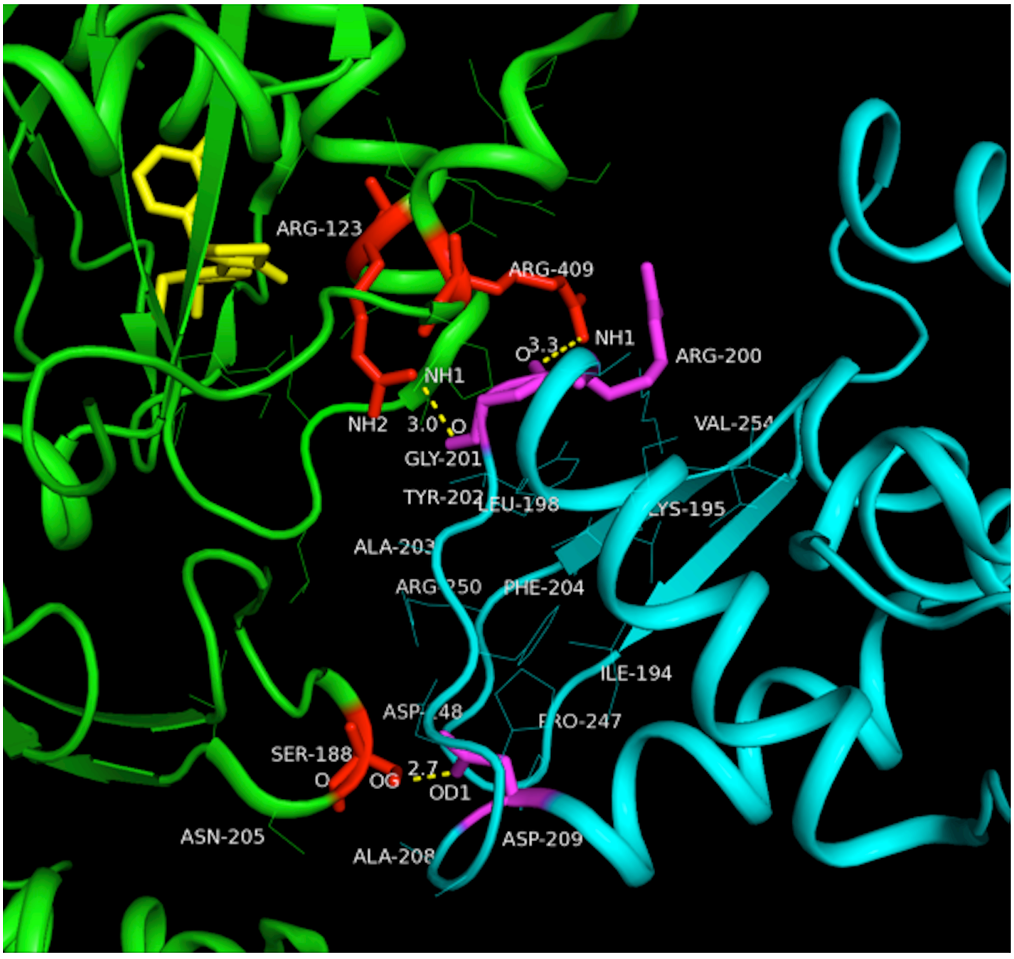

Figure 3.5: *Key residues present at the Arp2:Arp3 interface of the Arp2/3 complex. (PDB id 1K8K)* Green cartoon: Arp3; Cyan cartoon: Arp2; Red sticks: side chains of amino acid residues of Arp3 (R123, S188, and R409); Magenta sticks: side chains of interacting amino acid residues of Arp2 (D209, G201, and R200). Thin sticks: side chains of amino acid residues that are involved in the hydrophilic or hydrophobic interactions at the interface. Yellow sticks represent the Arp2/3 complex inhibitor CK-869 after superposition (PDB id: 3UKU). Alanine substitutions of each red residue individually are destabilizing to the complex.

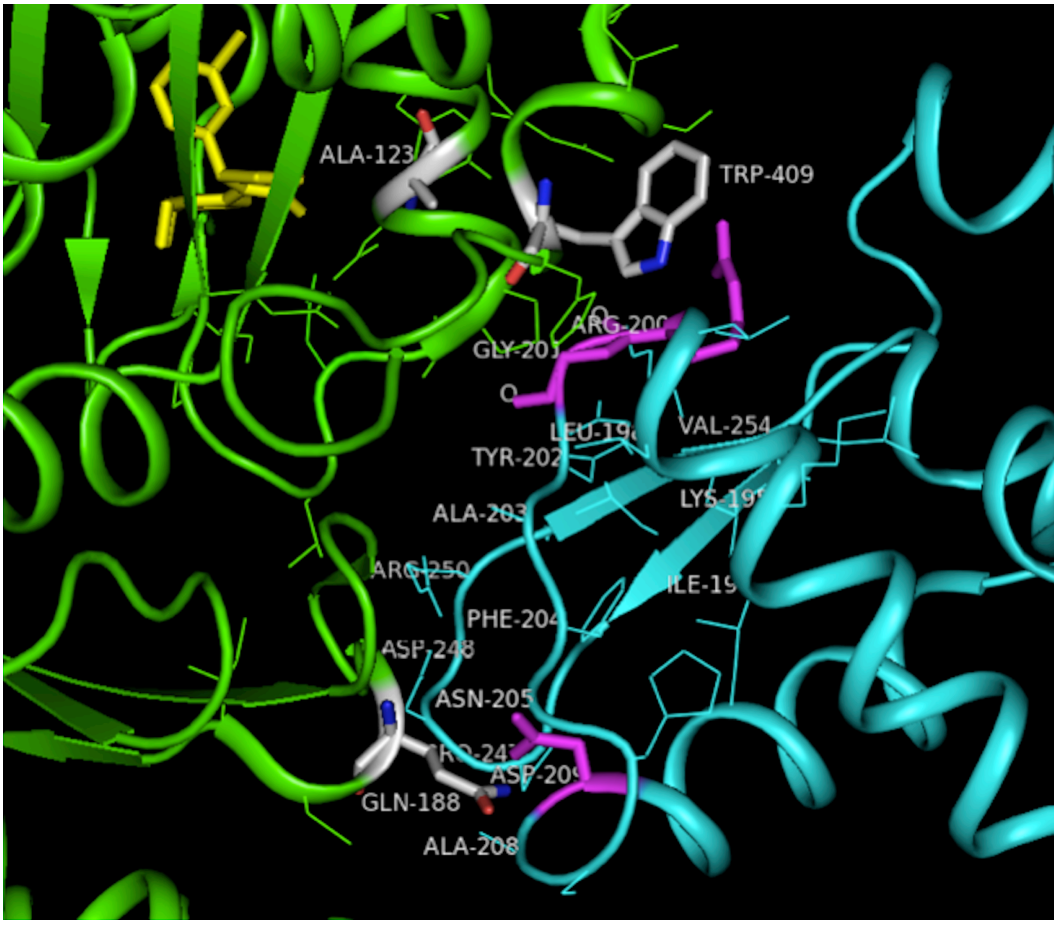

Figure 3.6: *Close view of R123A, S188Q, and R409W at the Arp2:Arp3 interface of the Arp2/3 complex (PDBid 1K8K).* Green cartoon: Arp3; Cyan cartoon: Arp2; White sticks: R123A, S188Q, and R409W mutant rotamers in Arp3. Magenta sticks: side chains of interacting amino acid residues of Arp2 (D209, G201, and R200). Thin sticks: side chains of amino acid residues that are involved in the hydrophilic or hydrophobic interactions at the interface. Yellow sticks represent the Arp2/3 complex inhibitor CK-869 after superposition (PDB id: 3UKU). Rotamer positions of mutants represent lowest strain coupled with highest probability (see Methods).

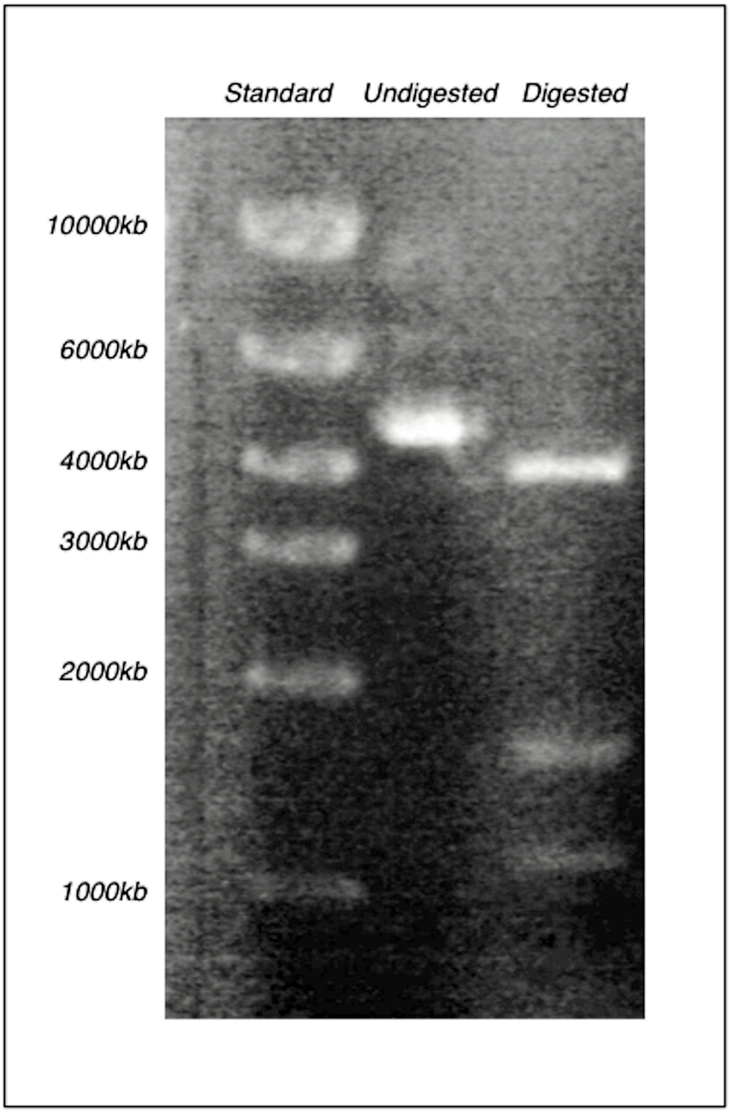

Figure 3.7: *Restriction digestion of recombinant GFP-Arp3 WT with BglI restriction enzyme.* 1.5% agarose gel electrophoresis was used to separate the fragments. The digest pattern of bands at 4000, 1800 and 1200 bp suggests that the vector contained Arp3 in the correct orientation.

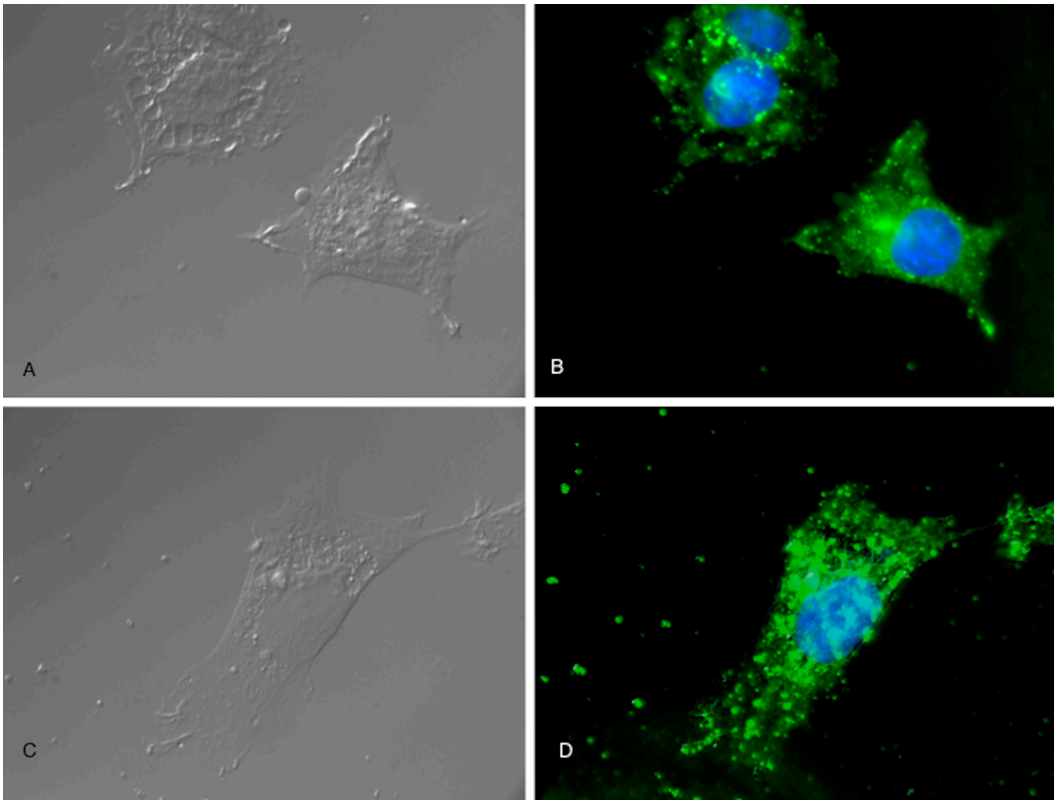

Figure 3.8: *Immunocytochemistry of GFP and GFP-tagged Arp3 transfected B35 neuroblastoma cells with Anti-GFP antibodies (100X).* (A,C) Differential Interference Contrast (DIC). (B,D) Fluorescence images. GFP/GFP-Arp3 expression (green) with nucleus specific DAPI staining (blue). (A,B): GFP expression; (C,D): GFP-Arp3 expression. Cells are viable and exhibit normal neurite morphology.

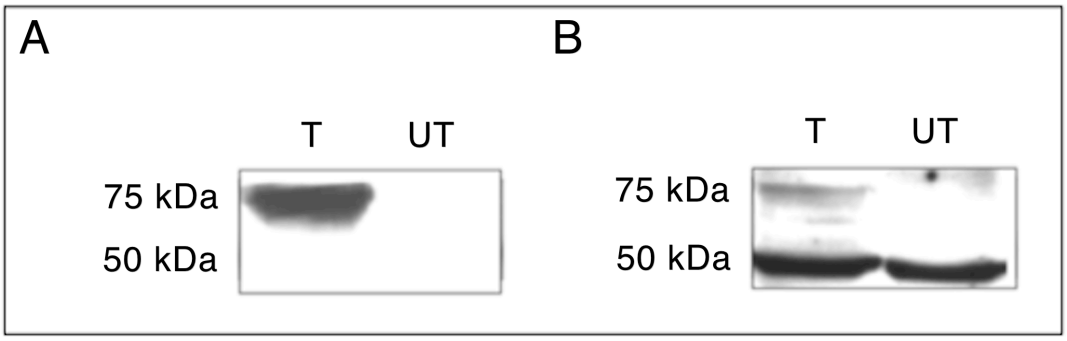

Figure 3.9: *Western blot analysis of B35 neuroblastoma cells to confirm the transfection of GFP-tagged Arp3. 50 kDA, 75 kDa: expected molecular weights of Arp3 and GFP-Arp3, respectively.* (A) *Anti-GFP antibodies*: The presence of only a 75 kDa band in the transfected lane (T) and absence of bands in the untransfected lane (UT) suggests cells were transfected either with empty GFP vector or GFP-Arp3 vector. (B) *Anti-Arp3 antibodies:* The presence of a 50 kDa band in both lanes confirms the expression of endogenous Arp3 was not prevented during the transfection. The presence a light band at 75kDa indicates the presence of GFP-Arp3.

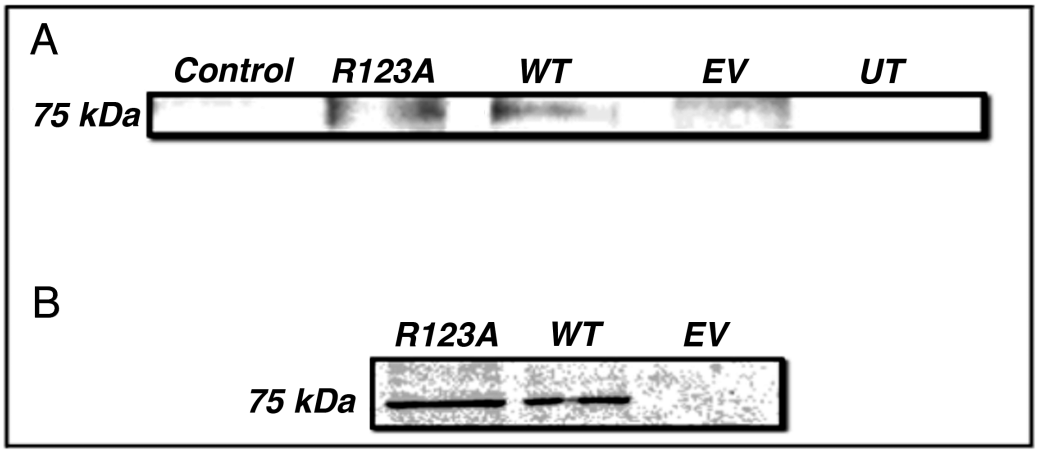

Figure 3.10: *Co-immunoprecipitation of B35 neuroblastoma cells using anti-Arp2 antibodies.*

UT: Untransfected; EV: empty vector, only GFP present; WT: wild type GFP-Arp3; R123A: GFP-Arp3:R123A; (b): Input blot with anti-Arp2 antibodies.

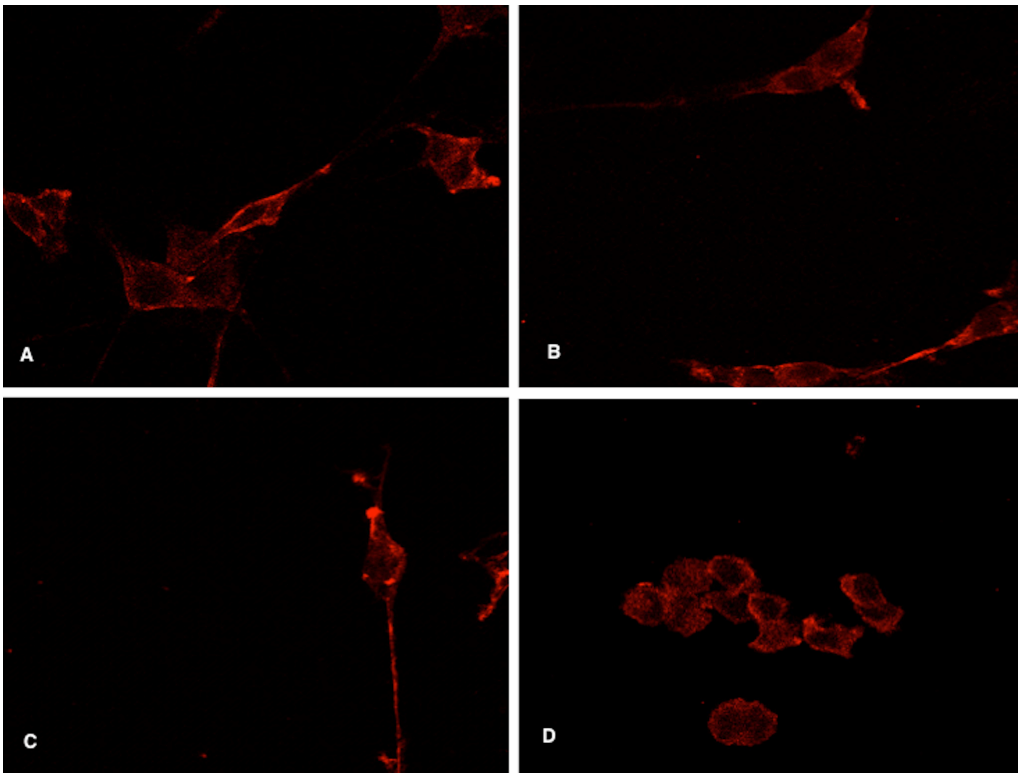

Figure 3.11: *Representative 100X images of B35 neuroblastoma cells stained with phalloidin.*

(A): Untransfected cells; (B): cells transfected with empty vector (GFP only); (c): cells transfected with w.t. GFP-Arp3; (d): cells transfected with GFP-Arp3:R123A.

CHAPTER IV

MUTATING Arp3 R161 DECREASES NEURITE OUTGROWTH WITHOUT DISRUPTING WAVE AND ARP2/3 COMPLEX INTERACTIONS

Sounick Haldar[1], Amruta C. Mahadik[1], Brian W. Beck[2] , and DiAnna L. Hynds[1†]

1 Department of Biology, Texas Woman's University, Denton, Texas, United States of America

2 Texas Advanced Computing Center, University of Texas at Austin,

Austin, Texas, United States of America

† Author to whom correspondence should be addressed: dhynds@twu.edu

Present address: Department of Biology, PO Box 425799, Denton, TX 76204-5799.

Telephone: 940-898-2359

Author Contributions:

- Haldar, Mahadik, Beck, and Hynds conceived the project, developed the protocols, and prepared the initial manuscript
- Haldar collected all bench-based experimental data.
- Mahadik collected all computational experimental data and prepared the final manuscript.

ABSTRACT

The Arp2/3 complex is an actin filament nucleator composed of two evolutionarily conserved major subunits, Arp2 and Arp3, and five accessory subunits (ARPC1, ARPC2, ARPC3, ARPC4, and ARPC5). During nucleation of actin branches, Arp2 and Arp3 undergo a conformational change to form an "actin-like" dimer and provide a template for actin monomers to polymerize into a daughter actin filament. The Arp2/3 complex is intrinsically inactive and its activation requires binding to an existing actin filament and to regulatory proteins called Nucleation Promoting Factors (NPFs). NPFs constitute a family of proteins, each of which contains a C-terminal VCA motif. NPFs modulate the Arp2/3 conformational activation via CA-domain interactions with Arp2 and Arp3 and V-domain binding to new daughter actins. In our recent work, we have identified residues critical to the stability of the native inactive state of the Arp2/3 complex. Upon Arp3: R161A mutation, we observed stable Arp2/3 complex formation, increased cortical actin, but reduced neurite outgrowth, suggesting a constitutively active Arp2/3 complex in B35 neuroblastoma cells.

Here we further characterize the effect of the Arp3:R161A mutant on actin filaments, including rate of filament formation, and alteration in the neurite outgrowth, including number of neurite bearing cells, number of neurites per cell, and branches of neurites per cell. Quantification of these characteristics suggests that not only is Arp3:R161A constitutively active, but that excess actin branch formation favors lamellipodia at the expense of filopodia, thus reducing neurite outgrowth.

ABBREVIATIONS AND SYMBOLS

A-domain: Acidic domain

Arp: Actin Related Protein

Arp 2/3 Complex: Actin Related Protein 2/3 Complex

CAS: Computational Alanine Scanning

C-domain: Central domain

CNS : Central Nervous System

DIC : Differential Inference Contrast

FRET : Fluorescence Resonance Energy Transfer

ICT : Immunocytochemistry

ITC : Isothermal Titration Calorimetry

NPF: Nucleation Promoting Factors

PDB: Protein Data Bank

RMSD: Root Mean Square Deviation

V-domain: Verprolin domain

WA Family: Wiskott-Aldrich Family

WASP: Wiskott-Aldrich Syndrome Protein

WAVE Wiskott-Aldrich syndrome Verprolin homolog

INTRODUCTION

Axon growth during development, regeneration, and plasticity of neurons results from extension of a sensory motile structure, the growth cone, located at the tips of extending axons. Forward extension of growth cones requires expansion of peripheral domain lamellipodia, structures containing an actin filament meshwork.[1] In particular, nucleation and polymerization of globular actin (G-actin) into filamentous actin (F-actin) near the leading plasma membrane of an extending growth cone is important for axon extension, a process regulated by the actin-related protein 2/3 complex (Arp2/3).[2-5] Arp2/3 complex is composed of two major subunits, Arp2 and Arp3, along with five accessory subunits (ARPC1, ARPC2, ARPC3, ARPC4, and ARPC5).[6, 7] The accessory subunits, ARPC1-5, facilitate the binding of the Arp2/3 complex to existing actin filaments (so-called "mother" filaments) by mediating quaternary interactions between cofactors and the existing mother filament.[8] Arp2 and Arp3 form a "short pitch" actin-like dimer that acts as a template for G-actin to polymerize into branching daughter filaments.[7-10] The Arp2/3 complex has been shown to exist in three major nucleotide-binding cleft conformations: open, intermediate, and closed, as well as in inactive and active quaternary conformations.[9, 10] During branching of the actin filament, the Arp2/3 complex interacts with the existing actin filament and nucleation promoting factors such as such as WASP, N-WASP, WAVE and WHAMM, each of which contain a conserved C-terminal VCA region.[11, 12] The VCA region of Wiskott-Aldrich (WA) family proteins regulates nucleation and branching, whereas other domains in the complex facilitate

cellular localization.[11, 13-15] The VCA region consists of V (verprolin), C (central), and A (acidic) domains that modulate interactions with actin (V domain) and the Arp2/3 complex (CA domain) at actin branch points.[16-18]

Upon interaction with an activating WA family protein, an open and inactive Arp2/3 complex bound to an existing mother filament adopts a closed and active conformation.[19, 20] It is this rearrangement of Arp2 and Arp3 subunits within the complex that allows formation of an F-actin-like surface for daughter actin filament polymerization.[17, 18, 21] The WA family V-domain has high affinity for actin, relative to the C-domain, which is thought to bind Arp2 and Arp3.[17] V-domain bound actin has strong affinity for Arp2 but activates the Arp2/3 complex weakly. On the other hand, V-domain bound actin has a lower affinity towards Arp3, but Arp3 binding results in strong activation of the complex.[17] However, ITC and FRET studies have shown that V-domain bound actin binds first to Arp2 and ArpC1. This in turn produces a partial conformational change at the barbed end of Arp3.[21] While both studies differ in whether V-domain bound actin binds primarily to Arp2 or Arp3, they confirm that conformational changes in Arp3 are involved in activating the Arp2/3 complex. CA domain binding to the hydrophobic cleft present in sub-domain 1 of Arp2 or Arp3 modulates the quaternary interactions between Arp2 and Arp3 subunits within the complex.[21]

In our previous work, we used computational alanine scanning (CAS) and site-directed mutagenesis to assess the quaternary interaction and relative importance of specific interfacial residues present at the Arp2:Arp3 dimer interface.[22] CAS uses simple energy functions to measure the change in the pseudo-free energy due to substitution of

alanine for individual interfacial wild type amino acids.[23] In that work, we identified Arp3 residues R161, S226, and R447 (*homo sapiens* sequence numbering) as playing a dominant role in inactive state conformational stability. We demonstrated that site-directed mutagenesis of Arp3 R161A followed by transient transfection in B35 rat neuroblastoma cells altered cell morphology, reduced neurite outgrowth, and increased cortical actin filament concentration. We suggested that Arp3 R161A likely constitutively activates the Arp2/3 complex by destabilizing the inactive state and promoting actin filament formation and branching.

Here, we expand the previous work by characterizing the phenotypic changes in neurite outgrowth and lamellipodia formation in B35 rate neuroblastoma cells upon Arp3 R161A mutation. We correlate these changes to observed variation in Arp2/3 complex formation and actin filament conformation and distribution. We hypothesize that: (1) Arp3:R161A mutants alter the Arp2/3 quaternary conformation without affecting the binding of other subunits in Arp2/3 complex; (2) Constitutive activation leads to increased oligomerization of actin filaments, particularly in the actin-rich lamellipodial structures; (3) Increases in the lamellipodial actin are the source of changes to neurite outgrowth. In this work, we used immunocytochemistry and phase contrast image analysis to quantify the effects of Arp3: R161A on neurite outgrowth and on actin polymerization in B35 neuroblastoma cells.

RESULTS

4.1 Expression of Arp3-R161A does not affect binding of other Arp2/3 members to WAVE

Using co-immunoprecipitation, we assessed whether mutating residue R161 in Arp3 prevents interaction with its activator, WAVE. GFP immunoprecipitates isolated from cell extracts of cells expressing wild-type or mutant Arp3 had Arp3 immunoreactive bands at approximately 75 kDa (the expected molecular weight of the GFP fusion proteins), whereas untransfected cells or cells transfected with GFP-only vectors (empty vectors) did not have these immunoreactive bands, suggesting that these two categories of cells expressed the GFP-Arp3 chimeric proteins (Figure 4.1). Negative control immunoprecipitation with normal rabbit serum confirmed successful immunoprecipitation. Reciprocal immunoprecipitation yielded similar results (data not shown). The lane of extracts from cells expressing mutant Arp3, however, showed increased Arp3 immunoreactivity, perhaps indicating an effect of the mutation on the efficacy of Arp3-antibody binding or increased production of the mutant compared to cells expressing the wild-type construct. When extracts of cells transfected with either wild-type or mutant Arp3 were co-immunoprecipitated with anti-Arp2 and blotted for WAVE, immunoreactive bands of approximately 62 kDa with similar band intensities were observed in the untransfected, empty vector, wild-type and mutant lanes, but not in cell extracts immunoprecipitated with normal rabbit serum (Figure 4.2).

Similar results were seen with reciprocal co-immunoprecipitations. Together these data suggest that the fusion proteins are being expressed and can be precipitated,

and that the interaction of members of the Arp2/3 complex with WAVE is not precluded by the Arp3 mutation.

4.2 Expression of Arp3-R161A decreases neurite outgrowth

We used image analysis to assess how expressing wild-type or mutant Arp3 in B35 cells affects neurite outgrowth. Immunocytochemical images of untransfected cells (Figure 4. 3 A-E) and cells transfected with GFP only (Figure 4. 3 F-J), GFP-Arp3 (WT; Figure 4.3 K-O), or GFP-Arp3-R161A (R161A; Figure 4.3 P-T) show similar cellular morphology for untransfected, empty vector (only GFP) and GFP-Arp3 (WT) transfected cells, with the majority of cells elaborating long neurites (Figure 4.3). In contrast, cells expressing GFP-Arp3 (R161A) elaborated few or no neurites and typically had a rounded cell morphology with increased phalloidin staining at the cell cortex (Figure 4.3 S and T). Untransfected cells did not show any GFP immunoreactivity.

The mean of the percentage of neurite-bearing cells in the R161A group was 23.94% ($p \leq 0.05$) (range 0% - 66.67%), as compared to 96.29% (range 66.67% - 100%), 90.74% (range 50% - 100%) and 91.66% (range 50% - 100%) for the untransfected, empty vector and wild type groups, respectively (Figure 4.4). This might suggest that the cells expressing the Arp3 mutant (R161A) had decreased neurite initiation. Similarly, the number of neurites per cell (only including cells with neurites) was significantly decreased in cells expressing Arp3-R161A, with a mean of 1.40 (range 1 to 2; $p \leq 0.05$), as compared to the mean of 1.68 (range 1 to 3), 1.96 (range 1 to 3) or 2.15 (range 1 to 4) for the wild-type, empty vector, or untransfected groups respectively (Figure 4.5). Additionally, the number of branches per neurite in cells expressing Arp3-R161A was

0.104 ($p \leq 0.05$), as compared to means of 0.85 in cells expressing wild-type Arp3, as well as untransfected and empty vector, suggesting that any neurite initiated from cells with mutant Arp3 might have a decreased tendency to branch (Figure 4.6). The neurite length per cell was also significantly decreased in cells expressing Arp3-R161A, with a mean of 35.05 microns ($p \leq 0.05$), as compared to means of 100.47, 78.57 and 74.51 for the untransfected, empty vector and wild-type groups, respectively (Figure 4.7). The longest neurite per cell was significantly decreased in cells expressing Arp3-R161A, with a mean of 32.03 microns ($p \leq 0.05$), as compared to a mean of 75.4 microns for untransfected cells (Figure 4.8).

4.3 Expression of Arp3-R161A increases lamellipodial actin filament content

The data presented above show that expressing Arp3-R161A decreases neurite outgrowth, but that this construct can still participate in the Arp2/3 complex. Therefore, we next determined how expressing Arp3-R161A affects the production of actin filament content in lamellipodia. Figure 9 shows the immunocytochemical images of untransfected cells (A-C) and cells transfected with GFP (D-F), GFP-Arp3 (WT: G-I), or GFP-Arp3-R161A (R161A: J-L). Comparison of the Arp3 mutant-expressing cells (Figure 4. 9 K) to those in the other treatment groups (Figure 4.9 B, E, and H) indicates higher cortical phalloidin intensity around cell bodies, suggesting increased actin filament content. Immunocytometry study provide a same field comparison of an untransfected cell and a cell expressing Arp3-R161A (Figure 4.9 M, N, O). The cell expressing GFP-Arp3-R161A (green) did not elaborate neurites and demonstrates increased phalloidin staining compared to the untransfected cell, which has typical morphology and a long

neurite. The cell body phalloidin fluorescence intensity was increased in cells expressing Arp3-R161A, with a mean of 24.64 relative fluorescence units ($p \leq 0.05$), as compared to means of 18.52, 17.01 and 17.98 arbitrary units for the untransfected, empty vector and wild-type, respectively (Figure 4.10).

It was difficult to compare the growth cone lamellipodial phalloidin fluorescence intensity between the different treatment groups due to the decreased number of growth cones in cells expressing Arp3-R161A. An estimate was made by measuring the phalloidin intensity of the lamellipodial regions, which showed an increase in the intensity in wild-type cells, perhaps due to overexpression of Arp3. Overall, lamellipodial intensity estimates decreased in the R161A group, though were still larger compared to the untransfected and empty vector groups (Table 4.1). The difference in the intensity was significant ($p \leq 0.05$) in WT as compared to UT or EV.

4.4 Extracts from cells expressing Arp3-R161A have an increased rate of actin polymerization

Extracts from cells transfected with R161A Arp3 demonstrated a near 2-fold increase in the *in-vitro* actin polymerization as compared to that from cells transfected with wild-type Arp3 (Figure 4.11). Slopes for the linear portion of each curve (minutes 5-15) were calculated through linear regression and demonstrated a near 2-fold increase in the actin polymerization rate for extracts of cells expressing Arp3- R161A (517 RFU/min), compared to that of extracts from cells expressing wild type Arp3 (371 RFU/min) or the assay positive control (374 RFU/min). Experiments were conducted in duplicate and repeated three times. Comparison of the slopes using

ANOVA with LSD post-hoc and $p < 0.05$ indicates that the rate of polymerization is significantly higher in cells expressing Arp3-R161A compared to cells expressing WT Arp3.

DISCUSSION

In this work, we have shown that a R161A point mutation in Arp3 decreases several measures of neurite outgrowth in B35 neuroblastoma cells, including initiation, elongation, and branching. Interestingly, Arp3-R161A expression increased cortical actin filament accumulation and the mutant Arp3 was still capable of interacting with Arp2. Furthermore, cells expressing Arp3-R161A have Arp2/3 complexes that interact with activating WAVE. These results initially seem somewhat incongruous since while Arp3-R161A can form a stable Arp2/3 complex that can interact with its activator, expression of the mutated Arp3 results in dramatic decreases in neurite outgrowth. Our current results continue to validate our prior modeling results suggesting that Arp3 R161 is an important contributor to the stability of the Arp2:Arp3 interface in the inactive state as mutating this residue has profound effects on cellular morphology and lamellipodial actin filament structure.[22] As immunoprecipation results indicated wild-type oligomerization, and *in vitro* actin polymerization assays demonstrated 2-fold rate enhancement, we suggest that R161A mutation does indeed alter the conformational equilibrium of the Arp2/3 complex, shifting it towards the active conformation. Over expression of this constitutively active complex results in excess accumulation of actin.

Several studies suggest that lamellipodia formation and cell motility require Arp2/3 mediated nucleation and polymerization within a narrow, optimal range.[1, 24] Cellular processes may be disrupted by increased actin branching and polymerization.[24] Mutant Arp3 has been reported as one of the major contributors to the abnormal actin assembly in rats with focal and segmental glomerulosclerosis (FSGC).[25]

Alternatively, R161A could potentially affect neurite outgrowth by altering the interaction between WAVE and Arp2/3 complex. Co-IP results suggest that the amounts of WAVE binding to Arp2 in the untransfected, empty vector, wild type, and mutant groups are not different. At the same time, WAVE can interact with the Arp2/GFP-Arp3 complex in the wild type and R161A groups since Arp2 was found to bind both GFP-Arp3 and GFP-Arp3-R161A. As a side note, all the Arp2 in our studies is endogenous, suggesting that expression levels of Arp2 may be responsive to the levels of Arp3.

Although the co-IP studies suggested that the amount of interaction between WAVE and Arp2/3 complex was not affected after Arp3 R161A mutation, immunocytochemistry and confocal imaging studies clearly showed that the cells transfected with Arp3 R161A have poor neurite initiation and growth. Neurite formation is an actin-dependent process and proteins that directly augment actin polymerization facilitate lamellipodial protrusion (e.g. cortactin).[26, 27] As such, one would expect that the mutation would either have little effect on the morphology of the cells, or that expression of Arp3-R161A would increase neurite outgrowth. At first glance, our immunoprecipitation and polymerization results seem to contradict this, as R161A not only did not appear to affect the actin branching process but appeared to enhance it.

In order to reconcile these results, we interpret the data reported here to suggest that the R161A mutation in Arp3 increases efficiency of the Arp2/3 complex for nucleation and actin polymerization. Arp2 is known to participate in the nucleation process and it has also been shown that nucleotide-binding to Arp3 is more important than nucleotide-binding to Arp2 for proper nucleation activity of the Arp2/3 complex.[28,29] The C-domain of WAVE is thought to facilitate Arp2 and Arp3 association with actin during the Arp2/3 nucleation process.[11] At the same time Wiskott-Aldrich Syndrome protein (WASP), a protein similar to WAVE, has been shown to bivalently bind both Arp2 and Arp3.[30] Since the amount of WAVE interacting with the Arp2/3 complex in this work was relatively invariant between treatment groups, we suggest that it is unlikely that the Arp3 R161A mutation altered the WAVE:Arp3 or WAVE:Arp2 affinity. This further suggests that the mutation is simply changing the quaternary conformation, thereby enhancing the nucleating capacity of Arp2/3 complex without affecting the WAVE-Arp2/3 complex interaction. Higher concentrations of highly branched actin may indeed favor lamellipodia formation, but have also been shown to impede filopodia formation.[1, 24] We suggest this is what is happening in our R161A mutants, with destabilization of the inactive conformation favoring the active state. Preliminary molecular dynamics computer simulations of WAVE bound to wild-type Arp2 or Arp3 in our lab suggest that WAVE binding to sub-domain 1 induces conformation changes in sub-domain 3 near R161 at the Arp2:Arp3 inactive interface. This is consistent with the idea that Wiskott-Aldrich proteins function to alter the relative inactive/active Arp2/3 equilibria by destabilizing the inactive conformation.

CONCLUSIONS

In this work, we show that R161A mutants in transiently transfected B35 rat neuroblastoma cells increase cortical actin without impacting oligomerization of WAVE with the Arp2/3 complex. This same mutation, however, dramatically reduces neurite morphology by favoring lamellipodia formation at the expense of filopodia formation. Overall, these results support the idea that Wiskott-Aldrich proteins activate actin branching by destabilizing the inactive conformation of the Arp2/3. Continued detailed characterization of this process will likely provide important clues towards manipulating actin nucleation to facilitate recovery from condition like central nervous system (CNS) injuries.

METHODS

The protocols for generation of GFP-tagged Arp3, site-directed mutagenesis of R161A Arp3, gel electrophoresis, transfection in B35 neuroblastoma cells, and co-immunoprecipitation are as described.[22] Other methods used are as follows.

4.1 Immunocytochemistry for co-localization

Immunocytochemistry was performed using anti-WAVE (1:200; Sigma, St. Louis, MO), anti-GFP (1:200; Sigma, St. Louis, MO) and anti-Arp3 (1:200; Sigma, St. Louis, MO) antibodies, and the immunolabeling was visualized with secondary antibodies (1:200) conjugated to Alexafluor 488, Alexafluor 555, or Alexaflour 649. Controls were untransfected cells (UT) and cells transfected with GFP only (empty vector, EV). Treatment groups for these experiments included the UT and EV controls,

GFP and V5 tagged wild-type Arp3 (WT), and GFP and V5 tagged mutant R161A Arp3 (R161A).

4.2 Analysis of outgrowth

Neurite outgrowth and actin filament content were analyzed using image analysis of phase contrast and fluorescent images. Cells were stained with Texas Red-phalloidin (165 nM in PBS) to analyze the actin filament content. Digital images were captured through 40X and 100X objectives for quantification of lamellipodia formation, actin filament content, and neurite outgrowth. For quantification of lamellipodia formation, areas in the growth cone with characteristic lamellipodial morphology and phalloidin labeling intensity 50% higher than growth cone central regions were defined as lamellipodia and outlined. Phalloidin labeling intensities in the cortical regions of the cell bodies and lamellipodial regions of the growth cones were used to quantify actin filament content. For neurite outgrowth analysis, the percentage of neurite bearing cells, number of neurites per cell, total neurite length per cell (sum of all processes), the length of the longest neurite for each cell and number of branches per neurite were assessed. Treatment groups for these experiments included the UT and EV controls, GFP-WT Arp3, and GFP-R161A-Arp3. Each group was assessed using triplicate cultures in 3 separate experiments (n = 9). One image was taken per condition per replica.

4.3 Actin polymerization assay

Actin Polymerization Biochem Kit (Cytoskeleton) was used to measure *in vitro* actin polymerization rates from B35 cells cells transfected with GFP-WT Arp3 or GFP-R161A Arp3.[31] In this assay, increased polymerization is measured by increased

fluorescence from pyrene-conjugated actin. Lysates from cells were incubated with pyrene-conjugated G-actin (0.4 mg/ml) in the presence of ATP and the samples were read with a fluorimeter (Tecan). The samples were read at 60 seconds intervals for 20 minutes without actin polymerization buffer (APB) and for 1 hour after the addition of APB. Baseline controls only had ATP and general actin buffer. Spontaneous actin polymerization for each treatment condition (at time = 1 min) was subtracted from each group (baseline control: 129 RFU, test buffer/positive control: 24318 RFU, wild-type: 25054 RFU, and mutant: 25003 RFU). The pyrene label has been shown to minimally alter the rate of actin polymerization.[32] The experiments were conducted in duplicate and repeated three times.

4.4 Statistics

All end-point assays for the lamellipodia formation, actin filament content, and neurite outgrowth yielded normally distributed data with similar variances across experimental groups. The experimental groups were individual cultures expressing wild type and mutant Arp3, whereas the control groups were untransfected cultures and cultures expressing only the GFP construct. Data were analyzed using univariate analysis of variance (ANOVA) with individual treatment groups as the independent variable and the morphological characteristics as the dependent variable. Differences between treatment groups were determined using the Least Significant Difference (LSD) post-hoc test at the 0.05 level of significance.

REFERENCES

1. Korobova F, Svitkina T. Arp2/3 complex is important for filopodia formation, growth cone motility, and neuritogenesis in neuronal cells. Mol Biol Cell 2008 Apr;19(4):1561-74.
2. Machesky LM, Atkinson SJ, Ampe C, Vandekerckhove J, Pollard TD. Purification of a cortical complex containing two unconventional actins from acanthamoeba by affinity chromatography on profilin-agarose. J Cell Biol 1994 Oct;127(1):107-15.
3. Aspenstrom P. The rho GTPases have multiple effects on the actin cytoskeleton. Exp Cell Res 1999 Jan 10;246(1):20-5.
4. Dickson BJ. Rho GTPases in growth cone guidance. Curr Opin Neurobiol 2001 Feb;11(1):103-10.
5. Garrity PA. Signal transduction in axon guidance. Cellular and Molecular Life Sciences CMLS 1999;55(11).
6. May RC. The Arp2/3 complex: A central regulator of the actin cytoskeleton. Cell Mol Life Sci 2001 Oct;58(11):1607-26.
7. Robinson RC, Turbedsky K, Kaiser DA, Marchand JB, Higgs HN, Choe S, Pollard TD. Crystal structure of Arp2/3 complex. Science 2001 Nov 23;294(5547):1679-84.
8. Rouiller I, Xu XP, Amann KJ, Egile C, Nickell S, Nicastro D, Li R, Pollard TD, Volkmann N, Hanein D. The structural basis of actin filament branching by the Arp2/3 complex. J Cell Biol 2008 Mar 10;180(5):887-95.

9. Nolen BJ, Pollard TD. Insights into the influence of nucleotides on actin family proteins from seven structures of Arp2/3 complex. Mol Cell 2007 May 11;26(3):449-57.

10. Rodal AA, Sokolova O, Robins DB, Daugherty KM, Hippenmeyer S, Riezman H, Grigorieff N, Goode BL. Conformational changes in the Arp2/3 complex leading to actin nucleation. Nat Struct Mol Biol 2005 Jan;12(1):26-31.

11. Chereau D, Kerff F, Graceffa P, Grabarek Z, Langsetmo K, Dominguez R. Actin-bound structures of wiskott-aldrich syndrome protein (WASP)-homology domain 2 and the implications for filament assembly. Proc Natl Acad Sci U S A 2005 Nov 15;102(46):16644-9.

12. Padrick SB, Cheng HC, Ismail AM, Panchal SC, Doolittle LK, Kim S, Skehan BM, Umetani J, Brautigam CA, Leong JM, Rosen MK. Hierarchical regulation of WASP/WAVE proteins. Mol Cell 2008 Nov 7;32(3):426-38.

13. Chen Z, Borek D, Padrick SB, Gomez TS, Metlagel Z, Ismail AM, Umetani J, Billadeau DD, Otwinowski Z, Rosen MK. Structure and control of the actin regulatory WAVE complex. Nature 2010;468(7323).

14. Dominguez R. Actin filament nucleation and elongation factors--structure-function relationships. Crit Rev Biochem Mol Biol 2009 Nov-Dec;44(6):351-66.

15. Ismail AM, Padrick SB, Chen B, Umetani J, Rosen MK. The WAVE regulatory complex is inhibited. Nat Struct Mol Biol 2009 May;16(5):561-3.

16. Machesky LM, Mullins RD, Higgs HN, Kaiser DA, Blanchoin L, May RC, Hall ME, Pollard TD. Scar, a WASp-related protein, activates nucleation of actin

filaments by the Arp2/3 complex. Proc Natl Acad Sci U S A 1999 Mar 30;96(7):3739-44.

17. Padrick SB, Doolittle LK, Brautigam CA, King DS, Rosen MK. Arp2/3 complex is bound and activated by two WASP proteins. Proc Natl Acad Sci U S A 2011 Aug 16;108(33):E472-9.

18. Ti SC, Jurgenson CT, Nolen BJ, Pollard TD. Structural and biochemical characterization of two binding sites for nucleation-promoting factor WASp-VCA on Arp2/3 complex. Proc Natl Acad Sci U S A 2011 Aug 16;108(33):E463-71.

19. Wegner AM, Nebhan CA, Hu L, Majumdar D, Meier KM, Weaver AM, Webb DJ. N-wasp and the arp2/3 complex are critical regulators of actin in the development of dendritic spines and synapses. J Biol Chem 2008 Jun 6;283(23):15912-20.

20. Nikolic M. The role of rho GTPases and associated kinases in regulating neurite outgrowth. Int J Biochem Cell Biol 2002 Jul;34(7):731-45.

21. Boczkowska M, Rebowski G, Kast DJ, Dominguez R. Structural analysis of the transitional state of Arp2/3 complex activation by two actin-bound WCAs. Nature Communications 2014;5.

22. Mahadik AC, Haldar S, Hynds DL, Beck BW. Specific interfacial residues control rearrangement of the Arp2:Arp3 dimer during activation of the Arp2/3 complex *(submitted to protein science, in review)*. .

23. Kortemme T, Kim DE, Baker D. Computational alanine scanning of protein-protein interfaces. Sci STKE 2004 Feb 3;2004(219):pl2.

24. Moulding DA, Blundell MP, Spiller DG, White MR, Cory GO, Calle Y, Kempski H, Sinclair J, Ancliff PJ, Kinnon C, Jones GE, Thrasher AJ. Unregulated actin polymerization by WASp causes defects of mitosis and cytokinesis in X-linked neutropenia. J Exp Med 2007 Sep 3;204(9):2213-24.

25. Akiyama K, Morita H, Suetsugu S, Kuraba S, Numata Y, Yamamoto Y, Inui K, Ideura T, Wakisaka N, Nakano K, Oniki H, Takenawa T, Matsuyama M, Yoshimura A. Actin -related protein 3 (Arp3) is mutated in proteinuric BUF/mna rats. Mamm Genome 2008 Jan;19(1):41-50.

26. Bryce NS, Clark ES, Leysath JL, Currie JD, Webb DJ, Weaver AM. Cortactin promotes cell motility by enhancing lamellipodial persistence. Curr Biol 2005 Jul 26;15(14):1276-85.

27. Siton O, Ideses Y, Albeck S, Unger T, Bershadsky AD, Gov NS, Bernheim-Groswasser A. Cortactin releases the brakes in actin- based motility by enhancing WASP-VCA detachment from Arp2/3 branches. Curr Biol 2011 Dec 20;21(24):2092-7.

28. D'Agostino JL, Goode BL. Dissection of Arp2/3 complex actin nucleation mechanism and distinct roles for its nucleation-promoting factors in saccharomyces cerevisiae. Genetics 2005 Sep;171(1):35-47.

29. Martin AC, Xu XP, Rouiller I, Kaksonen M, Sun Y, Belmont L, Volkmann N, Hanein D, Welch M, Drubin DG. Effects of Arp2 and Arp3 nucleotide-binding pocket mutations on Arp2/3 complex function. J Cell Biol 2005 Jan 17;168(2):315-28.

30. Kiselar JG, Mahaffy R, Pollard TD, Almo SC, Chance MR. Visualizing Arp2/3 complex activation mediated by binding of ATP and WASp using structural mass spectrometry. Proc Natl Acad Sci U S A 2007 Jan 30;104(5):1552-7.

31. Cytoskeleton, inc. - the protein experts. <http://www.cytoskeleton.com/>. Accessed 2014 4/27/2014.

32. Criddle AH, Geeves MA, Jeffries T. The use of actin labelled with N-(1-pyrenyl)iodoacetamide to study the interaction of actin with myosin subfragments and troponin/tropomyosin. Biochem J 1985 Dec 1;232(2):343-9.

Condition	Lamellipodia Phalloidin Stain Fluorescence Intensity (RFU ± SEM)
Untransfected	12.13 ± 1.82 (n = 14)
Empty Vector	10.15 ± 1.93 (n = 8)
Wild Type	27.38 ± 8.61 (n = 10)
R161A mutant	19.92 ± 9.96 (n = 3)

Table 4.1: *Quantification of lamellipodial phalloidin fluorescence intensity in different treatment groups*.

FIGURES

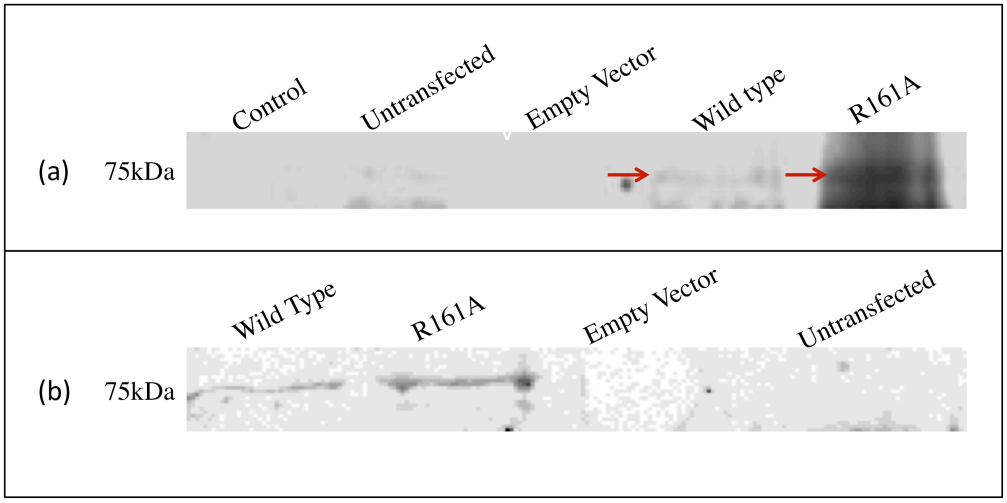

Figure 4.1: Co-*immunoprecipitation of extracts from untransfected (UT) cells and cells transfected with empty vector (EV: only GFP), wild type Arp3 (WT) and mutant Arp3 (R161A)*. (a) Co-immunoprecipitated with anti-GFP antibodies and blotted with anti-Arp3 antibodies. Bands 75 kDa are present in the WT and R161A lanes. (b) Input blot. Blots are representative of three separate experiments, all of which showed similar results.

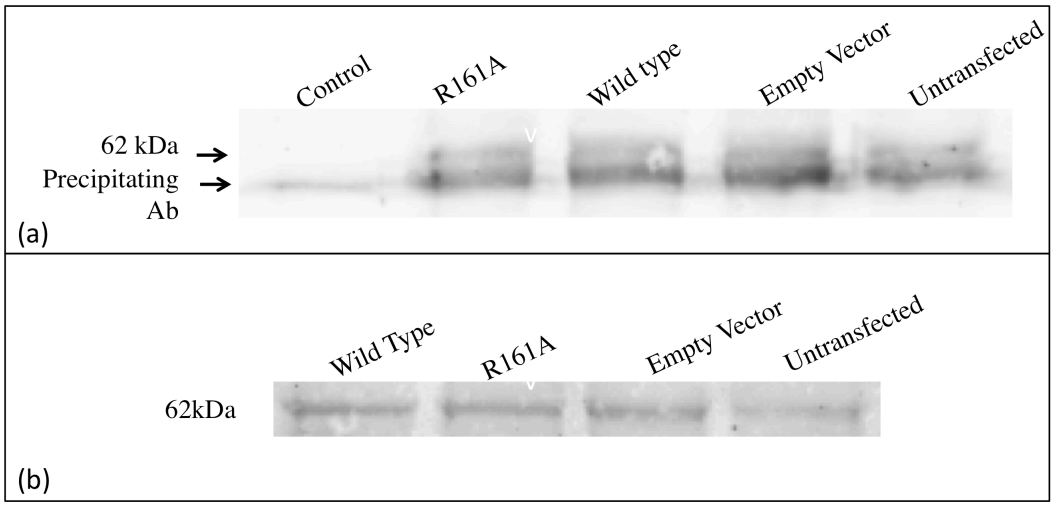

Figure 4.2: *Co-immunoprecipitation of extracts from untransfected (UT) cells and cells transfected with empty vector (EV: only GFP), wild-type Arp3 (WT) and mutant Arp3 (R161A)*. (a) Co-immunoprecipitated with anti-Arp2 antibodies and blotted with anti-WAVE1 antibodies. Bands of 62 kDa are present in the UT, EV, WT and R161A lanes. (b) Input blot. Blots are representative of three separate experiments, all of which showed similar results.

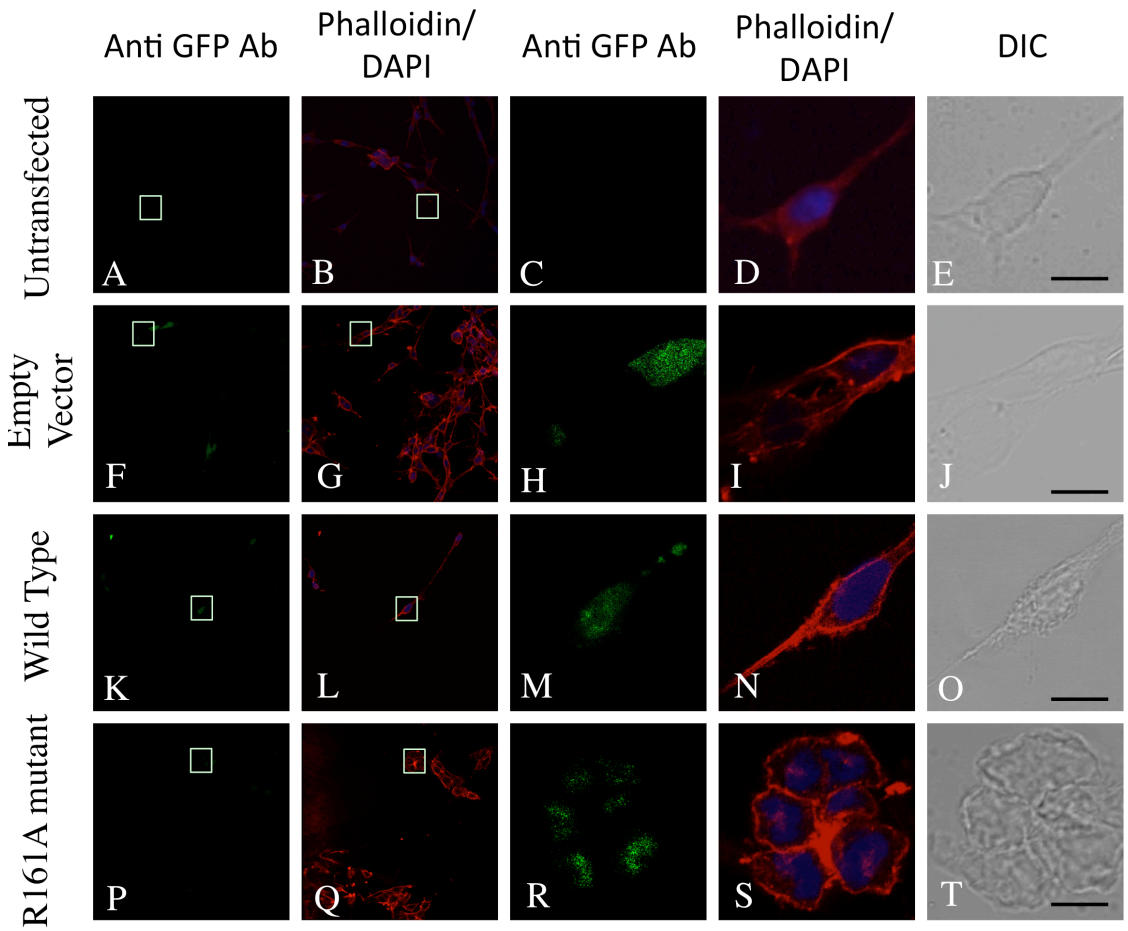

Figure 4.3: *Immunocytochemistry of untransfected cells (a-e) or cells expressing only GFP (f-j), GFP-Arp3(WT) (k-o), or GFP-Arp3-R161A (R161A; p-t) with anti-GFP antibodies (green), Texas-red phalloidin (red) and DAPI (blue) staining (40X).* Panels e, j, o, t are DIC images of d, I, n and s, respectively. Panels c, h, m, r are enlarged areas of a, f, k, p, respectively. Panels d, i, n, sare enlarged areas of b, g, l, q, respectively. Scale is 20μm.

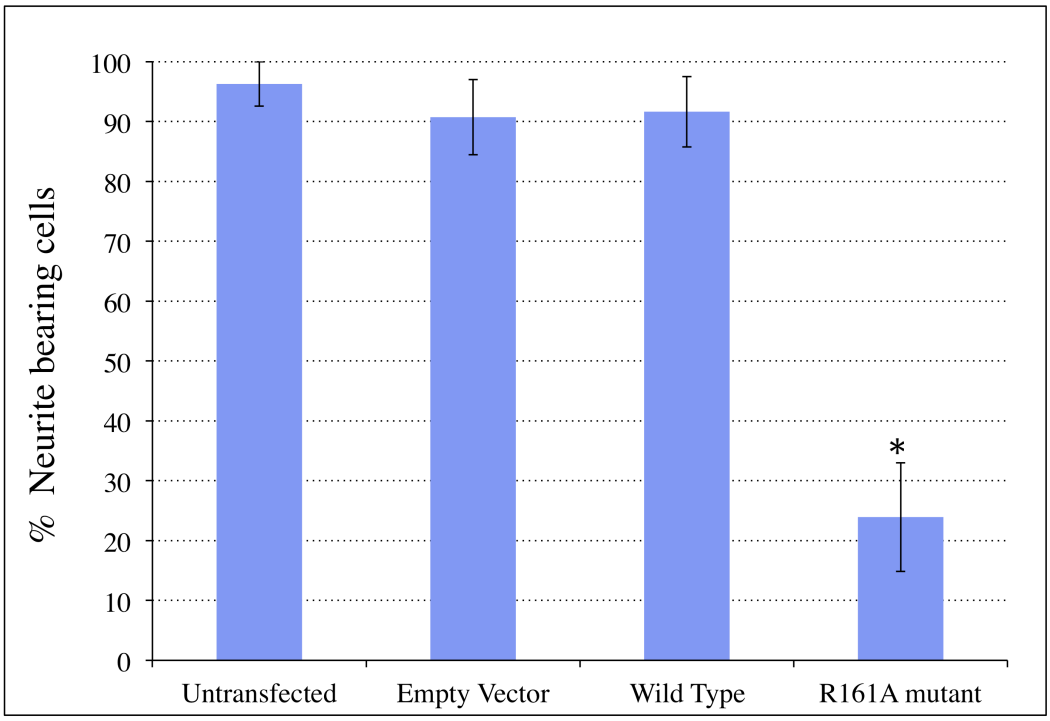

Figure 4.4: *Quantification of the percentage of neurite bearing cells in different treatment groups*. Data are means ± SEM for n = 9. Asterisk indicates significant difference from all other groups at $p \leq 0.05$ (ANOVA with LSD post-hoc).

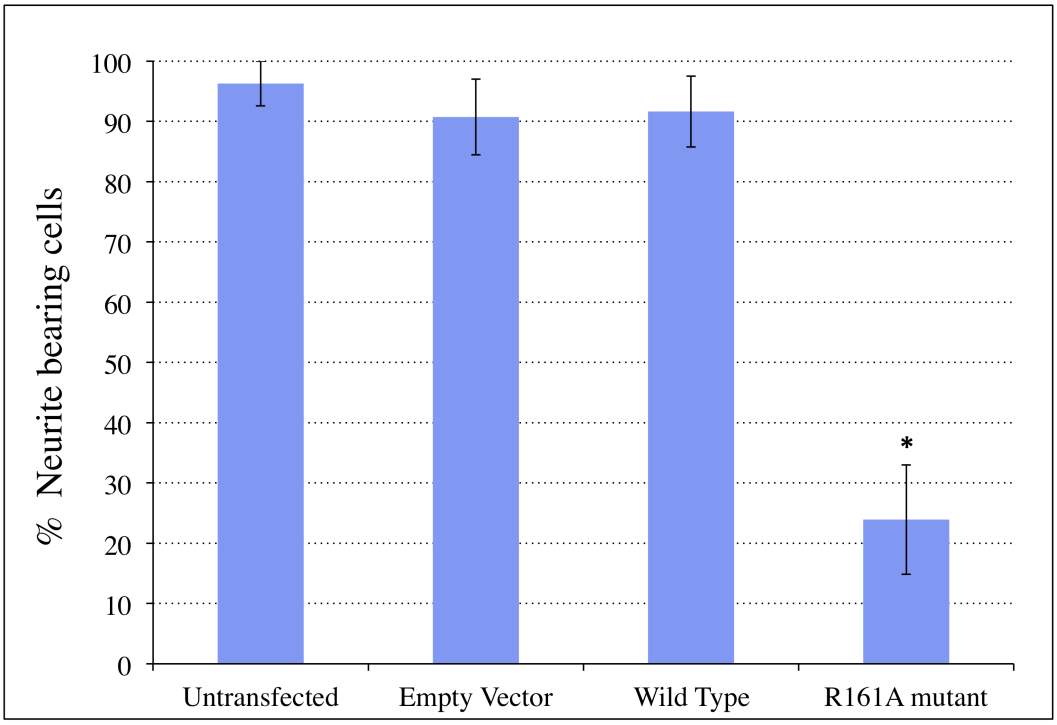

Figure 4.5: *Quantification of the number of neurites per cell in different treatment groups (including only cells with neurites).* Data are means ± SEM for n = 9. Asterisk indicates significant difference from all other groups at $p < 0.05$ (ANOVA with LSD post-hoc).

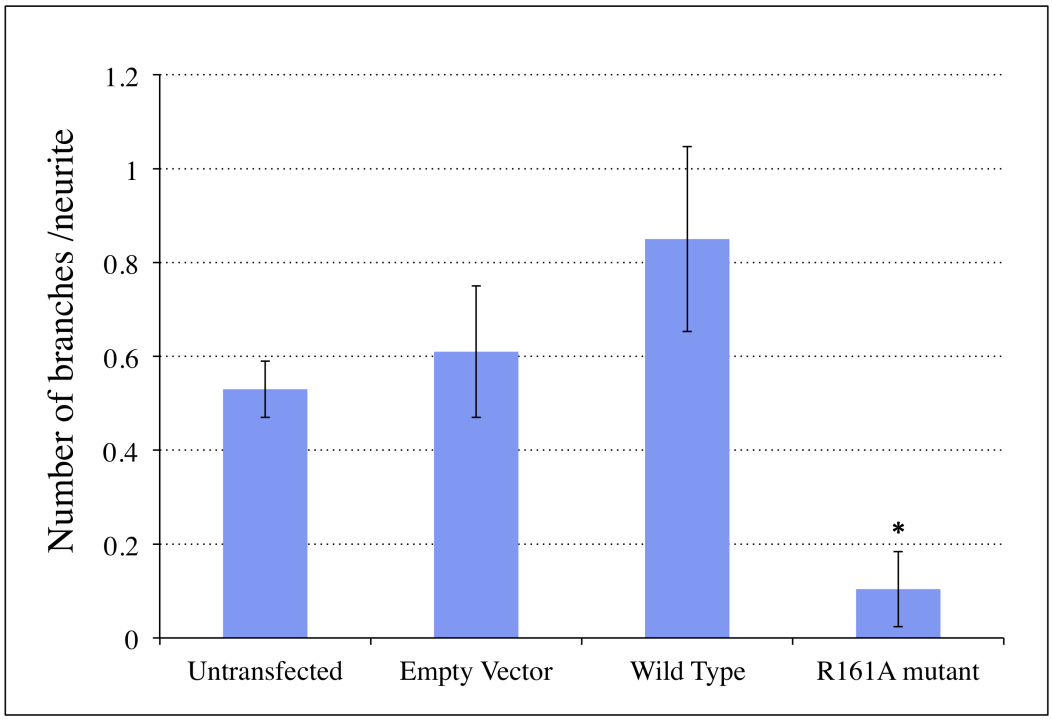

Figure 4.6: *Quantification of the number of branches per neurite in different treatment groups*. Data are means ± SEM for n = 9. Asterisk indicates significant difference from all other groups at $p \leq 0.05$ (ANOVA with LSD post-hoc).

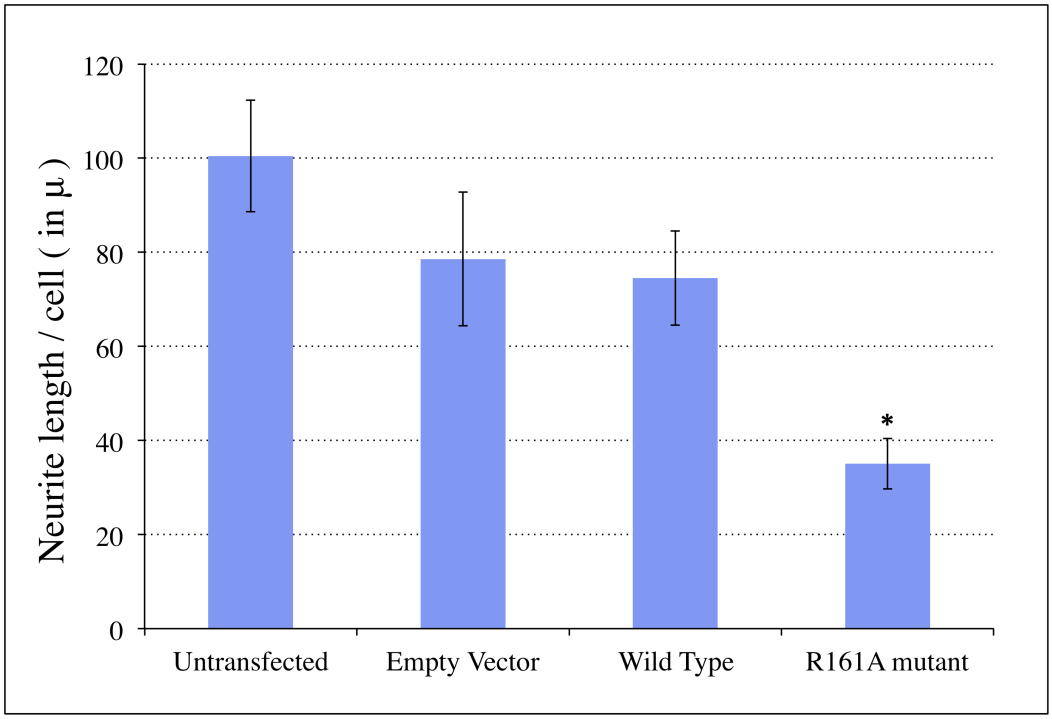

Figure 4.7: *Quantification of the neurite length per cell in different treatment groups*. Data are means ± SEM for n = 9. Asterisk indicates significant difference from all other groups at $p \leq 0.05$ (ANOVA with LSD post-hoc).

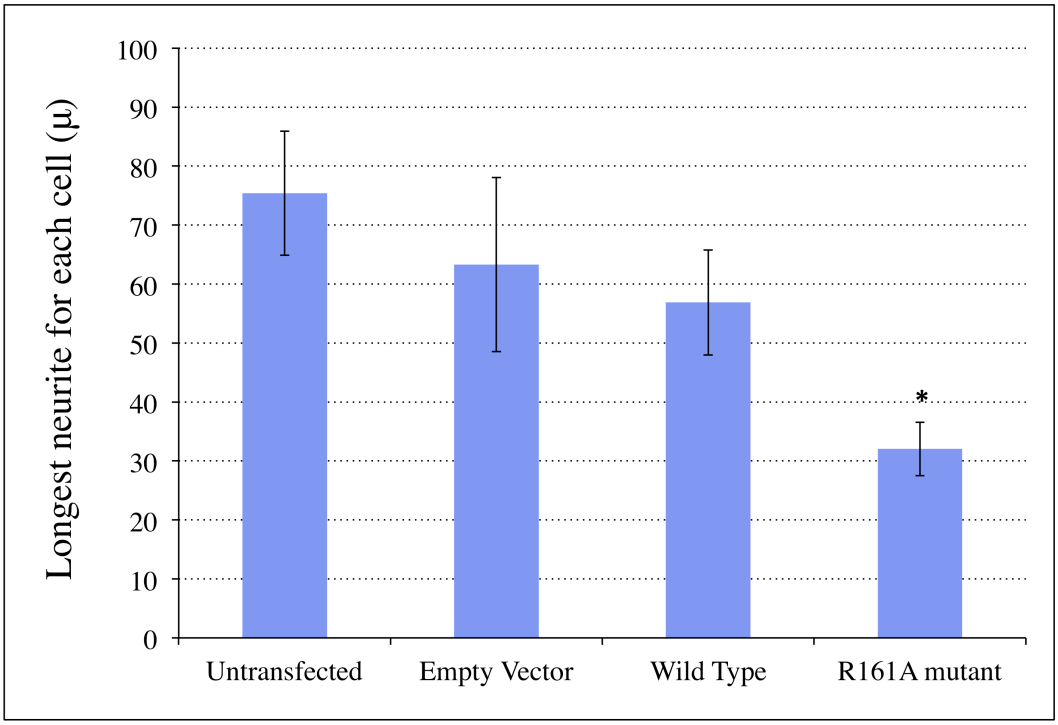

Figure 4.8: *Quantification of the longest neurite per cell in different treatment groups*. Data are means ± SEM for n = 9. Asterisk indicates significant difference from UT at $p \leq 0.05$ (ANOVA with LSD post-hoc).

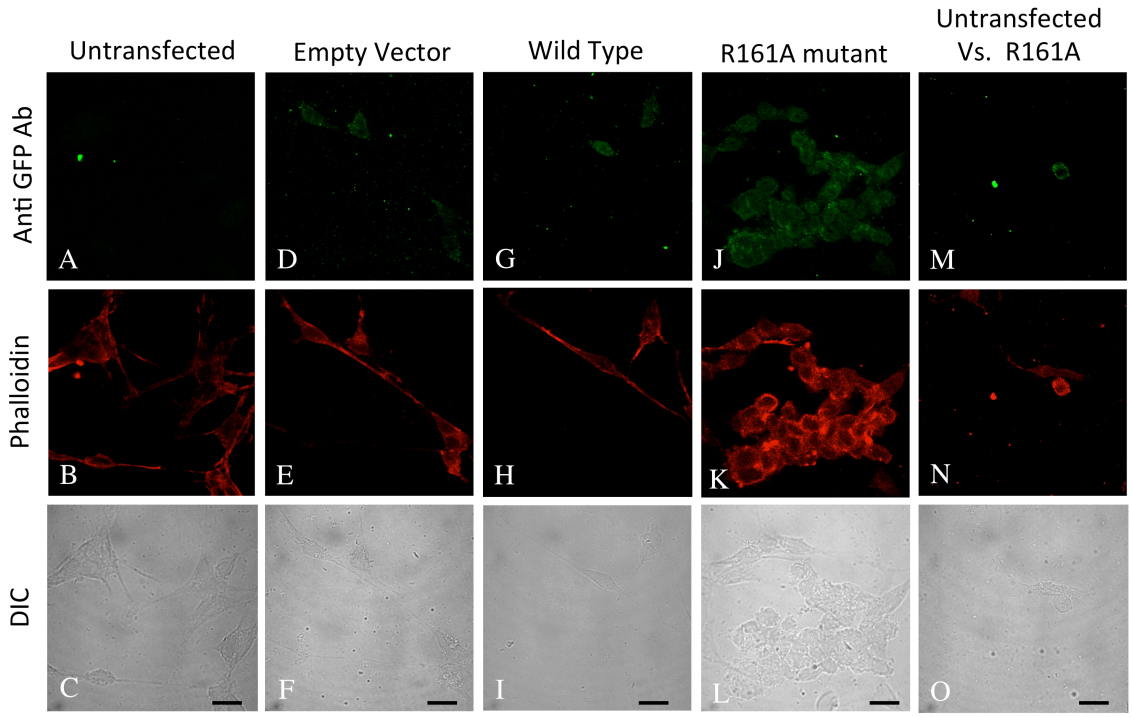

Figure 4.9: *Immunocytochemistry of untransfected cells (a-c) or cell transfected with GFP (d-f), GFP-Arp3(WT; g-i), or GFP-Arp3-R161A (R161A; j-l) with anti-GFP antibodies (a,d,g,j,m; green) along with phalloidin (b,e,h,k,n; red) staining (100X).* Panels m-o show a same field comparison of an untransfected cell to a GFP-Arp3-R161A transfected cell immunostained with anti-GFP antibodies (m; green) and stained with phalloidin (n; red) (100X). Scale is 40μm.

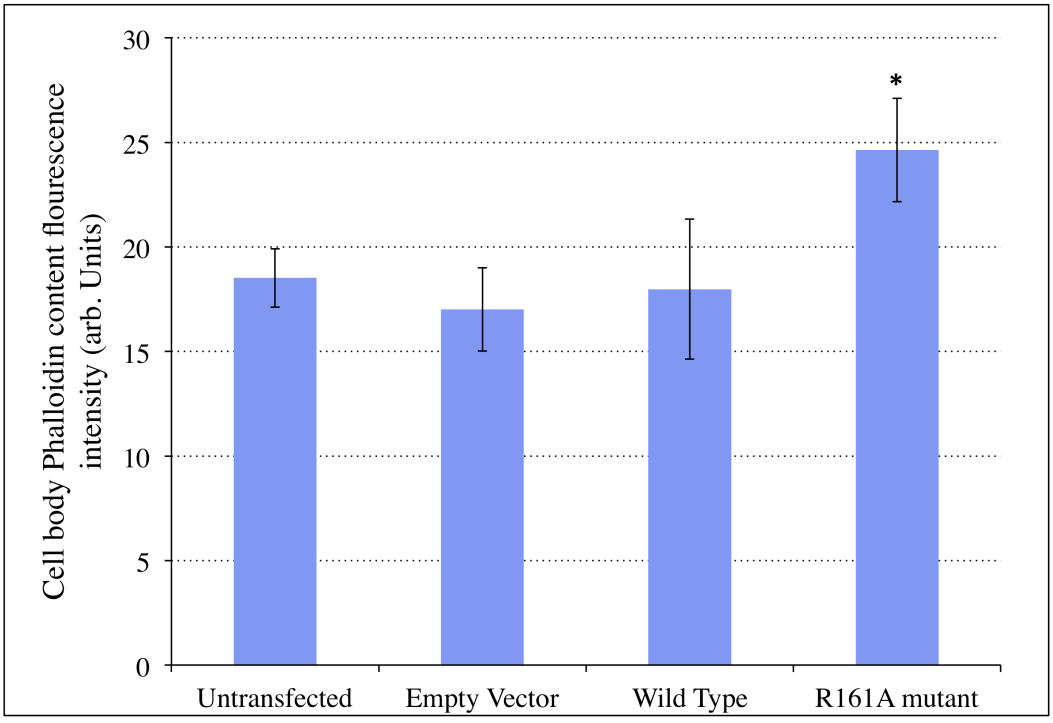

Figure 4.10: *Quantification of cell body phalloidin stain fluorescence intensity in different treatment groups*. Data are means ± SEM for n = 9. Asterisk indicates significant difference from all groups at $p \leq 0.05$ (ANOVA with LSD post-hoc).

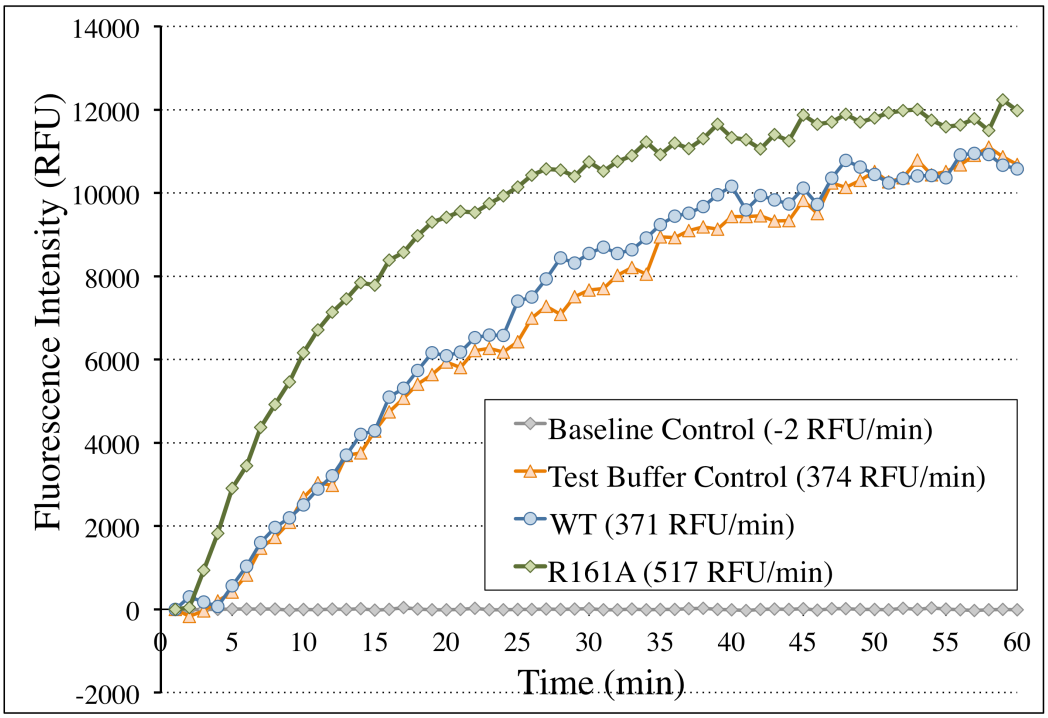

Figure 4.11: *In-vitro actin polymerization of cell extracts from cells transfected separately with WT or R161A Arp3*. The experiments were conducted in duplicate and repeated three times. Comparison of the regression slopes of the linear portion of each curve between 5 and 15 minutes (values in parentheses in key) indicates that the rate of polymerization is significantly higher in cells expressing Arp3-R161A, compared to cells expressing WT Arp3 (ANOVA with LSD post-hoc and $p < 0.05$). Data shown are from a representative experiment.

CHAPTER V

CONCLUSION

Here (as described in Chapters 2, 3, and 4), we used computational methods to characterize the mechanism of activation of the Arp2/3 protein complex, an actin cytoskeletal nucleator. We further validated these computational predictions with *in vivo* cell biology studies. Similar efforts have been made over the course of the last decade in understanding the mechanism of the activation of the Arp2/3 complex.[1-4]

Following the identification of the Arp2/3 complex as one of the major cellular actin nucleators [5, 6], substantial progress towards understanding the molecular mechanism of Arp2/3 complex activity and function in actin assembly has been made.[7-11] However, we still lack residue and atomistic details of the activation of the Arp2/3 complex. In our attempt to understand the activation mechanism, we used computational methods, such as molecular dynamics (MD) simulations (Chapter 2) and Computational Alanine Scanning (CAS, Chapters 3 and 4), to understand the conformational changes in actin, Arp2, and Arp3 in the presence and absence of known Wiskott-Aldrich (WA) protein regulatory V or C peptides. It is well established that the nucleation and branching activities of the Arp2/3 complex require binding of V bound actin molecules to the complex.[12] However, the mechanism by which the V bound actin molecule activates the complex as well as the role of the C peptide in the activation was poorly understood previously.[3, 13]

Molecular details underlying binding of the V or C peptide to actin, Arp2, and Arp3

In Chapter 2, we assessed the binding of V peptide or C peptide to actin, Arp2, and Arp3 molecules in the presence and absence of nucleotide. The activation of the Arp2/3 complex followed by side-branching of the actin filaments involves many sub-interactions including: (i) Association of V bound actin with the appropriate Arp (Arp2 or Arp3) binding site; (ii) Interaction of the C peptide with the remaining Arp (Arp2 or Arp3) binding site with concomitant tertiary structure changes; (iii) Quaternary rearrangement between Arp2 and Arp3 to a conformation that promotes nucleation of activated actin into short-pitch dimers; and (iv) Interaction of other protein subunits (ARPC1-C5) with the existing actin filament. In order to study these sub-interactions, we performed 18 individual MD simulations that include monomeric actin, Arp2, Arp3 (each in nucleotide bound and nucleotide free form, and each with V peptide, C peptide, or peptide-free states).

Our MD and energetic data suggest binding of V peptide to nucleotide bound actin has the lowest energy conformation among possible V binding partners (Figure 2.12), whereas the binding of the C peptide to Arp3 produces the largest increase in compact conformation (Figure 2.9 (vi)). Sub-domain 3 in Arp3 underwent conformational changes upon C peptide binding that may destabilize the quaternary interactions required for the known relative enhanced stability of the *inactive* Arp2/3 complex (Figure 5.1 (a)).

It is known that different sub-interactions are required during the overall activation of the complex but the sequence of these events was previously not well-

established.[14] A number of different models exist to explain the possible sequence of the sub-interactions during the activation of the Arp2/3 complex.[2, 4] Our studies indicate that the conformational changes in sub-domain 3 of Arp3 are important and suggest that the interface between Arp2 and Arp3 plays a crucial role in the activation of the complex.

Interface residues of Arp3 play an important role in conformational changes of the Arp2/3 complex

In Chapters 3 and 4, we successfully used a combination of computational and experimental approaches to define functionally important surfaces of Arp2 and Arp3 proteins that are required in such Arp2/3 complex activities as nucleation and branching.

We identified functionally important residues in Arp3 that stabilize the inactive state of the Arp2:Arp3 dimer. We used a computational alanine scanning method to design Arp3 mutants that destabilize this inactive interface. One of the computational Arp3 mutants, R123A, "rescues" the complex from inactive to a constitutively active state, resulting in substantial accumulation of actin filaments in B35 neuroblastoma cells (Figures 3.6, 5.1(b)). Although the Arp2:Arp3 dimer interface is thought to form an active short-pitch actin-like dimer template with the interface thus playing a critical role in filament formation, the remaining five ARPC1-5 subunits, which are known to bind existing actin filaments, will likely also play an important role in regulating side-branching.

Thus, while our results are extremely promising, in order to obtain a complete molecular picture of the Arp2/3 complex bound to existing actin filaments, future investigation of the molecular details of the other sub-interactions using similar

approaches would also need to take place (though that is beyond the scope of this work). However, the fact that CK-666 and CK-869 (small organic heterocycles developed by Nolen) each inhibit activation of the Arp2/3 complex by trapping the complex in the "OFF" state (Figure 5.1 (C)) is corroborative data supporting our model. In future work, it would be interesting to use these heterocycle inhibitors in conjunction with our R123A mutant.[15] If our model is correct, our R123A mutant should not experience the inhibitory effects of CK-666 and CK-869.

Implications of the C-tail in Arp2 and Arp3

Our studies suggest that the C-tails extensions in Arp2 and Arp3, relative to actin, play important roles in modulating tertiary and quaternary conformations. In both proteins, the C-tail folds into an otherwise hydrophobic groove of Arp2 and Arp3. The displacement of the C-tail by the C peptide in the nucleotide bound Arp3 suggests that, under physiological conditions, binding of the C peptide/tail-free state will dominate over either V peptide or tail-bound states. It would likely be illuminating to test the specificity of binding of the V peptide with Arp3 when the C-tail is absent (either via structural modeling or mutagenesis approaches). The absence of the C-tail may change the binding specificity and lead to conformational changes in Arp3 that more closely mimic those of actin whose conformations that lack the C-tail motif. Such a conformational change may negate the steric clash with Arp3 that we earlier posed, thus permitting Arp2 to much more easily adopt a short pitch actin-like dimer conformation. Thus, the conformational changes in Arp3 may promote the rearrangement between Arp2 and Arp3 that leads to the formation of "active" actin dimer at the barbed end of the complex.

Many attempts have been performed to understand the mechanism of activation of the Arp2/3 complex, but much less is known about the structures of actin nucleators such as Arp2/3 complex and NPF's in their activated states. In addition to this, multiple NPF's have been identified with similar cellular mechanisms of activating Arp2/3 complex; suggesting a tight regulatory control for Arp2/3 complexes *in vivo*.

Our MD simulations studies reveal the importance of the quaternary interactions at the Arp2:Arp3 interface in the activation of Arp2/3 complex. Our designed Arp3-R123A interface mutant "rescued" the complex from inactive to a constitutively active state, resulting in substantial accumulation of actin filaments in B35 neuroblastoma cells. It would be interesting to study the effect of constitutively active Arp2/3 mutant complex on its upstream regulators RhoA/RAC. Besides nucleating actin filaments, Arp2/3 complex may influence cell motility by altering Rho GTPase signaling.

Based on our findings, we propose that the conformational rearrangement due to quaternary interfacial interactions plays an important role in activating the Arp2/3 complex, whereas regulation by NPF's controls the process of actin nucleation. Future studies that involve both control parameters simultaneously will allow us to better understand the detailed mechanism of activation of the Arp2/3 complex.

REFERENCES

1. Dalhaimer P, Pollard TD. Molecular dynamics simulations of Arp2/3 complex activation. Biophys J 2010 Oct 20;99(8):2568-76.

2. Boczkowska M, Rebowski G, Kast DJ, Dominguez R. Structural analysis of the transitional state of Arp2/3 complex activation by two actin-bound WCAs. Nature Communications 2014;5.

3. Rodal AA, Sokolova O, Robins DB, Daugherty KM, Hippenmeyer S, Riezman H, Grigorieff N, Goode BL. Conformational changes in the Arp2/3 complex leading to actin nucleation. Nat Struct Mol Biol 2005 Jan;12(1):26-31.

4. Padrick SB, Doolittle LK, Brautigam CA, King DS, Rosen MK. Arp2/3 complex is bound and activated by two WASP proteins. Proc Natl Acad Sci U S A 2011 Aug 16;108(33):E472-9.

5. Miller KG, Field CM, Alberts BM. Actin-binding proteins from drosophila embryos: A complex network of interacting proteins detected by F-actin affinity chromatography. J Cell Biol 1989 Dec;109(6 Pt 1):2963-75.

6. Robinson RC, Turbedsky K, Kaiser DA, Marchand JB, Higgs HN, Choe S, Pollard TD. Crystal structure of Arp2/3 complex. Science 2001 Nov 23;294(5547):1679-84.

7. Bailly M, Ichetovkin I, Grant W, Zebda N, Machesky LM, Segall JE, Condeelis J. The F-actin side binding activity of the Arp2/3 complex is essential for actin nucleation and lamellipod extension. Curr Biol 2001 Apr 17;11(8):620-5.

8. Le Clainche C, Pantaloni D, Carlier MF. ATP hydrolysis on actin-related protein 2/3 complex causes debranching of dendritic actin arrays. Proc Natl Acad Sci U S A 2003 May 27;100(11):6337-42.

9. D'Agostino JL, Goode BL. Dissection of Arp2/3 complex actin nucleation mechanism and distinct roles for its nucleation-promoting factors in saccharomyces cerevisiae. Genetics 2005 Sep;171(1):35-47.

10. Pfaendtner J, Volkmann N, Hanein D, Dalhaimer P, Pollard TD, Voth GA. Key structural features of the actin filament Arp2/3 complex branch junction revealed by molecular simulation. J Mol Biol 2012 Feb 10;416(1):148-61.

11. Nolen BJ, Pollard TD. Insights into the influence of nucleotides on actin family proteins from seven structures of Arp2/3 complex. Mol Cell 2007 May 11;26(3):449-57.

12. Chereau D, Kerff F, Graceffa P, Grabarek Z, Langsetmo K, Dominguez R. Actin-bound structures of wiskott-aldrich syndrome protein (WASP)-homology domain 2 and the implications for filament assembly. Proc Natl Acad Sci U S A 2005 Nov 15;102(46):16644-9.

13. Panchal SC, Kaiser DA, Torres E, Pollard TD, Rosen MK. A conserved amphipathic helix in WASP/scar proteins is essential for activation of Arp2/3 complex. Nat Struct Biol 2003 Aug;10(8):591-8.

14. Beltzner CC, Pollard TD. Pathway of actin filament branch formation by Arp2/3 complex. J Biol Chem 2008 Mar 14;283(11):7135-44.

15. Hetrick B, Han MS, Helgeson LA, Nolen BJ. Small molecules CK-666 and CK-869 inhibit actin-related protein 2/3 complex by blocking an activating conformational change. Chem Biol 2013;20(5).

FIGURES

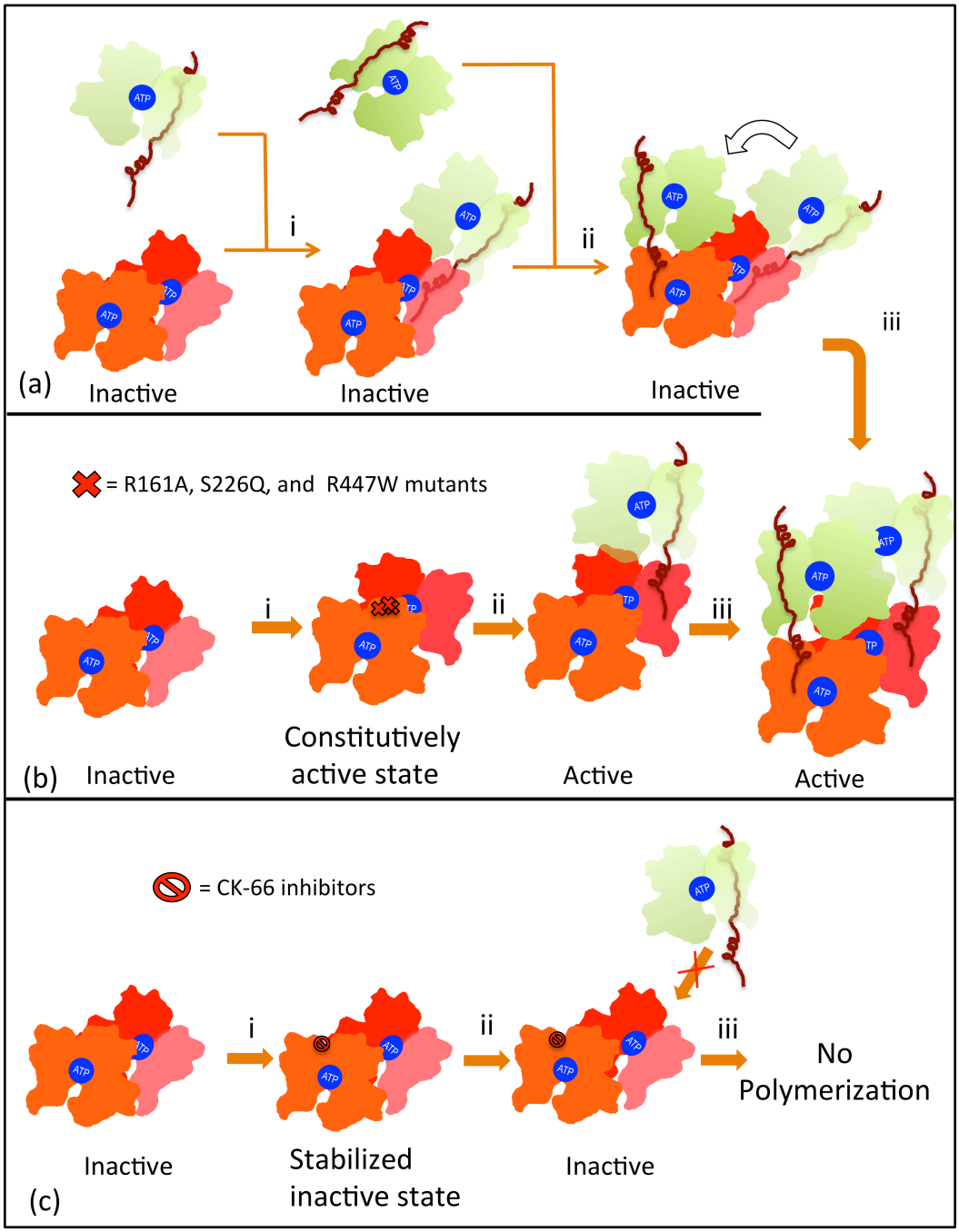
(a)
Inactive
Inactive
Inactive
i
ii
iii
= R161A, S226Q, and R447W mutants
(b)
Inactive
Constitutively active state
Active
Active
i
ii
iii
= CK-66 inhibitors
(c)
Inactive
Stabilized inactive state
Inactive
No Polymerization
i
ii
iii

Figure 5.1: *Hypothetical Model for the activation of Arp2/3 complex due to conformational rearrangement between Arp2:Arp3 dimer*. (A) V bound actin is delivered to the Arp2 site followed by the delivery of V bound actin to the Arp3 site. Binding of a C peptide to Arp3 induces a conformational shift that compacts Arp3, destabilizes the Arp3:Arp2 inactive interface, allowing for rearrangement of Arp2 relative to Arp3 into an active state, thus leading to polymerization. (B) Arp3 if mutated for R161A/S226Q/R447W. Mutations alter the quaternary interactions at the interface of Arp2:Arp3, destabilizing the inactive to active state of the complex and allowing for constitutive actin polymerization. (C) CK-66 inhibitors stabilize the complex in an inactive state and inhibit actin polymerization. Key: ATP (blue solid circles), Arp3 (orange subunit), Rearranged Arp2 (red subunit), Arp2 with unresolved sub-domain 1 and 2 (red and salmon subunit); actin (Green subunit); VCA region of Wiskott-Aldrich complex (brown helical structure), R161A, S226Q, R447W mutants in Arp3 (✖), CK-66 inhibitors (x), (Some concepts from: Padrick and Rosen et al., 2011; Ti and Pollard et al., 2011; Rouiller and Hanein et al., 2008.)

COMBINED REFERENCES

1. Regulation of WASP/WAVE proteins <http://www.ncbi.nlm.nih.gov/pmc/articles/PMC2172026/>.

2. Cytoskeleton, inc. The protein experts <http://www.cytoskeleton.com/>.

3. Abercrombie M, Heaysman JEM, Pegrum SM. The locomotion of fibroblasts in culture Exp Cell Res 1970;62(2-3).

4. Abraham VC, Krishnamurthi V, Taylor DL, Lanni F. The actin-based nanomachine at the leading edge of migrating cells Biophys J 1999 Sep;77(3):1721-32.

5. Akiyama K, Morita H, Suetsugu S, Kuraba S, Numata Y, Yamamoto Y, Inui K, Ideura T, Wakisaka N, Nakano K, Oniki H, Takenawa T, Matsuyama M, Yoshimura A. Actin -related protein 3 (Arp3) is mutated in proteinuric BUF/Mna rats Mamm Genome 2008 Jan;19(1):41-50.

6. Alto LT, Havton LA, Conner JM, Hollis ER,II, Blesch A, Tuszynski MH. Chemotropic guidance facilitates axonal regeneration and synapse formation after spinal cord injury Nat Neurosci 2009; 2009;12(9):1106 <last_page> 1113.

7. Aspenstrom P. The rho GTPases have multiple effects on the actin cytoskeleton Exp Cell Res 1999 Jan 10;246(1):20-5.

8. Baas PW, Luo L. Signaling at the growth cone: The scientific progeny of cajal meet in madrid Neuron 2001 Dec 20;32(6):981-4.

9. Bailly M, Ichetovkin I, Grant W, Zebda N, Machesky LM, Segall JE, Condeelis J. The F-actin side binding activity of the Arp2/3 complex is essential for actin nucleation and lamellipod extension Curr Biol 2001 Apr 17;11(8):620-5.

10. Baker D. Robetta: Full-chain protein structure prediction server <http://robetta.bakerlab.org/>. .

11. Beltzner CC, Pollard TD. Pathway of actin filament branch formation by Arp2/3 complex J Biol Chem 2008 Mar 14;283(11):7135-44.

12. Beltzner CC, Pollard TD. Identification of functionally important residues of Arp2/3 complex by analysis of homology models from diverse species J Mol Biol 2004 Feb 13;336(2):551-65.

13. Berman HM, Battistuz T, Bhat TN, Bluhm WF, Bourne PE, Burkhardt K, Feng Z, Gilliland GL, Iype L, Jain S, Fagan P, Marvin J, Padilla D, Ravichandran V, Schneider B, Thanki N, Weissig H, Westbrook JD, Zardecki C. The protein data bank Acta Crystallogr D Biol Crystallogr 2002 Jun;58(Pt 6 No 1):899-907.

14. BERTANI G. Sensitivities of different bacteriophage species to ionizing radiations J Bacteriol 1960 Mar;79:387-93.

15. Boczkowska M, Rebowski G, Dominguez R. Glia maturation factor (GMF) interacts with Arp2/3 complex in a nucleotide state-dependent manner J Biol Chem 2013 Sep 6;288(36):25683-8.

16. Boczkowska M, Rebowski G, Petoukhov MV, Hayes DB, Svergun DI, Dominguez R. X-ray scattering study of activated Arp2/3 complex with bound actin-WCA Structure 2008 May;16(5):695-704.

17. Boczkowska M, Rebowski G, Kast DJ, Dominguez R. Structural analysis of the transitional state of Arp2/3 complex activation by two actin-bound WCAs Nature Communications 2014;5.

18. Brooks BR, Bruccoleri RE, Olafson BD, States DJ, Swaminathan S, Karplus M. CHARMM: A program for macromolecular energy, minimization, and dynamics calculations Journal of Computational Chemistry 1983;4(2).

19. Bryce NS, Clark ES, Leysath JL, Currie JD, Webb DJ, Weaver AM. Cortactin promotes cell motility by enhancing lamellipodial persistence Curr Biol 2005 Jul 26;15(14):1276-85.

20. Carlier MF, Pantaloni D. Control of actin dynamics in cell motility J Mol Biol 1997 Jun 20;269(4):459-67.

21. Chaponnier C, Janmey PA, Yin HL. The actin filament-severing domain of plasma gelsolin J Cell Biol 1986 Oct;103(4):1473-81.

22. Chen LF, Winkler H, Reedy MK, Reedy MC, Taylor KA. Molecular modeling of averaged rigor crossbridges from tomograms of insect flight muscle J Struct Biol 2002 Apr-May;138(1-2):92-104.

23. Chen Z, Borek D, Padrick SB, Gomez TS, Metlagel Z, Ismail AM, Umetani J, Billadeau DD, Otwinowski Z, Rosen MK. Structure and control of the actin regulatory WAVE complex Nature 2010;468(7323):533 <last_page> 538.

24. Chereau D, Kerff F, Graceffa P, Grabarek Z, Langsetmo K, Dominguez R. Actin-bound structures of wiskott-aldrich syndrome protein (WASP)-homology domain 2 and the implications for filament assembly Proc Natl Acad Sci U S A 2005 Nov 15;102(46):16644-9.

25. Chik JK, Lindberg U, Schutt CE. The structure of an open state of beta-actin at 2.65 A resolution J Mol Biol 1996 Nov 8;263(4):607-23.

26. Clackson T, Wells JA. A hot spot of binding energy in a hormone-receptor interface Science 1995 Jan 20;267(5196):383-6.

27. Courtemanche N, Pollard TD. Interaction of profilin with the barbed end of actin filaments Biochemistry 2013 Sep 17;52(37):6456-66.

28. Criddle AH, Geeves MA, Jeffries T. The use of actin labelled with N-(1-pyrenyl)iodoacetamide to study the interaction of actin with myosin subfragments and troponin/tropomyosin Biochem J 1985 Dec 1;232(2):343-9.

29. D'Agostino JL, Goode BL. Dissection of Arp2/3 complex actin nucleation mechanism and distinct roles for its nucleation-promoting factors in saccharomyces cerevisiae Genetics 2005 Sep;171(1):35-47.

30. Dalhaimer P, Pollard TD. Molecular dynamics simulations of Arp2/3 complex activation Biophys J 2010 Oct 20;99(8):2568-76.

31. Dalhaimer P, Pollard TD, Nolen BJ. Nucleotide-mediated conformational changes of monomeric actin and Arp3 studied by molecular dynamics simulations J Mol Biol 2008 Feb 8;376(1):166-83.

32. Dayel MJ, Holleran EA, Mullins RD. Arp2/3 complex requires hydrolyzable ATP for nucleation of new actin filaments Proc Natl Acad Sci U S A 2001 Dec 18;98(26):14871-6.

33. Dent EW, Gupton SL, Gertler FB. The growth cone cytoskeleton in axon outgrowth and guidance Cold Spring Harb Perspect Biol 2011 Mar 1;3(3):10.1101/cshperspect.a001800.

34. Dickson BJ. Rho GTPases in growth cone guidance Curr Opin Neurobiol 2001 Feb;11(1):103-10.

35. Dominguez R. Actin filament nucleation and elongation factors--structure-function relationships Crit Rev Biochem Mol Biol 2009 Nov-Dec;44(6):351-66.

36. Dominguez R. Actin filament nucleation and elongation factors--structure-function relationships Crit Rev Biochem Mol Biol 2009 Nov-Dec;44(6):351-66.

37. Dominguez R, Holmes KC. Actin structure and function Annu Rev Biophys 2011;40:169-86.

38. Dou F, Huang L, Yu P, Zhu H, Wang X, Zou J, Lu P, Xu XM. Temporospatial expression and cellular localization of oligodendrocyte myelin glycoprotein (OMgp) after traumatic spinal cord injury in adult rats J Neurotrauma 2009 Dec;26(12):2299-311.

39. Dunbrack RL,Jr, Cohen FE. Bayesian statistical analysis of protein side-chain rotamer preferences Protein Sci 1997 Aug;6(8):1661-81.

40. Egile C, Rouiller I, Xu XP, Volkmann N, Li R, Hanein D. Mechanism of filament nucleation and branch stability revealed by the structure of the Arp2/3 complex at actin branch junctions PLoS Biol 2005 Nov;3(11):e383.

41. Eswar N, Webb B, Marti-Renom MA, Madhusudhan MS, Eramian D, Shen MY, Pieper U, Sali A. Comparative protein structure modeling using MODELLER Curr Protoc Protein Sci 2007 Nov;Chapter 2:Unit 2.9.

42. Falet H, Hoffmeister KM, Neujahr R, Italiano JE,Jr, Stossel TP, Southwick FS, Hartwig JH. Importance of free actin filament barbed ends for Arp2/3 complex function in platelets and fibroblasts Proc Natl Acad Sci U S A 2002 Dec 24;99(26):16782-7.

43. Forscher P, Lin CH, Thompson C. Novel form of growth cone motility involving site-directed actin filament assembly Nature 1992 Jun 11;357(6378):515-8.

44. Fujii T, Iwane AH, Yanagida T, Namba K. Direct visualization of secondary structures of F-actin by electron cryomicroscopy Nature 2010; 2010;467(7316):724 <last_page> 728.

45. Garrity PA. Signal transduction in axon guidance Cellular and Molecular Life Sciences CMLS 1999;55(11).

46. Goldberg DJ, Foley MS, Tang D, Grabham PW. Recruitment of the Arp2/3 complex and mena for the stimulation of actin polymerization in growth cones by nerve growth factor J Neurosci Res 2000 May 15;60(4):458-67.

47. Goley ED, Rammohan A, Znameroski EA, Firat-Karalar EN, Sept D, Welch MD. An actin-filament-binding interface on the Arp2/3 complex is critical for nucleation and branch stability Proc Natl Acad Sci U S A 2010 May 4;107(18):8159-64.

48. Hall A. Rho GTPases and the actin cytoskeleton Science 1998;279(5350):509 <last_page> 514.

49. Hanson J, Lowy J. The structure of F-actin and of actin filaments isolated from muscle J Mol Biol 1963;6(1).

50. Heisenberg C, Pinyol R, Haeckel A, Ritter A, Qualmann B, Kessels MM. Regulation of N-WASP and the Arp2/3 complex by Abp1 controls neuronal morphology Plos One 2007;2(5):e400.

51. Hetrick B, Han MS, Helgeson LA, Nolen BJ. Small molecules CK-666 and CK-869 inhibit actin-related protein 2/3 complex by blocking an activating conformational change Chem Biol 2013;20(5).

52. Higgs HN, Blanchoin L, Pollard TD. Influence of the C terminus of wiskott-aldrich syndrome protein (WASp) and the Arp2/3 complex on actin polymerization Biochemistry 1999 Nov 16;38(46):15212-22.

53. Holder T. 2011 <https://raw.githubusercontent.com/Pymol-Scripts/Pymol-script-repo/master/show_bumps.py>. .

54. Homologene. <http://www.ncbi.nlm.nih.gov/homologene>. .

55. Ismail AM, Padrick SB, Chen B, Umetani J, Rosen MK. The WAVE regulatory complex is inhibited Nat Struct Mol Biol 2009 May;16(5):561-3.

56. Kabsch WW. Atomic structure of the actin:DNase I complex. Nature (London) 1990;347(6288):37-44.

57. Kaksonen M, Toret CP, Drubin DG. Harnessing actin dynamics for clathrin-mediated endocytosis Nat Rev Mol Cell Biol 2006 Jun;7(6):404-14.

58. Katoh H, Yasui H, Yamaguchi Y, Aoki J, Fujita H, Mori K, Negishi M. Small GTPase RhoG is a key regulator for neurite outgrowth in PC12 cells Mol Cell Biol 2000 Oct;20(19):7378-87.

59. Kelleher JF, Atkinson SJ, Pollard TD. Sequences, structural models, and cellular localization of the actin-related proteins Arp2 and Arp3 from acanthamoeba J Cell Biol 1995 Oct;131(2):385-97.

60. Kim AS, Kakalis LT, Abdul-Manan N, Liu GA, Rosen MK. Autoinhibition and activation mechanisms of the wiskott-aldrich syndrome protein Nature 2000 Mar 9;404(6774):151-8.

61. Kiselar JG, Mahaffy R, Pollard TD, Almo SC, Chance MR. Visualizing Arp2/3 complex activation mediated by binding of ATP and WASp using structural mass spectrometry Proc Natl Acad Sci U S A 2007 Jan 30;104(5):1552-7.

62. Koestler SA, Rottner K, Lai F, Block J, Vinzenz M, Small JV. F- and G-actin concentrations in lamellipodia of moving cells PLoS One 2009;4(3):e4810.

63. Kolafa J, Perram JW. Cutoff errors in the ewald summation formulae for point charge systems. Molecular Simulation 1992;9(5):351.

64. Korobova F, Svitkina T. Arp2/3 complex is important for filopodia formation, growth cone motility, and neuritogenesis in neuronal cells Mol Biol Cell 2008 Apr;19(4):1561-74.

65. Kortemme T, Kim DE, Baker D. Computational alanine scanning of protein-protein interfaces Sci STKE 2004 Feb 3;2004(219):pl2.

66. Krissinel,E.,Henrick,K. Detection of protein assemblies in crystals. 2005.

67. Kudryashov DS, Sawaya MR, Adisetiyo H, Norcross T, Hegyi G, Reisler E, Yeates TO. The crystal structure of a cross-linked actin dimer suggests a detailed molecular interface in F-actin Proc Natl Acad Sci U S A 2005 Sep 13;102(37):13105-10.

68. Kurisu S, Takenawa T. The WASP and WAVE family proteins Genome Biol 2009;10(6):226,2009-10-6-226. Epub 2009 Jun 15.

69. Le Clainche C, Pantaloni D, Carlier MF. ATP hydrolysis on actin-related protein 2/3 complex causes debranching of dendritic actin arrays Proc Natl Acad Sci U S A 2003 May 27;100(11):6337-42.

70. Lee SH, Kerff F, Chereau D, Ferron F, Klug A, Dominguez R. Structural basis for the actin-binding function of missing-in-metastasis Structure 2007 Feb;15(2):145-55.

71. Leung DW, Otomo C, Chory J, Rosen MK. Genetically encoded photoswitching of actin assembly through the Cdc42-WASP-Arp2/3 complex pathway Proc Natl Acad Sci U S A 2008 Sep 2;105(35):12797-802.

72. Lichtarge O, Bourne HR, Cohen FE. An evolutionary trace method defines binding surfaces common to protein families J Mol Biol 1996 Mar 29;257(2):342-58.

73. Liu SL, Needham KM, May JR, Nolen BJ. Mechanism of a concentration-dependent switch between activation and inhibition of Arp2/3 complex by coronin J Biol Chem 2011 May 13;286(19):17039-46.

74. Lodish, H. F., A. Berk, C. Kaiser, M. Krieger, A. Bretscher, H. Ploegh, A. Amon, and M. Scott, Matsudaira.'. Molecular cell biology. 7th ed. ed. W. H. Freeman and Company, N. Y.; (2012).

75. Lu P, Yang H, Jones LL, Filbin MT, Tuszynski MH. Combinatorial therapy with neurotrophins and cAMP promotes axonal regeneration beyond sites of spinal cord injury J Neurosci 2004 Jul 14;24(28):6402-9.

76. Luan Q, Nolen BJ. Structural basis for regulation of Arp2/3 complex by GMF Nat Struct Mol Biol 2013 Sep;20(9):1062-8.

77. Machesky LM, Atkinson SJ, Ampe C, Vandekerckhove J, Pollard TD. Purification of a cortical complex containing two unconventional actins from acanthamoeba by affinity chromatography on profilin-agarose J Cell Biol 1994 Oct;127(1):107-15.

78. Machesky LM, Mullins RD, Higgs HN, Kaiser DA, Blanchoin L, May RC, Hall ME, Pollard TD. Scar, a WASp-related protein, activates nucleation of actin filaments by the Arp2/3 complex Proc Natl Acad Sci U S A 1999 Mar 30;96(7):3739-44.

79. Mahadik AC, Haldar S, Hynds DL, Beck BW. Specific interfacial residues control rearrangement of the Arp2:Arp3 dimer during activation of the Arp2/3 complex *(submitted to protein science, in review)*.

80. Marchand JB, Kaiser DA, Pollard TD, Higgs HN. Interaction of WASP/Scar proteins with actin and vertebrate Arp2/3 complex Nat Cell Biol 2001 Jan;3(1):76-82.

81. Martin AC, Xu XP, Rouiller I, Kaksonen M, Sun Y, Belmont L, Volkmann N, Hanein D, Welch M, Drubin DG. Effects of Arp2 and Arp3 nucleotide-binding pocket mutations on Arp2/3 complex function J Cell Biol 2005 Jan 17;168(2):315-28.

82. Maruyama K, Kurokawa H, Oosawa M, Shimaoka S, Yamamoto H, Ito M, Maruyama K. Beta-actinin is equivalent to cap Z protein J Biol Chem 1990 May 25;265(15):8712-5.

83. May RC. The Arp2/3 complex: A central regulator of the actin cytoskeleton Cell Mol Life Sci 2001 Oct;58(11):1607-26.

84. May RC, Knecht DA, LaFleur RA, Kahsai AW, Argueta CE, Beshir AB, Fenteany G. Cucurbitacin I inhibits cell motility by indirectly interfering with actin dynamics Plos One 2010;5(11):e14039.

85. McLaughlin PJ, Gooch JT, Mannherz HG, Weeds AG. Structure of gelsolin segment 1-actin complex and the mechanism of filament severing Nature 1993 Aug 19;364(6439):685-92.

86. Meyer G, Feldman EL. Signaling mechanisms that regulate actin-based motility processes in the nervous system J Neurochem 2002 Nov;83(3):490-503.

87. Millard TH, Sharp SJ, Machesky LM. Signalling to actin assembly via the WASP (wiskott-aldrich syndrome protein)-family proteins and the Arp2/3 complex Biochem J 2004 May 15;380(Pt 1):1-17.

88. Miller KG, Field CM, Alberts BM. Actin-binding proteins from drosophila embryos: A complex network of interacting proteins detected by F-actin affinity chromatography J Cell Biol 1989 Dec;109(6 Pt 1):2963-75.

89. Mogilner A, Oster G. Cell motility driven by actin polymerization Biophys J 1996 Dec;71(6):3030-45.

90. Moulding DA, Blundell MP, Spiller DG, White MR, Cory GO, Calle Y, Kempski H, Sinclair J, Ancliff PJ, Kinnon C, Jones GE, Thrasher AJ. Unregulated actin polymerization by WASp causes defects of mitosis and cytokinesis in X-linked neutropenia J Exp Med 2007 Sep 3;204(9):2213-24.

91. Mueller BK. Growth cone guidance: First steps towards a deeper understanding Annu Rev Neurosci 1999;22:351-88.

92. Mullins RD. How WASP-family proteins and the Arp2/3 complex convert intracellular signals into cytoskeletal structures Curr Opin Cell Biol 2000 Feb;12(1):91-6.

93. Mullins RD, Heuser JA, Pollard TD. The interaction of Arp2/3 complex with actin: Nucleation, high affinity pointed end capping, and formation of branching networks of filaments Proc Natl Acad Sci U S A 1998 May 26;95(11):6181-6.

94. Nikolic M. The role of rho GTPases and associated kinases in regulating neurite outgrowth Int J Biochem Cell Biol 2002 Jul;34(7):731-45.

95. Nolen BJ, Littlefield RS, Pollard TD. Crystal structures of actin-related protein 2/3 complex with bound ATP or ADP Proc Natl Acad Sci U S A 2004 Nov 2;101(44):15627-32.

96. Nolen BJ, Littlefield RS, Pollard TD. Crystal structures of actin-related protein 2/3 complex with bound ATP or ADP Proc Natl Acad Sci U S A 2004 Nov 2;101(44):15627-32.

97. Nolen BJ, Pollard TD. Structure and biochemical properties of fission yeast Arp2/3 complex lacking the Arp2 subunit J Biol Chem 2008 Sep 26;283(39):26490-8.

98. Nolen BJ, Pollard TD. Insights into the influence of nucleotides on actin family proteins from seven structures of Arp2/3 complex Mol Cell 2007 May 11;26(3):449-57.

99. Otey,C.A.,Boukhelifa,M., Maness,P. B35 neuroblastoma cells: An easily transfected, cultured cell model of central nervous system neurons. In: Hollenbeck,P., Bamburg,J., editor. Neurons: Methods and applications for the cell biologist. ; 2003.

100. Otterbein LR, Graceffa P, Dominguez R. The crystal structure of uncomplexed actin in the ADP state Science 2001 Jul 27;293(5530):708-11.

101. Padrick SB, Cheng HC, Ismail AM, Panchal SC, Doolittle LK, Kim S, Skehan BM, Umetani J, Brautigam CA, Leong JM, Rosen MK. Hierarchical regulation of WASP/WAVE proteins Mol Cell 2008 Nov 7;32(3):426-38.

102. Padrick SB, Doolittle LK, Brautigam CA, King DS, Rosen MK. Arp2/3 complex is bound and activated by two WASP proteins Proc Natl Acad Sci U S A 2011 Aug 16;108(33):E472-9.

103. Panchal SC, Kaiser DA, Torres E, Pollard TD, Rosen MK. A conserved amphipathic helix in WASP/Scar proteins is essential for activation of Arp2/3 complex Nat Struct Biol 2003 Aug;10(8):591-8.

104. Pantaloni D, Le Clainche C, Carlier MF. Mechanism of actin-based motility Science 2001 May 25;292(5521):1502-6.

105. Pfaendtner J, Volkmann N, Hanein D, Dalhaimer P, Pollard TD, Voth GA. Key structural features of the actin filament Arp2/3 complex branch junction revealed by molecular simulation J Mol Biol 2012 Feb 10;416(1):148-61.

106. Pollard TD, Beltzner CC. Structure and function of the Arp2/3 complex Curr Opin Struct Biol 2002 Dec;12(6):768-74.

107. Pollard TD, Borisy GG. Cellular motility driven by assembly and disassembly of actin filaments Cell 2003;112(4).

108. Robinson RC, Turbedsky K, Kaiser DA, Marchand JB, Higgs HN, Choe S, Pollard TD. Crystal structure of Arp2/3 complex Science 2001 Nov 23;294(5547):1679-84.

109. Rodal AA, Sokolova O, Robins DB, Daugherty KM, Hippenmeyer S, Riezman H, Grigorieff N, Goode BL. Conformational changes in the Arp2/3 complex leading to actin nucleation Nat Struct Mol Biol 2005 Jan;12(1):26-31.

110. Rohatgi R, Ma L, Miki H, Lopez M, Kirchhausen T, Takenawa T, Kirschner MW. The interaction between N-WASP and the Arp2/3 complex links Cdc42-dependent signals to actin assembly Cell 1999 Apr 16;97(2):221-31.

111. Rouiller I, Xu XP, Amann KJ, Egile C, Nickell S, Nicastro D, Li R, Pollard TD, Volkmann N, Hanein D. The structural basis of actin filament branching by the Arp2/3 complex J Cell Biol 2008 Mar 10;180(5):887-95.

112. Sali A. *Salign.py* : A script for multiple sequence alignment using modeller. <http://salilab.org/modeller/tutorial/advanced.html>. .

113. Sali A, Blundell TL. Comparative protein modelling by satisfaction of spatial restraints. J Mol Biol 1993 Dec 5;234(3):779-815.

114. Schaefer AW, Schoonderwoert VTG, Ji L, Mederios N, Danuser G, Forscher P. Coordination of actin filament and microtubule dynamics during neurite outgrowth Developmental Cell 2008;15(1).

115. Schmidt H, Rathjen FG. Signalling mechanisms regulating axonal branching in vivo Bioessays 2010 Nov;32(11):977-85.

116. Schrödinger. The PyMOL Molecular Graphics System, Version 1.5.04 Schrodinger, LLC [computer program]. .

117. Schutt CE, Myslik JC, Rozycki MD, Goonesekere NC, Lindberg U. The structure of crystalline profilin-beta-actin Nature 1993 Oct 28;365(6449):810-6.

118. Shakir MA, Jiang K, Struckhoff EC, Demarco RS, Patel FB, Soto MC, Lundquist EA. The Arp2/3 activators WAVE and WASP have distinct genetic interactions with rac GTPases in caenorhabditis elegans axon guidance Genetics 2008 Aug;179(4):1957-71.

119. Sheterline P, Clayton J, Sparrow J. Actin Protein Profile 1995;2(1):1-103.

120. Siton O, Ideses Y, Albeck S, Unger T, Bershadsky AD, Gov NS, Bernheim-Groswasser A. Cortactin releases the brakes in actin- based motility by enhancing WASP-VCA detachment from Arp2/3 branches Curr Biol 2011 Dec 20;21(24):2092-7.

121. Skaper SD, Moore SE, Walsh FS. Cell signalling cascades regulating neuronal growth-promoting and inhibitory cues Prog Neurobiol 2001 Dec;65(6):593-608.

122. Smith BA, Daugherty-Clarke K, Goode BL, Gelles J. Pathway of actin filament branch formation by Arp2/3 complex revealed by single-molecule imaging Proc Natl Acad Sci U S A 2013 Jan 22;110(4):1285-90.

123. Song H, Poo M. The cell biology of neuronal navigation Nat Cell Biol 2001 Mar;3(3):E81-8.

124. Suetsugu S, Yamazaki D, Kurisu S, Takenawa T. Differential roles of WAVE1 and WAVE2 in dorsal and peripheral ruffle formation for fibroblast cell migration Developmental Cell 2003;5(4):595 <last_page> 609.

125. Svitkina TM, Borisy GG. Arp2/3 complex and actin depolymerizing factor/cofilin in dendritic organization and treadmilling of actin filament array in lamellipodia J Cell Biol 1999 May 31;145(5):1009-26.

126. Ti SC, Jurgenson CT, Nolen BJ, Pollard TD. Structural and biochemical characterization of two binding sites for nucleation-promoting factor WASp-VCA on Arp2/3 complex Proc Natl Acad Sci U S A 2011 Aug 16;108(33):E463-71.

127. To C, Shilton BH, Di Guglielmo GM. Synthetic triterpenoids target the Arp2/3 complex and inhibit branched actin polymerization J Biol Chem 2010 Sep 3;285(36):27944-57.

128. Verkhovsky AB, Chaga OY, Schaub S, Svitkina TM, Meister JJ, Borisy GG. Orientational order of the lamellipodial actin network as demonstrated in living motile cells Mol Biol Cell 2003 Nov;14(11):4667-75.

129. Volkmann N, Amann KJ, Stoilova-McPhie S, Egile C, Winter DC, Hazelwood L, Heuser JE, Li R, Pollard TD, Hanein D. Structure of Arp2/3 complex in its

activated state and in actin filament branch junctions Science 2001 Sep 28;293(5539):2456-9.

130. Wegner A, Isenberg G. 12-fold difference between the critical monomer concentrations of the two ends of actin filaments in physiological salt conditions Proc Natl Acad Sci U S A 1983 Aug;80(16):4922-5.

131. Wegner AM, Nebhan CA, Hu L, Majumdar D, Meier KM, Weaver AM, Webb DJ. N-wasp and the arp2/3 complex are critical regulators of actin in the development of dendritic spines and synapses J Biol Chem 2008 Jun 6;283(23):15912-20.

132. Welch MD, Mullins RD. Cellular control of actin nucleation Annu Rev Cell Dev Biol 2002;18:247-88.

133. Wilson AJ. Inhibition of protein-protein interactions using designed molecules Chem Soc Rev 2009 Dec;38(12):3289-300.

134. Winter D, Lechler T, Li R. Activation of the yeast Arp2/3 complex by Bee1p, a WASP-family protein Curr Biol 1999 May 6;9(9):501-4.

135. Yarar D, To W, Abo A, Welch MD. The wiskott-aldrich syndrome protein directs actin-based motility by stimulating actin nucleation with the Arp2/3 complex Curr Biol 1999 May 20;9(10):555-8.

136. Zhu X, Lopes PE, Mackerell AD,Jr. Recent developments and applications of the CHARMM force fields Wiley Interdiscip Rev Comput Mol Sci 2012 Jan;2(1):167-85.